UNIVERSIDAD AUTÓNOMA DE MADRID

Facultad de Ciencias
Departamento de Biología Molecular
Programa de Doctorado en Biociencias Moleculares

Development of genetic circuits and synthetic receptors in *Escherichia coli* for detecting tumor-associated metabolites and protein antigens

Doctoral Thesis

Álvaro Ceballos Munuera

Madrid 2023

Tesis presentada por D. Álvaro Ceballos Munuera para optar al grado de Doctor en Biociencias Moleculares por la Universidad Autónoma de Madrid.

Director de la tesis doctoral:
Dr. Luis Ángel Fernández Herrero
Investigador Científico del Consejo Superior de Investigaciones Científicas.

Este trabajo ha sido realizado en el Departamento de Biotecnología Microbiana del Centro Nacional de Biotecnología del Consejo Superior de Investigaciones Científicas (CNB-CSIC), gracias al contrato de Formación de Profesorado Universitario FPU16/01427 y a la financiación de los proyectos BIO2017-89081-R (AEI/MINECO), H2020 FET Open 965018- BIOCELLPHE (Unión Europea) y PLEC2021-007739 (MICIN - Líneas estratégicas), así como la ayuda Research and Training Grant FEMS-GO-2020-249 (FEMS).

“This is insanity!”

“No, this is scholarship! I don’t know what kind of view I can get through the water, but I have to try.”

Brandon Sanderson, Words of Radiance.

AGRADECIMIENTOS

Pues… parece que sí. Tras releer varias veces el nombre en la portada, todo parece indicar que he conseguido acabar la tesis. Sigo en proceso de creérmelo. Han sido años de trabajo, esfuerzo y altibajos, pero también de vivencias importantes y personas que han pasado a ser fundamentales en mi vida. Decía Newton aquello de que si había podido ver más lejos era porque había subido a hombros de gigantes. Yo quisiera añadirle algo más: la importancia de aquellas personas que te sostienen la escalera al subir. Personas a las que estaré eternamente agradecido, puesto que sin ellas no existiría esta tesis.

En primer lugar, a mi director de tesis, Luis Ángel, por confiar en mí para un proyecto tan arriesgado y darme la oportunidad de unirme a un estupendo equipo. Gracias por las buenas ideas y tener siempre la puerta abierta, pero, sobre todo, por seguir teniendo fe en el proyecto y animarme a continuar a pesar de los baches en el camino.

En segundo lugar, pero no menos importante, a mi familia del 241, porque esta tesis es tan suya como mía. A Carmen, Eva, Lidia, Bea, Elena, Alba, Mercedes y a Alejandro, gracias por todo lo que habéis hecho y seguís haciendo por mí día a día (y por vuestra paciencia infinita para aguantar las payasadas continuas). No puedo dejar de hacer una mención especial a Alex y Yago, porque además de ser un gran apoyo a lo largo de toda la tesis se han convertido en grandes amigos dentro y fuera del laboratorio. Gracias por creer siempre en mí más que yo mismo.

A mis queridas Almu y Raquel, por su cariño, su apoyo y las quedadas espontáneas post CNB.

A los compañeros del departamento de BiMi, y con especial cariño a Julia, Samu, Pablo, Fernando, Leti, Rubén y Marcos. Gracias por tantísimos buenos momentos por los pasillos del CNB, apretujados en el 714, las cenas, las cañas, las fiestas con indumentarias horribles, los juegos de mesa, los “planes culturales” y tantas otras batallitas. Y, por supuesto, gracias a Guille, que ha estado en casi todos esos momentos y muchos más y sigue soportándome con estoicismo como el gran amigo en que se ha convertido.

A huge thank you to the wonderful people of the Bonnet lab in Montpellier. First of all, to Jérôme, for giving me the chance to work with the team and helping me with the integrases project. Mil gracias a Ana por su ayuda constante en el laboratorio y con la burocracia francesa, pero sobre todo por convertirse en una verdadera amiga. Trabajar con ella es un lujo. A Diego, por su ayuda, por su amabilidad y por haber hecho posible ese cuarto mes. Thanks, Peter, for the

laughs and the mushroom growing lessons. Also, thanks to Miguel, Gabriel, Pauline, Paul, Carlos, Annika, Ashley and everyone else for the good moments outside the CBS. Merci, mes amis!

A Jass, por su apoyo, su amistad y tantísimas risas. A Jose, Lazas y Alex de la primera planta, por los planes de barrio y las patrullitas del OW.

Gracias a M. Carmen y Miguel Ángel del servicio de citometría, siempre dispuestos a echarme una mano con el Gallios. A Florencio Pazos, por su inestimable ayuda con AlphaFold. También a Esteban Martínez y Belén Calles, por ayudarme a pelear con el Spectramax y el Victor2.

Gracias a Jorge y Antonio del departamento de Bioquímica de la UCA, por guiarme en los comienzos de mi aventura científica. Si hoy estoy aquí es en gran parte gracias a ellos.

Fuera del mundo científico, en primer lugar, por supuesto, gracias a mi familia. A mis padres y a Celia, gracias por vuestro cariño, vuestro apoyo incondicional y vuestra confianza ciega. Prometo que algún día os daré una explicación en condiciones sobre lo que hago. Gracias por estar siempre ahí y hacer por mí todo lo que está en vuestra mano. Os quiero.

Gracias a Loren, Noe, Gabi y Sara, por ser ese trocito del sur en Madrid. Con vosotros el exilio en la meseta siempre fue más llevadero. A Diego, por aguantarme casi a diario y estar siempre ahí cuando necesito que me escuchen. A Manu y a Somi, porque no importa lo poco que la vida nos deja vernos, siempre parece que fue ayer, y porque más que amigos, son familia. A Alexander, por tantos años de payum payum. A Sergio, por todas las anécdotas desde la carrera hasta hoy. Gracias por esa hospitalidad lionesa, el Super Soaker al final lo consiguió.

A Vincen, Santi y Mariela, porque hay pocas cosas más importantes que sentirte a gusto en tu propia casa.

Mil gracias a todos. Porque sin vosotros aguantando mi escalera probablemente me habría abierto la cabeza.

TABLE OF CONTENTS

LIST OF FIGURES

ABBREVIATIONS

2-ME	β-mercaptoethanol
6xHis	Hexa histidine-tag
AC	Autochaperone region
Amp	Ampicillin
AT	Autotransporter
aTc	Anhydrotetracycline
BAC	Bacterial Artificial Chromosome
BAM	β-barrel assembly machinery
BCG	Bacillus Calmette-Guérin
BSA	Bovine serum albumin
CAR-T	Chimeric Antigen Receptor T
CDR	Complementarity determining region
CFU	Colony forming units
Cm	Chloramphenicol
DAPA	Diaminopimelic acid
DSP	Dithiobis(succinimidyl propionate)
EDTA	Ethylenediaminetetraacetic acid
EGFR	Epidermal growth factor receptor
EHEC	Enterohemorrhagic *E. coli*
EPEC	Enteropathogenic *E. coli*
Fc	Antibody fragment crystallizable region
FNR	Fumarate and nitrate reductase
FRAP	Fluorescence recovery after photobleaching
GFP	Green fluorescent protein
H_2O_2	Oxygen peroxide
HCAbs	Heavy-chain only antibodies
Ig	Immunoglobulin
IM	Inner membrane
iNOS/NOS2	Inducible nitric oxide synthase
IPTG	Isopropyl-ß-D-thiogalactopyranoside
Km	Kanamycin

L-ara	L-arabinose
LB	Lysogeny Broth
mAb	Monoclonal antibody
Nb	Nanobody
NK	Natural killer cell
NMIBC	Non-muscle invasive bladder cancer
NO	Nitric oxide
O/N	Overnight
$O_2^{\bullet-}$	Superoxide radical
OD_{600}	Optical density at 600 nm
OM	Outer membrane
OMP	Outer membrane protein
PAGE	Polyacrylamide gel electrophoresis
PBS	Phosphate-buffered saline
PCA	Protein complementation assay
PCR	Polymerase Chain Reaction
PD-L1	Programmed death-ligand 1
PG	Peptidoglycan
POD	Peroxidase
POTRA	Polypeptide-transport-associated
PVDF	Polyvinylidene difluoride membrane
RBD	Receptor binding domain
RBS	Ribosomal binding site
ROS	Reactive oxygen species
SA	Synthetic adhesin
SBOL	Synthetic Biology Open Language
scFv	Single-chain variable fragment
SDS	Sodium dodecyl sulphate
SIEC	Synthetic Injector *E. coli*
SP	Signal peptide
SPER/NO	Spermine NONOate
T3SS	Type III secretion system
T5SS	Type V secretion system

TEV	Tobacco etch virus
TF	Transcription factor
Tir	Translocated intimin receptor
TIRF	Total internal reflection fluorescence
TME	Tumor microenvironment
TSS	Transformation and Storage Solution
VHH	Variable heavy chain region
WT	Wild type

SUMMARY

Anaerobic and facultative bacteria are promising tools in the treatment of cancer since they are able to colonize solid tumors, proliferating in the tumor microenvironment characterized by hypoxic and immunosuppressive conditions, with metabolite gradients that differ from healthy homeostatic concentrations. Due to their active motility, bacteria can also reach tumor regions that cannot be accessed by passive therapeutics. With the advances in synthetic biology, researchers are engineering bacteria to produce different proteins with cytotoxic and immunomodulatory activities within the tumor. In order to increase the safety of bacterial therapies the induction of these activities requires specificity to avoid enacting their effects outside the tumor. In this PhD thesis we have aimed to develop inductions systems that avoid relying in classical chemical inducers and focus on detecting specific tumor cues such as tumor-associated metabolites and proteins, as well as genetic circuit tools to program a more specific response to those signals.

We have characterized several promoters that respond to increased concentrations of L-lactate, reactive oxygen species and nitric oxide (NO), which are common characteristic of the tumor microenvironment. Promoters were analyzed by using *gfp* as reporter gene while integrated in the chromosome of *E. coli* K-12, with two NO promoters (P_{norV} and P_{hmp}) showing good characteristics for *in vivo* applications and a L-lactate promoter (a mutated version of P_{lldP}) presenting promising results that could be further improved. Next, we tested the possibility of using serine integrases to design genetic logic circuits and generate genetic memory using targets placed in the chromosome of *E. coli*. We found that three different serine integrases (Bxb1, Tp901 and Int7) can successfully catalyze the excision and inversion of chromosome-integrated targets, with excision appearing more efficient. Bxb1 and Tp901 targets were used to produce functional AND logic circuits based on excision or inversion. The NO-responsive P_{hmp} promoter and Bxb1 were used to create a NO biosensor *E. coli* that generates genetic memory after exposure, with all the genetic elements integrated in the chromosome of *E. coli*.

Detection of tumor-associated proteins could also allow the specific activation of therapeutic bacteria. Previous works from our laboratory engineered *E. coli* cell surface display systems based on protein fusions between single-domain antibodies (nanobodies) and the β-barrel domain of outer membrane proteins (OMPs) belonging to

the type V secretion system (T5SS). Building from those results, in this work we engineered different types of chimeric OMP receptors, based on the β-barrel of T5SS proteins such as intimin, invasin and EhaA, which simultaneously display a nanobody on the bacterial cell surface and protein fragments of a reporter system in the bacterial periplasm. We obtained functional chimeric proteins that display a nanobody binding the human epidermal growth factor receptor (EGFR), a tumor-associated antigen, and that express in the periplasm the two fragments of a split luciferase reporter (NanoBiT) or peptides for covalent protein fusions (SpyTag and SnoopTag). By co-expressing intimin- and invasin-based chimeric receptors having the anti-EGFR nanobody and the NanoBiT fragments, we have demonstrated that *E. coli* bacteria can function as a biosensor, decreasing its bioluminescence signal in the presence of soluble EGFR and in a dose-dependent manner. Given the modularity of these chimeric proteins, these results open the way to generate bacterial antigen receptors (BAR) for biosensors detecting multiple extracellular protein antigens associated to human diseases (infection, inflammation, cancer) as well as the presence of toxins and pathogens in environmental samples.

RESUMEN

Las bacterias anaeróbicas y facultativas son prometedoras herramientas en el tratamiento del cáncer dada su capacidad para colonizar tumores sólidos, proliferando en un microambiente tumoral caracterizado por condiciones hipóxicas e inmunosupresoras y gradientes de metabolitos que difieren de las concentraciones homeostáticas sanas. Debido a su movilidad activa, las bacterias también son capaces de alcanzar regiones tumorales a las que las terapias pasivas no pueden acceder. Gracias a los avances en biología sintética, se están diseñando bacterias capaces de producir diferentes proteínas con actividades citotóxicas e inmunomoduladoras desde el interior del tumor. Para incrementar la seguridad de las terapias bacterianas la inducción de estas actividades requiere una alta especificidad que evite que sus efectos puedan manifestarse fuera del tumor. En la presente tesis doctoral hemos trabajado en el desarrollo de sistemas de inducción que eviten la necesidad de utilizar inductores químicos clásicos y en cambio se basen en la detección de señales específicas del tumor, como son la presencia de altos niveles de metabolitos y proteínas asociadas al ambiente tumoral. Además, también se han desarrollado circuitos genéticos destinados a programar una respuesta más específica a dichas señales.

En primer lugar, caracterizamos promotores que responden a altas concentraciones de L-lactato, especies reactivas de oxígeno y óxido nítrico (NO), características comunes del microambiente tumoral. Los promotores fueron analizados usando *gfp* como gen reportero estando integrados en el cromosoma de *E. coli* K-12. Dos promotores sensibles a NO (P_{norV} and P_{hmp}) demostraron buenas características para su uso en aplicaciones *in vivo* y un promotor sensible a L-lactato (una versión mutada de P_{lldP}) presentó resultados prometedores que podrían ser mejorados en el futuro. A continuación, estudiamos la posibilidad de usar serin-integrasas para diseñar circuitos genéticos lógicos y generar memoria genética usando dianas situadas en el cromosoma de *E. coli*. Determinamos que tres serin-integrasas distintas (Bxb1, Tp901 y Int7) pueden catalizar la excisión e inversión de dianas integradas en el cromosoma, con una mayor eficiencia en el caso de la excisión. Empleando dianas para Bxb1 y Tp901 se diseñaron circuitos lógicos tipo AND funcionales basados tanto en la excisión como en la inversión. Mediante el control de la expresión de Bxb1 por el promotor sensible a NO P_{hmp} se generó una cepa de *E. coli* biosensora de NO que genera memoria genética tras la exposición a dicha molécula, con todos los componentes genéticos integrados en el cromosoma de la bacteria.

La detección de proteínas asociadas a tumores también podría permitir una activación especifica de bacterias terapéuticas. En trabajos previos de nuestro laboratorio se diseñaron sistemas de presentación en la membrana de *E. coli* basados en fusiones proteicas entre anticuerpos de dominio único (nanoanticuerpos o *nanobodies*) y el dominio barril β de proteínas de membrana externa (OMPs) pertenecientes al sistema de secreción tipo V (T5SS). Partiendo de estos resultados, en este trabajo hemos generado diferentes tipos de receptores basados en OMP quiméricas utilizando el dominio barril β de proteínas del T5SS como intimina, invasina y EhaA, capaces de presentar simultáneamente un nanoanticuerpo en la superficie bacteriana y un fragmento proteico de un sistema reportero en el periplasma bacteriano. Se produjeron proteínas quiméricas funcionales que presentan un nanoanticuerpo capaz de unirse al factor de crecimiento epidérmico humano (EGFR), un antígeno asociado a tumores, y que expresan en el periplasma los fragmentos complementarios del sistema reportero NanoBiT, basado en una luciferasa fragmentada, o los péptidos de los sistemas SpyTag y SnoopTag, que permiten fusiones covalentes a otras proteínas. Mediante la expresión simultánea de los receptores quiméricos basados en intimina e invasina con el nanoanticuerpo contra EGFR y los fragmentos de NanoBiT hemos demostrado que la bacteria *E. coli* puede funcionar como un biosensor, disminuyendo su señal bioluminiscente en la presencia de EGFR soluble de manera dosis-dependiente. Dada la naturaleza modular de estas proteínas quiméricas, estos resultados abren la puerta a generar receptores bacterianos de antígeno (BAR, bacterial antigen receptors) para la creación de biosensores capaces de detectar múltiples proteínas extracelulares asociadas a enfermedades humanas (infecciones, inflamación, cáncer) así como la presencia de toxinas y patógenos en muestras ambientales.

INTRODUCTION

1. Bacteria in human health and cancer.

When discussing human health, bacteria are mainly seen by the general public as pathogenic agents that harbor infections. However, nowadays we are aware that these organisms play a key role in the correct functioning of the human body. Together with archaea, viruses, and eukaryotic microbes, more than 1000 species of bacteria form the human microbiome and play a fundamental role in maintaining health. Generating nutrients from substrates indigestible by the human host, training the immune system for its proper function, and protecting from pathogens are several examples of the roles accomplished by bacteria that have a huge impact in our bodies (Shreiner et al., 2015). As our understanding of the behavior and composition of the microbiota in homeostasis grew thanks to advances in metagenomic and transcriptomic techniques the possibility of using bacteria as living therapeutics became a promising concept. Some examples include their use as antigen delivery or presentation vehicles for vaccines, or the transplantation of fecal microbiota to counter opportunistic infections due to the homeostasis disruption caused by antibiotic treatments (Kelly et al., 2020). But perhaps the most extended use of bacteria as therapeutic agents can be found in probiotics, dietary supplements and foods that contain "*live microorganisms which when administered in adequate amounts confer a health benefit on the host*"(FAO and WHO, 2002). Lactic acid bacteria from the genera *Lactobacillus* and *Bifidobacterium* are the most commonly used in probiotics, as their production of lactic, acetic, and propionic acid reduces the intestinal pH and hinders the growth of pathogenic bacteria. Other species used as probiotics include *Escherichia coli* strains such as Nissle 1917 (Sonnenborn, 2016). Strong evidence supports the beneficial effects of probiotics in the treatment of acute diarrhea, but there are also promising reports in the prevention of other affections such as *Clostridium difficile* infections, irritable bowel syndrome, ulcerative colitis, Crohn's disease, and vulvovaginal candidiasis (Beimfohr, 2016; Senok et al., 2005; Williams, 2010).

Bacteria have also revealed as promising therapeutics against cancer. Back in the 19th century, spontaneous remission of certain tumors was first reported in patients infected by *Streptococcus pyogenes*. Decades later, the same observations led Dr. B. Coley to start administering systemically this bacterium to treat patients affected by sarcomas, myelomas and other types of cancer, a treatment that would eventually develop to also include *Serratia marcescens* (Coley, 1910, 1891). Mixtures of live or heat-inactivated bacteria became known as "Coley's toxins" and were frequently capable of inducing total and prolonged tumor regressions. Results, however, were variable and the inoculation of bacteria in an era before the discovery of antibiotics sometimes resulted in the death

of the patients, which together with the advent of new treatments in the form of radiotherapy and chemotherapy resulted in a loss of interest in bacterial cancer therapy (Hoption Cann et al., 2003; McCarthy, 2006). However, there is an example of an approved clinical application of bacteria against cancer. This is the use of the live Bacillus Calmette-Guérin (BCG) against non-muscle invasive bladder cancer (NMIBC) (Alhunaidi and Zlotta, 2019). This bacterium is an attenuated strain of *Mycobacterium bovis* that was originally used as a tuberculosis vaccine (Gandhi et al., 2013). Since the 1970s, BCG has been administered by intravesical instillations to high-grade NMIBC patients. It is believed that BCG triggers a strong local immune response leading to the destruction of tumor cells in the bladder (Alhunaidi and Zlotta, 2019; Pettenati and Ingersoll, 2018). A modern analysis of Coley's treatment has also attributed the remission of tumors to the stimulation of the immune system and activation of lymphocytes, which is considered one of the first forms of cancer immunotherapy (Forbes et al., 2018; Mellman et al., 2011; Tsung and Norton, 2006). Other antitumoral effects of bacteria include nutrient depletion inside the tumor (Song et al., 2018), secretion of toxins and bacteriocins with cytotoxic activity (Kaur and Kaur, 2015; Middlebrook and Dorland, 1984) as well as the creation of biofilms that hinder metastasis (Song et al., 2018).

Nowadays, we understand that this localized antitumoral activity is a consequence of the preferential growth inside the necrotic cores of solid tumors displayed by several species of obligate and facultative anaerobic bacteria. With this key information, researchers have identified additional genera capable of colonizing solid tumor such as *Salmonella* (Forbes et al., 2003; Hernández-Luna and Luria-Pérez, 2018; Pawelek et al., 1997), *Bifidobacterium* (Kimura et al., 1980), *Clostridium* (Lambin et al., 1998; Malmgren and Flanigan, 1955), *Listeria* (Flickinger et al., 2018) or *Escherichia* (Jiang et al., 2010; Stritzker et al., 2007; Yu et al., 2004). Although it was unknown at Coley's time, this preferential localization of bacteria within the tumor is not by mere chance, but a direct consequence of the specific characteristics of the chaotic and fast proliferation of the tumor.

2. The tumor microenvironment.

Solid tumors are heterogeneous, dynamic and highly disorganized pseudoorgans. The rapid proliferation of tumor cells results in a deficient vascularization, with chaotic and leaky blood vessels that commonly fail to meet the needs of nutrients delivery, waste removal and gas exchange. All these factors have important consequences in the tumor microenvironment (TME) that make it display several differences compared to healthy tissue (Lyssiotis and Kimmelman, 2017) (Figure 1).

As oxygen delivery is directly dependent on the deficient vascular access, tumors usually present increasingly hypoxic areas towards their center, where the lack of oxygen and nutrients becomes fatal for cells and the deficient removal of their waste products leads to the formation of a necrotic core (Carmeliet and Jain, 2011; Chaplain, 1993). The resulting gas gradient modifies the metabolism of the tumor cells and creates a cooperative organization of the catabolism of carbohydrates: cells in hypoxic regions metabolize D-glucose incompletely by producing L-lactate, which in turn is used by cells in well-oxygenated areas in the final steps of respiration. This creates a decreasing gradient of L-lactate from the core to the vessels, which due to the acidic nature of this metabolite also entails a reduction of the pH towards the center of the tumor (Choi et al., 2013; Sonveaux et al., 2008).

The TME also presents differences in the availability of amino acids. Tryptophan is avidly consumed by tumor cells to generate several metabolites, especially kynurenine, with detrimental consequences to the activity of immune cells (Lyssiotis and Kimmelman, 2017; Mellor and Munn, 2008). Another amino acid commonly depleted in tumors is arginine, which is transformed by nitric oxide synthases, mainly the inducible nitric oxide synthase (iNOS/NOS2), to generate citrulline and nitric oxide (NO). Overexpression of NOS2 has been observed in more than 50% of gliomas, melanomas, breast, prostate, pancreatic, liver, cervical, colon, stomach and several other cancer patients (Cheng et al., 2014). NO is highly diffusible, but its concentration is only decreased near the blood vessel barriers, which favors its accumulation in the poorly irrigated tumor areas (Chen et al., 2007). Studies regarding the role of NO in the biology of tumors show complex and sometimes contradictory interactions depending of its concentration and the tumor stage, including stimulating cancer cell proliferation and metastasis but also cell cycle arrest and apoptosis, as well as metabolic and immune function regulation (Somasundaram et al., 2019). NO is also implicated in the high levels of oxidative stress suffered by tumor cells, which adapt by producing antioxidant metabolites such as glutathione, increasing their demand of its amino acid precursor, cysteine (Sullivan and Chandel, 2014). Tumors also have an increased production of reactive oxygen species (ROS), highly reactive radicals, ion and molecules with an unpaired electron that include the superoxide radical ($O_2^{\bullet-}$), organic radicals or hydrogen peroxide (H_2O_2), among many other examples (Liou and Storz, 2010). Hypoxia has been proven to stimulate the production of these substances in cancer cells, mainly by the mitochondria. ROS detoxifying mechanisms include the superoxide dismutase enzymes that catalyze their conversion into H_2O_2 and later into H_2O. As a result, increased levels of peroxide have been observed in cancer cell lines (Szatrowski and Nathan, 1991). In a similar manner

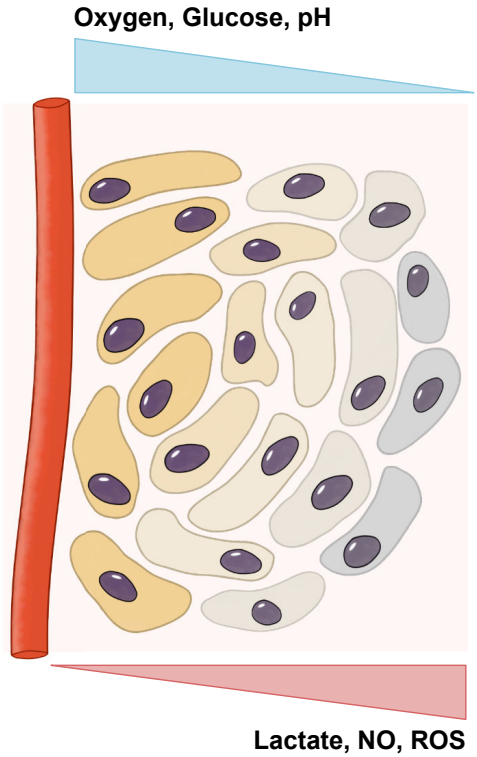

Figure 1. Metabolic and physicochemical gradients in tumors. Inside solid tumors, the pH, as well as the oxygen and glucose concentrations are higher near the blood vessels. Due to the chaotic vasculature and the high metabolic activity of cancer cells, tumor regions far from the vessels are subjected to hypoxic conditions, acidity and increased concentrations of L-lactate, nitric oxide (NO) and reactive oxygen species (ROS).

to NO, ROS species have a variety of effects in tumor cells depending on their concentration, from stimulating cell proliferation and angiogenesis to immunomodulation (Weinberg et al., 2019).

The differences between healthy tissue and the TME create conditions where anaerobic and facultative bacteria can thrive, resulting in a preferential growth inside tumors rather than other normal tissues (St. Jean et al., 2008). The faulty vasculature facilitate both the access of bacteria to the tumor from the blood vessels as well as their retention inside them (Maeda, 2013). Once inside, the active motility of bacteria allows them to reach the necrotic core, where the accumulated debris of dead cells are exploited as nutrients, creating a chemotactic signal that drives bacterial accumulation (Forbes, 2010; Kasinskas and Forbes, 2006; Lyssiotis and Kimmelman, 2017). The low oxygen concentration, the accumulation of metabolites such as L-lactate and NO, and immunosuppressive substances such as kynurenine hinder the immunologic functions inside the tumor. This immunosuppressive environment reduces the cytotoxic activity of Natural Killer (NK) and CD8+ T cells against the tumor (Bader et al., 2020; Liu et al., 2022) as well as the antibacterial activity of macrophages and neutrophils to eliminate bacteria (Westphal et al., 2008). Interestingly, many human tumors are found naturally

colonized with different bacteria (Nejman et al., 2020). These resident bacteria are an actual tumor microbiome that influences cancer treatments and progression (Fu et al., 2022; Geller et al., 2017).

3. Synthetic biology.

3.1. Designing microorganisms.

The improvements in molecular tools and genetic engineering techniques that arose during the last decades of the 20th century led to the development of synthetic biology, a scientific field that focuses on the application of engineering principles for the rational design of organisms equipped with new and predictable functions as well as modified to present specific characteristics. For this purpose, researchers combine different biological parts such as genes with the desired traits, but also genetic elements like promoters, terminators and transcription factors (TFs) that control how and when those genes are expressed, often creating intricate and complex genetic circuits to achieve a tight control of the transcription and translation. These components are deployed into an organism that will provide the elements to support their functioning, which is commonly referred in the field as the “chassis”. The selection of a chassis depends on the benefits presented by its natural traits to the intended application, but they can be also modified to reduce or eliminate any unnecessary or detrimental feature naturally present in them. In the last decades, researchers have created increasingly sophisticated biological machines, a process that started in the year 2000 with the creation of the toggle switch (Gardner et al., 2000) and the repressilator (Elowitz and Leibler, 2000), and has grown to the point where a method for standardizing biological parts is becoming a clear need in the field, which has led to the creation of initiatives such as the iGEM Registry of Standard Biological Parts (http://parts.igem.org), the Standard European Vector Architecture (SEVA) (Silva-Rocha et al., 2013) or the Synthetic Biology Open Language (Galdzicki et al., 2014).

3.2. Synthetic biology for engineering improved therapeutic bacteria.

Synthetic biology has become a powerful ally in the development of therapeutic bacteria. Several species have been modified to contain genetic modules that increase their safety and therapeutic potential or even transform them into biosensors for diagnostic applications. The selection of a bacterial chassis is mainly driven by two characteristics: the ease of genetic manipulation and the general safety of the species. Lactic acid bacteria such as *Lactococcus lactis* present a long history of use in human nutrition and has been widely engineered for both industrial and clinical applications (Landete, 2017;

Plavec and Berlec, 2020). Pathogenic strains of bacteria with a natural tropism for tumor tissue such as *Listeria monocytogenes* (Brockstedt et al., 2004; Wallecha et al., 2009) or *Salmonella typhimurium* (Curtiss and Kelly, 1987; Pawelek et al., 1997) have also been modified to reduce pathogenicity while maintaining anti-tumoral effects; however, extensive attenuation has been proved detrimental for therapeutic activity (Zhou et al., 2018). Several characteristics of *E. coli* present this microorganism as an ideal vector for cancer therapy. As a model organism, it has been widely studied, and its biological processes are better understood than those of other bacteria, moreover, its genetic manipulation is easy, including modification of its chromosome. Strains of *E. coli* include non-pathogenic human commensal strains with the capacity to colonize solid tumors such as the laboratory K-12 MG1655 strain or the probiotic *E. coli* Nissle 1917 (Danino et al., 2015; Loessner et al., 2009). *E. coli* Nissle 1917, commercialized as MUTAFLOR®, has been administered to humans for nearly 100 years to treat infections and intestinal inflammatory diseases (Fábrega et al., 2017; Sonnenborn, 2016). These characteristics have made *E. coli* an ideal microorganism for cancer therapy (Chien et al., 2017) and our laboratory's selected chassis for the development of synthetic biology modules that increase the therapeutic potential of the bacteria.

The anti-tumoral activity of bacteria can be enhanced by equipping them with different therapeutic molecules that can be delivered to malignant tissue. Such molecules include toxins, like hemolysin E from *E. coli* (Jiang et al., 2010; Ryan et al., 2009) or ADP-ribosilating toxins like exotoxin A from *Pseudomonas aeruginosa* (Leshem and Pastan, 2019; Zahaf et al., 2017); apoptosis inducing factors and cytotoxic cytokines such as FAS ligand or tumor necrosis factor alpha (Markus Loeffler et al., 2008; Theys et al., 1999); pro-drug converting enzymes like cytosine deaminase and the thymidine kinase from the herpes simplex virus (Lehouritis et al., 2013; Theys et al., 2001); immunomodulatory proteins such as interleukins 2 and 18 (al-Ramadi et al., 2009; M. Loeffler et al., 2008); agonists of the stimulator of interferon genes (Leventhal et al., 2020) or even small antibodies for inactivation of intracellular proteins (Böldicke, 2017; Van Audenhove and Gettemans, 2016). The delivery of these molecules has been approached through simple methods such as releasing them using membrane vesicles or fusing them to pore-forming cytolysins, but more complex strategies include the invasion of the target cell through the expression of *Yersinia'*s invasin (Critchley et al., 2004) and subsequent lysis of the phagosome through the listeriolysin O (Castagliuolo et al., 2005), or the use of the type III secretion system (T3SS), commonly found as a virulence factor of some pathogenic bacteria, to inject the therapeutic proteins directly into the cytoplasm of mammalian cells (Chabloz et al., 2020; Lim et al., 2020). This last

approach has been undertkaken in our laboratory by engineering a non-pathogenic *E. coli* K-12 with a functional T3SS capable of delivering small antibodies to target cells, named Synthetic Injector *E. coli* (SIEC) (Ruano-Gallego et al., 2015).

Engineered therapeutic bacteria are still living beings and need to be controlled for their safe application in patients. Biocontainment is also a fundamental issue, and the spread of modified bacteria to the environment must be prevented. Several strategies have been developed in this direction such as increasing the targeting of bacteria to the tumor to reduce the administered dosage (Piñero-Lambea et al., 2015), maintaining antibiotic sensitivity using toxin-antitoxin systems or implementing artificial auxotrophies for metabolites such as thymine, biotin or diaminopimelic acid (Isabella et al., 2018; Lee et al., 2018; Leventhal et al., 2020). Limiting the propagation of modified genetic material through horizontal gene transfer is also important and for this reason therapeutic bacteria should be free of mobile elements such as transposons and plasmids. Chromosomal integration of the modified genetic elements is the preferable choice as it does not require antibiotic use to maintain them, reduces the possibility of their propagation, and contributes to their genetic stability (Lee et al., 2018).

3.3. *In vivo* control of the expression of therapeutic proteins and delivery systems.

An important issue when engineering bacteria to treat tumors is assuring that the therapeutic proteins, especially cytotoxins, are expressed and delivered exclusively to the malignant cells, as their uncontrolled activity could harm healthy tissue. A common approach is the use of inducible promoters to activate the expression of both therapeutic proteins and their delivery systems only when a small molecule, the inducer, is added. However, traditional expression systems widely used in laboratory conditions such as the P_{tac} promoter present problems such as the low half-life and toxicity of its inducer, isopropyl β-D-1-thiogalactopyranoside (IPTG), as well as the leakiness of this promoter (Dvorak et al., 2015; Kosinski et al., 1992; Wyborski and Short, 1991). Other promoters successfully used *in vivo* include P_{tet}, induced by tetracycline derivatives such as anhydrotetracycline (aTc) (Bertram and Hillen, 2008), P_{BAD}, induced by arabinose (Loessner et al., 2007), or P_m, induced by acetyl salicylic acid (Royo et al., 2007). Alternative approaches include inducing the activation of the promoters through physical means, such as directed γ-radiation to trigger the SOS response (Nuyts et al., 2001) or increasing the temperature through ultrasounds, activating the P_L/P_R phage lambda thermally inducible promoters (Abedi et al., 2022). Quorum sensing has also been

employed to initiate the therapeutic activity when the population of bacteria reaches a high-enough density in the tumor (Anderson et al., 2006; Din et al., 2016; Prindle et al., 2012).

However, when aiming to restrict the therapeutic activity to the tumor microenvironment, the ideal situation would be for bacteria to activate any treatment exclusively when they are inside the tumor itself. With this objective, many groups have placed their genetic devices under control of signals belonging to the tumor microenvironment. The hypoxic conditions of the tumor core have been used to induce promoters regulated by the fumarate and nitrate reductase (FNR) TF (Deyneko et al., 2016; Lara et al., 2017; Leventhal et al., 2020; Mengesha et al., 2006; Yu et al., 2012). The increased concentration of lactic acid in the deeper parts of the tumor can be employed as an induction signal for genes under control of the P_{lldP} promoter, and due to the consequent decrease in pH due to accumulation of this molecule, for genes under control of the acid-activated P_{cadC} promoter (Chien et al., 2021). In an inverse approach, the depletion of glucose towards the core can also be used as a signal (Panteli and Forbes, 2016). While most of the bacterial biosensors for NO have been developed for gut inflammation, their capacity to detect this metabolite could be repurposed for tumor therapies (Archer et al., 2012; McKay et al., 2018; Riglar et al., 2017). To further increase the specificity of bacterial therapies, some authors have created complex circuits that integrate several of these tumor signals using Boolean logic gates that compute them and produce one or more responses based on the received inputs, thereby conditioning any treatment to the simultaneous presence of several of the tumor conditions (Chien et al., 2021; Riglar et al., 2017; Rubens et al., 2016). Some of these genetic circuits relay in the use of recombinases that trigger permanent and heritable changes in the DNA of the engineered bacteria, which can also generate genetic memory and a sustained response through time (Abedi et al., 2022; Archer et al., 2012; Rubens et al., 2016).

One of the aims of this work is the characterization of tumor-sensing promoters in the context of our non-pathogenic *E. coli* chassis derived from the commensal K-12 MG1655 strain (Blattner et al., 1997). For increased biocontainment, and to avoid the need for antibiotics, the promoters will be tested while integrated in the bacterial chromosome. We will also test the feasibility of using those promoters to control the expression of site-specific recombinases, serine integrases, for the creation of chromosome-integrated genetic logic gates that compute different signals into a determined signal and generate genetic memory (Figure 2).

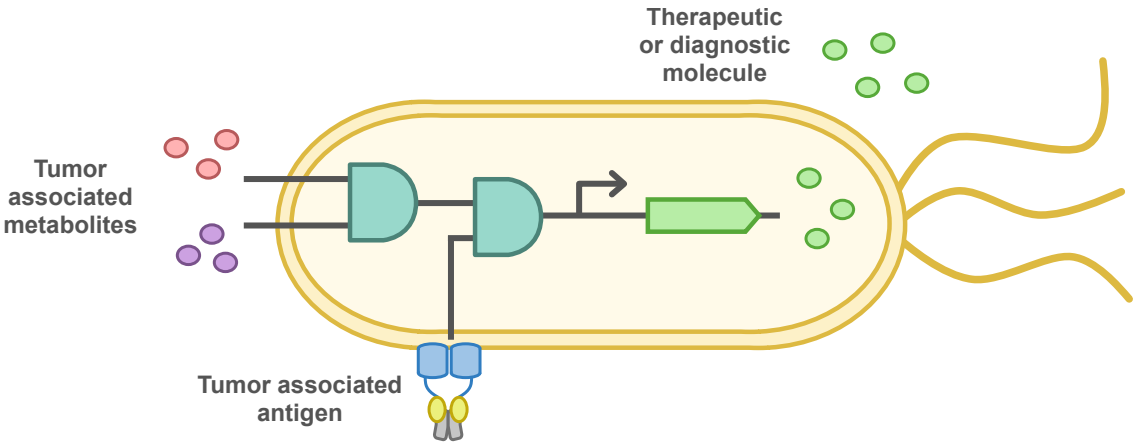

Figure 2. Conceptual genetic circuit for a bacterium that triggers expression of a therapeutic or diagnostic cargo in the tumor microenvironment. The presence of tumor-associated metabolites activate the first AND gate, whose signal, together with the one generated by the presence of a tumor-associated antigen, activate a second AND gate, triggering the gene expression of a therapeutic or diagnostic cargo.

4. Site-specific recombination: the serine integrases and their applications.

Site-specific recombination is the term that encompasses several specialized recombination processes that perform mutual exchange of DNA between specific sites without the requirement for DNA synthesis or high-energy nucleotides. Examples of this type of recombination can be found in the integration of the bacteriophage λ of *E. coli*, the transposition of Tn3-related transposons or the DNA modifications that activate the phase-variation switching in *E. coli* and *Salmonella* (Craig NL et al., 2002; Klemm, 1986). The outcome of this kind of recombination depends on the initial configuration of the recognized DNA sites, with a highly directional sensitivity. If the specific sites reside in different molecules, and at least one of them is circular, an integration event occurs. When both sites are present in the same molecule, their relative orientation determines the result: if both sites have the same orientation, the sequence between them suffers an excision, alternatively, if they are inversely oriented, the sequence is inverted (Figure 3). Site-specific recombinases are proteins capable of recognizing these specific sites and catalyze the breaking and rejoining of the DNA with conservation of the phosphodiester bond energy. DNA strands are not cleaved by hydrolysis, but by a phosphoryl transfer to the side chain of a residue in the recombinase. The two possible residues distinguish the two different families: tyrosine recombinases and serine recombinases (Grindley et al., 2006).

Serine integrases, as a subfamily of serine recombinases, present some mechanistic differences to tyrosine recombinases that include the formation of a double strand break

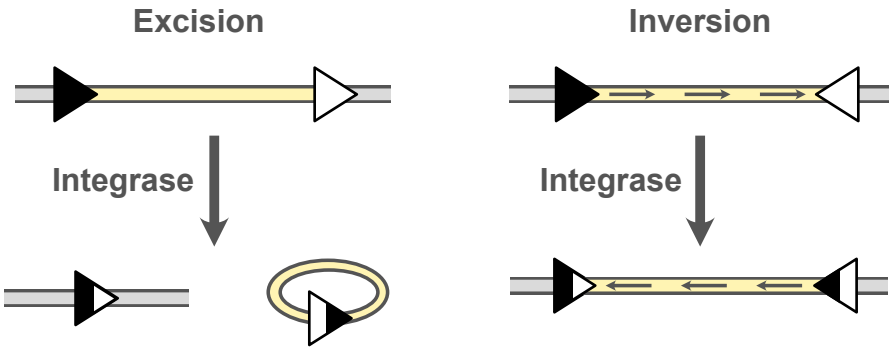

Figure 3. Examples of DNA rearrangement by excision and inversion mediated by serine integrases. The initial *attB* and *attR* sites are represented by full black or white triangles, while the resulting *attL* and *attR* sites are marked as half black-half white triangles. In excision (left) the serine integrase cleaves the sequence situated between the *att* sites with the same orientation. In inversion (right) the sequence between the inversely oriented *att* sites is inverted by the serine integrase.

of the DNA prior to the religation. The use of serine integrases as a genetic engineering tool offers several advantages over tyrosine recombinases. These include the absence of the need for cofactors and the small size of the recognized DNA sequences, which are often less than 50 base pairs. Since the original purpose of these enzymes is the integration of phages in the chromosome of bacteria, the initial sequences of the recognized sites are termed *attP* (phage) and *attB* (bacteria) attachment sites, whose sequence is distinct from the resulting *attL* (left) and *attR* (right) sites that arise after the recombination (Merrick et al., 2018). The various possible configurations of attachment sites enable the insertion, excision, and inversion of sequences. As a result, these sites have been widely utilized for the insertion and replacement of sequences in the chromosomes of both eukaryotic and prokaryotic cells (Andreas et al., 2002; Karow et al., 2011; Kuhstoss et al., 1991); and the assembly of linear DNA (Colloms et al., 2014; Zhang et al., 2011).

One of the most interesting applications of serine integrases resides in their implementation in the development of genetic circuits that allow biological systems to record stimulus in a permanent manner, creating genetic memory. These genetic devices can also be designed to behave as genetic logic circuits that utilize the serine integrases to compute multiple signals into different outputs. While alternative methods exist for achieving memory and computation (Bonnet et al., 2012; Manzoni et al., 2016), memory and logic circuits based on serine integrases have important advantages, reacting to inputs by creating a permanent and heritable modification of DNA with just a single activation of the integrase expression, with a reduced consumption of cellular resources (Merrick et al., 2018). Genetic circuits executing all the different Boolean logic

gates have been developed by rearranging the sequence of promoters, terminators and reporter genes using multiple and orthogonal serine integrases such as Bxb1, Tp901 or phiC31 by controlling their expression with different inducers (Bonnet et al., 2013; Siuti et al., 2013). These circuits have shown promising results for medical applications in the analysis of clinical samples by whole-cell biosensors (Courbet et al., 2015). The discovery of new integrases have increased the amount of information than can be stored by these genetics devices (Yang et al., 2014). The overlapping of attachments sites for different integrases have also allowed the creation of systems capable of permanently recording the temporal order of the inputs (Ham et al., 2008; Zúñiga et al., 2020). All these advancements present serine integrases as valuable tools in the development of biosensors with the capacity to maintain a programmed response once the specific combination of signals has been detected.

5. Nanobodies, surface display in *E. coli* and synthetic adhesins.

Previous work in our laboratory showed that it was possible to display small single domain antibodies, called nanobodies (Nbs), on the surface of *E. coli* by their fusion with the outer membrane-anchored β-barrel domains of proteins belonging to the type V secretion system (T5SS) (Marin et al., 2010; Salema et al., 2013). Nbs are formed by the recombinant expression of the variable heavy chain region (VHH) of the heavy-chain only antibodies (HCAbs) found in the *Camelidae* (e.g., dromedaries, llamas, alpacas) (Figure 4). Contrary to conventional antibodies, camelid HCAbs lack a light (L) chain and are able to bind the antigen with a single VHH domain (Muyldermans, 2013). The small size of Nbs (~15 kDa) and their longer complementarity determining regions (CDRs) allow them to access cryptic epitopes of the antigens that are non-accessible by conventional antibodies with VH and VL domains. Despite their simplicity, Nbs maintain high affinity and specificity for their antigen, are generally monomeric and have high solubility and protein stability. These properties, along with their similarity to human sequences and low immunogenicity, explain their interest in human therapy and other applications (Arezumand et al., 2017; Harmsen and De Haard, 2007; Muyldermans, 2013).

In the work of Salema et al., 2013, Nbs were fused to the β-barrel domains of EhaA and intimin proteins from enterohaemorrhagic *E. coli* (EHEC). These chimeric proteins were able to display functional, antigen-binding Nbs on the surface of *E. coli*, facilitating the selection of high-affinity Nbs from immune VHH libraries (Figure 5). Among the two display systems utilized, fusions to the EHEC intimin N-terminal fragment, termed Neae

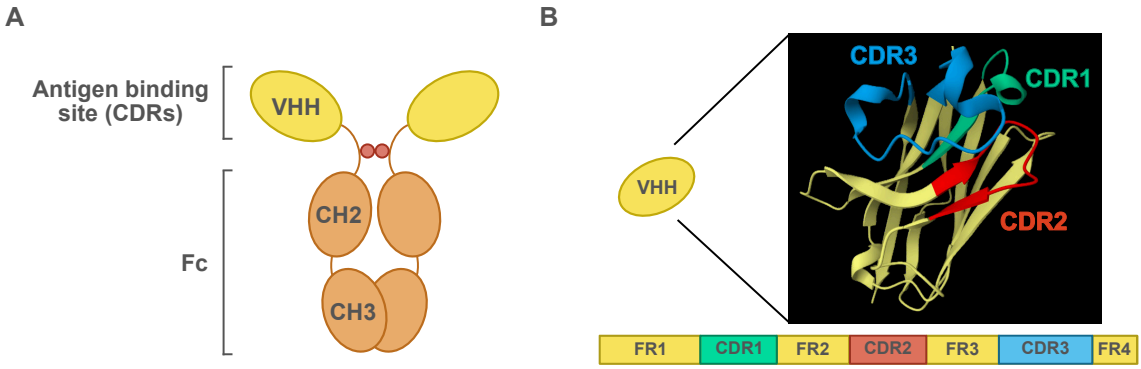

Figure 4. Heavy-chain only antibodies and nanobodies. (A) Schematic representation of the structure of camelid heavy-chain only antibodies (HCAbs). A single variable domain, termed VHH or nanobody, when expressed as recombinant protein, provides the antigen-binding capabilities. **(B)** 3D structure of a VHH/nanobody. AlphaFold predicted structure of the VEGFR2 Nb (Salema et al., 2016b) used in this work. Framework regions (FR) are colored yellow while complementarity determining regions (CDRs) are marked with different colors (CDR1, green, CDR2, red, CDR3, blue). A linear diagram using the same colors can be found at the bottom.

(residues 1-654), which contains the β-barrel domain that inserts in the bacterial outer membrane (OM), presented higher stability, expression, surface display levels and antigen-binding capabilities. This intimin *E. coli* display system (Salema and Fernández, 2017) has been employed in our laboratory for the screening of immune libraries of VHHs to select high-affinity Nbs binding the human fibrinogen (Salema et al., 2016a), the human epidermal growth factor receptor (EGFR) (Salema et al., 2016b), which is expressed on the surface of epithelial tumor cells, the translocated intimin receptor (Tir) of EHEC (Ruano-Gallego et al., 2019; Salema et al., 2013) and the receptor binding domain (RBD) of the Spike protein of SARS-CoV-2 (Casasnovas et al., 2022).

The display of Nbs with intimin showed an even greater potential when our laboratory demonstrated that these fusions can modify the adhesion properties of *E. coli* for the specific attachment of bacteria to abiotic surfaces, cells and tumors expressing a target antigen recognized by the Nb (Piñero-Lambea et al., 2015). Thus, the intimin-Nb fusion constituted a synthetic adhesion module, called synthetic adhesin (SA), when expressed by the engineered bacteria. Gene cassettes containing a strong constitutive promoter driving expression of the intimin-Nb fusion were stably integrated into the chromosome of an *E. coli* K-12 chassis strain engineered to reduce non-specific attachment to cells and abiotic surfaces by deletion of the genes encoding for type I fimbriae (*fim*) (Lillington et al., 2014), the *E. coli* common fimbriae (*ecp*/*mat*) (Lehti et al., 2010) and the antigen 43 (*flu*) adhesin (van der Woude and Henderson, 2008). The engineered strain expressing SAs with Nbs binding a model antigen (GFP) was able to bind specifically

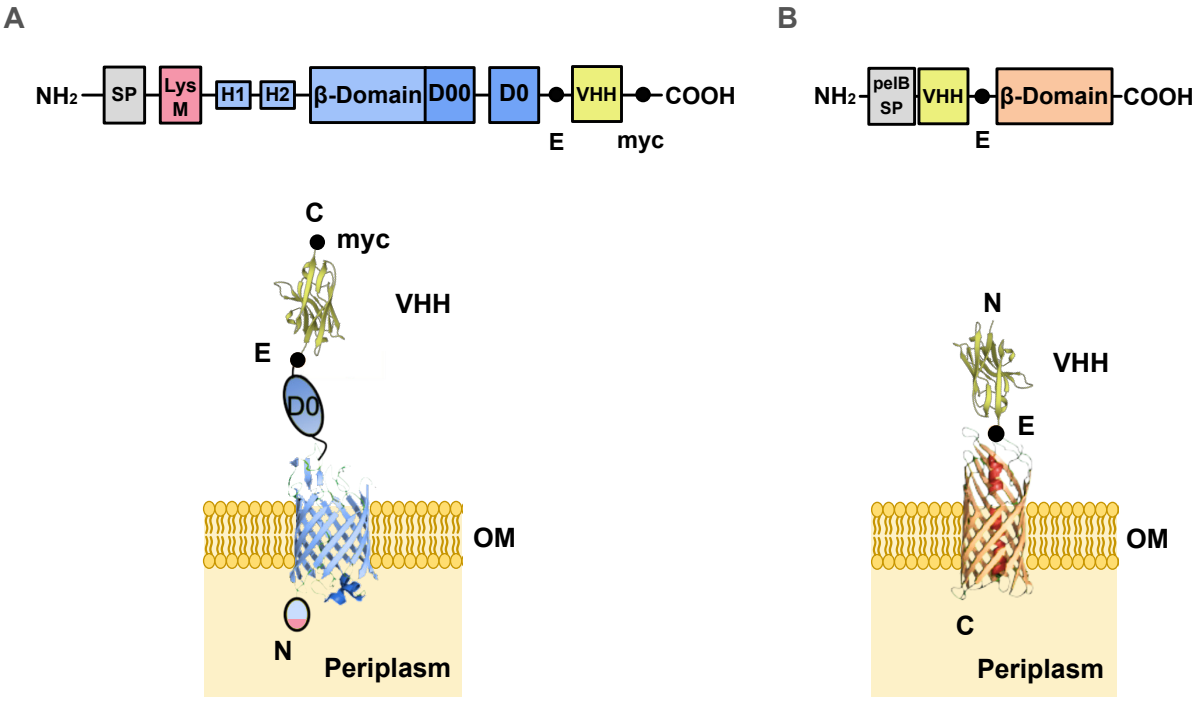

Figure 5. Nanobody surface display systems in *E. coli* based on fusion to intimin and EhaA. Display systems based on fusions to (**A**) intimin and **(B)** EhaA β-domains**.** Up**,** schematic representation of the chimeric proteins used for the Nb display systems. Size is not proportional to maintain visual clarity. SP = Signal peptide, H = helix, D = Ig-like domain, E = E-tag, myc = c-myc-tag. Down, model of the chimeric proteins in the outer membrane, modified from Salema et al., 2013.

and in high numbers to HeLa cells transfected to express GFP anchored in the plasma membrane. Moreover, when administered to athymic Nude mice bearing a subcutaneous tumor xenograft model of the same transfected HeLa-GFP cells, the bacteria were able to colonize and proliferate in the tumors even when a low bacterial dose of 10^5 CFU were administered systemically to the mice. In the absence of the SA binding GFP, a much higher bacterial dose (10^7 CFU) was needed to achieve a similar colonization level (Piñero-Lambea et al., 2015).

6. The Type V Secretion System.

6.1. Autotransporters, the Type V Secretion System.

Bacteria require the secretion of different proteins in order to accomplish a wide variety of functions such as nutrient transport, communication, adhesion or infection. In the case of gram-negative bacteria, secreted proteins must traverse two different membranes and the periplasm, and for this purpose they have evolved several mechanisms termed secretion systems. Due to their great diversity, the different secretion systems have been classified into different categories, from type I through type IX, which distinguish

mechanisms that go from single proteins to complex nanomachines formed by dozens of proteins that span the two membranes (Green and Mecsas, 2016).

From all these categories, the T5SS is one of the smallest, being exclusively situated in the OM and with only one to three polypeptides involved in the secretion process. The periplasm lacks chemical energy such as ATP and no stable ion gradients are present in the OM, resulting in no evident energy sources for the secretion. This leads to the consideration of a self-sufficient method for secretion, earning the proteins of the T5SS the name of "Autotransporters" (ATs) (Henderson et al., 2004; Klauser et al., 1993; Leo et al., 2012). However, it is currently accepted that ATs utilize different conserved secretion machineries of the bacterial cell for their translocation (Bernstein, 2007; Leyton et al., 2012). The variability of ATs has also generated a second classification, from type Va through type Ve, based in their different topologies and characteristics (Grijpstra et al., 2013) (Figure 6). Regardless of their type, all ATs share two main regions, an OM-anchored β-barrel, referred as β-domain, which is situated in the C-terminal except for the Ve type, and the secreted domain, also known as passenger or α-domain, which is situated in the N-terminal except for Ve type. Some ATs contain additional features such as autochaperone regions (AC) that help in the folding of the passenger (Drobnak et al., 2015; Meuskens et al., 2019). Except for the type Vb ATs, which are formed by two

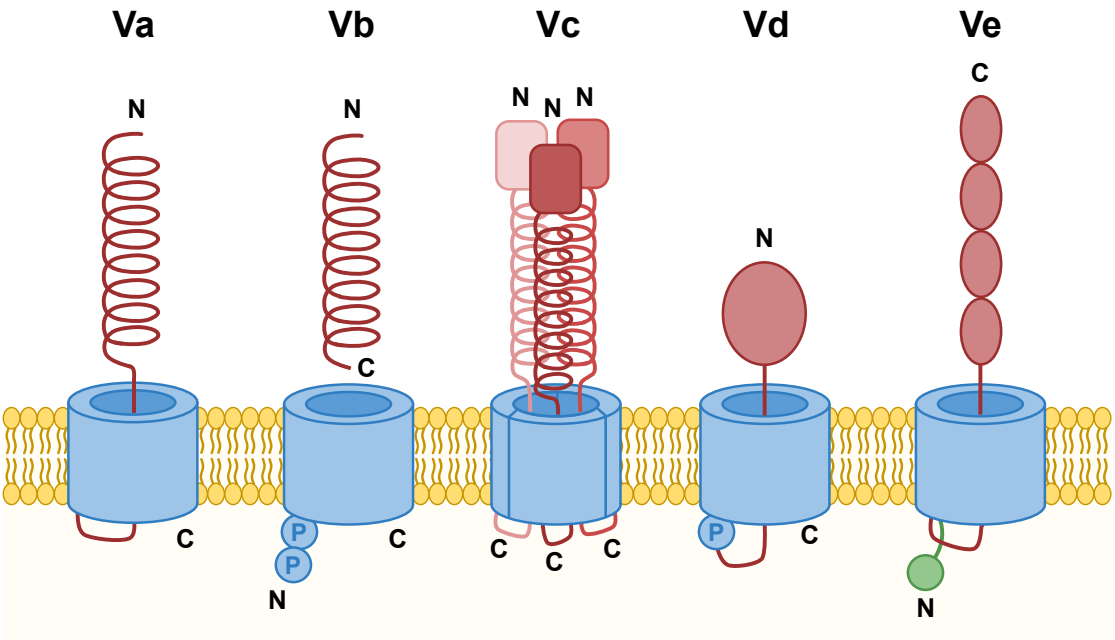

Figure 6. The different T5SS types. Cartoon representation of the topology of the different T5SS types from Va to Ve, indicating N and C terminal ends, β-barrels (blue) and POTRA domains (labelled P). Secreted passenger domains are also labelled in red. Different shades of red are used for the trimeric components of the Vc type. The periplasmic domain of the Ve type (intimins) is colored in green.

different polypeptide chains, all ATs are encoded by a single protein (Guérin et al., 2017). Among all T5SS, we will describe in the following section the major group, the type Va or classical ATs, and the type Ve, or inverse ATs, given their importance for this PhD thesis.

6.2 The structure and function of classical and inverse autotransporters.

The type Va or classical ATs include many important adhesins and virulence proteins in *E. coli* and other gram-negative bacteria (Henderson et al., 2004), such as the adhesins AIDA-I (Laarmann and Schmidt, 2003), EhaA (Wells et al., 2008), the auto-agglutination factor Ag43 (Sherlock et al., 2006) and the serine protease EspP (Roman-Hernandez et al., 2014). The β-barrel of these proteins is located in the C-terminal end and is formed by 12 amphipathic β-strands with an internal central hydrophilic pore of approximately 12 Å in diameter that is filled by an α-helix that connects with the N-terminal passenger domain (Gawarzewski et al., 2013; Oomen et al., 2004). The crystal structures of the β-barrels of classical ATs revealed that these proteins are mostly monomers (Barnard et al., 2007; Oomen et al., 2004; van den Berg, 2010). However, some ATs show different oligomerization states (Marin et al., 2010; Veiga et al., 2002). The secreted passenger domains of these proteins, which follow immediately after the N-terminal signal peptide (SP), are responsible for their biological function and typically fold into a repetitive β-helix fold, although other conformations are possible (Meuskens et al., 2019; van Ulsen et al., 2014). Most passenger domains, such as the ones in AIDA-I and EspP, are cleaved from the β-domain after secretion (Khan et al., 2011; Meuskens et al., 2019; Suhr et al., 1996).

Type Ve receive the name of inverse ATs due to the configuration of their domains being the opposite to the rest of ATs, placing the OM-anchored β-domain in the N-terminal region of the polypeptide, and the secreted passenger domain in the C-terminal region (Heinz et al., 2016; Leo et al., 2015b). The Ve β-barrels are similar to the Va ones, with 12 amphipathic β-strands and a central narrow pore that is filled with a segment of the polypeptide chain connecting with the C-terminal passenger domains (Fairman et al., 2012; Tsai et al., 2010). At least in the case of intimin, the β-barrels form stable dimers in the OM (Touzé et al., 2003). Important examples of the inverse ATs include the intimins from EHEC and other enteropathogenic *E. coli* (EPEC) strains and the invasins from *Yersinia* spp (Leo et al., 2015b), but many other examples are found in the genomes of gram-negative bacteria (Goh et al., 2019; Heinz et al., 2016). Intimin proteins are adhesins that promote the intimate attachment of these bacteria to the enterocyte during

infection by binding and clustering of the Tir, triggering polymerization of actin-rich pedestals underneath the attached bacterium (Leo et al., 2015b; Luo et al., 2000; Marchès et al., 2000; McKee et al., 1995). Invasins are protein found in the enteropathogenic *Yersinia* species, such as *Y. enterocolitica* and *Y. pseudotuberculosis*, which play a fundamental role in the early invasion of cells by adhering to the β_1 integrins in their apical surface. The binding of invasin triggers cytoskeletal rearrangements that internalize the bacteria through a zipper mechanism (Isberg et al., 1987; Isberg and Leong, 1990; Leo et al., 2015b; Leo and Skurnik, 2011; Palumbo and Wang, 2006).

Intimins and invasins share high similarity in their topology, with an N-terminal SP followed by a short periplasmic domain formed by two α-helices that continue into the β-barrel. Intimins, but not invasins, frequently contain an additional periplasmic domain after the SP called LysM. LysM contains a lysin motif that has been shown to bind to the peptidoglycan (PG) at low pH (<6). In addition, the LysM linker region together with the second periplasmic α-helix can participate in the dimerization of intimin (Leo et al., 2015a). After the β-barrel, the C-terminal passenger of intimins and invasins is constituted by several repeats of immunoglobulin (Ig)-like domains capped by a C-type lectin domain, the domain responsible of the receptor recognition. In intimin, four Ig-like domains (D00-D0-D1-D2) precede the C-lectin domain (Luo et al., 2000; Weikum et al., 2020). The passenger domain of invasin presents five Ig-like domains (D00-D1-D2-D3-D4) followed by the C-lectin domain, although the D00 domain has not been yet proven experimentally and it is only predicted from its sequence. While invasin from *Y. pseudotuberculosis* is reported to form dimers, invasin from *Y. enterocolitica* is monomeric. The reason for this difference has been attributed to the D2 domain of the passenger of *Y. pseudotuberculosis*, which seems to promote self-association (Chauhan et al., 2016; Dersch and Isberg, 2000; Hamburger et al., 1999).

6.3. Biogenesis of autotransporters.

From their translation in the cytosol to their insertion in the OM, all ATs must cross the inner membrane (IM) and the periplasm in a secretion-competent state. An N-terminal SP (Hegde and Bernstein, 2006) directs the nascent AT polypeptides in the cytosol to the general Sec-translocon of the IM, which translocate these polypeptides through the IM in a fully unfolded state (Tsirigotaki et al., 2017). Once in the periplasm, to prevent both folding and aggregation the ATs are assisted by periplasmic chaperones such as SurA, Skp and DegP (Pavlova et al., 2013; Weirich et al., 2017). Insertion in the OM of the β-barrel is carried out by the β-barrel assembly machinery (BAM) complex (Hagan et

al., 2011; Noinaj et al., 2017, 2013). In *E. coli* the BAM complex is formed by five proteins that include the main catalyst of the insertion, BamA (previously Omp85), which is an essential protein in *E. coli*, and four associated lipoproteins, BamBCDE. There is evidence that BamA participates in insertion of classical and inverse ATs in the OM (Bodelon et al., 2009; Doyle and Bernstein, 2021; Ieva and Bernstein, 2009). BamA is composed of an OM inserted β-barrel and five periplasmic polypeptide-transport-associated (POTRA) domains, while the four lipoproteins remain anchored to the inner side of the same membrane (Sklar et al., 2007; Tomasek et al., 2020; Wu et al., 2005). Although the process of catalyzing the folding and insertion in the OM of β-barrels by the BAM complex is not yet entirely understood, two models have been proposed. In the "assisted" model BamA helps the insertion of partially folded outer membrane proteins (OMPs) by destabilizing and thinning the OM, creating a favorably insertion point in terms of energy. However, recent evidence seems to reinforce an alternative "budding" model. This model proposes a progressive process where the weak interaction of the first and last β-strands of the BamA β-barrel create a lateral gate. Unfolded OMPs carry a "signature sequence" comprised of hydrophobic and aromatic residues in the final β-strand of their barrel which is recognized by the BAM machinery (Konovalova et al., 2017; Robert et al., 2006). This signature sequence is aligned to the first strand of the gate creating a nascent β-barrel that nucleates the folding of the subsequent strands until the barrel is complete and released into the membrane (Noinaj et al., 2017; Wu et al., 2020; Xiao et al., 2021). ATs use the BAM-complex for both insertion of the β-domain in the OM and simultaneous secretion of the passenger domains (Doyle and Bernstein, 2021). In some cases, additional BamA-like proteins seem to play an active role assisting BamA during AT secretion, like the translocation and assembly module protein TamA (Babu et al., 2018; Bamert et al., 2017; Gruss et al., 2013).

As there is no chemical energy (e.g., ATP) or ion gradients in the periplasm, the secretion of the passenger domains might be the result of the intrinsic folding capacity of the ATs that is able to drive the export directly. Alternatively, the process could be driven by the inability of the passenger to go back once folded outside the cell. Due to their topological differences, there should be variations in the mechanisms of transport and secretion of the passenger across the different AT types. In the translocation of Va ATs, the passenger forms a hairpin-loop in its C-terminus inside the β-barrel and later releases itself folded outside the cell, subsequently followed in sequential order by the rest of the passenger (Junker et al., 2006; Peterson et al., 2010). An analogous process occurs for Ve ATs, although due to their inverse topology the hairpin-loop is formed by the N-

terminus and starts the secretion driven by the sequential folding of the Ig-like domains (Leo et al., 2016; Oberhettinger et al., 2015, 2012). However, despite the fact that the final folding of the passenger can be acquired upon translocation, strong evidence also supports that partial folding of both natural and heterologous passenger domains of ATs with disulfide bonds (e.g. Nbs) occurs in the periplasm prior to secretion (Skillman et al., 2005; Veiga et al., 2004).

7. Surface dynamics of outer membrane proteins.

Once inserted by the BAM machinery, OMPs may face two different possibilities: they could diffuse freely along the bacterial surface or, on the contrary, they could find their movement confined to their immediate surroundings or even completely restricted. Although specific studies regarding the fate of inserted ATs are missing, several groups have investigated the dynamics of OMPs in general.

Studies using confocal microscopes to perform fluorescence recovery after photobleaching (FRAP) (Pucadyil and Chattopadhyay, 2006) resulted in the conclusion that OMP are not mobile, at least on the long-range (Rassam et al., 2015). This conclusion was also valid for OmpA when its PG-binding domain was removed, discarding the attachment to this component as the cause (Verhoeven et al., 2013). Several other cellular components and forces such as TonB, porins or even the proton motive force were also proven to not be hindering the diffusion of OMPs (Rassam et al., 2015). Nevertheless, researchers using total internal reflection fluorescence (TIRF) microscopes to perform single particle tracking found that OMPs are actually able to diffuse, but in a very limited space. OMPs LamB, BtuB and OmpF were shown to follow a Brownian movement pattern for diffusion on short timescales, while presenting a confined behavior on longer ones (Gibbs et al., 2004; Oddershede et al., 2002; Rothenberg et al., 2011; Spector et al., 2010). This lack of free movement seems to agree with the differences in diffusion for the IM and the OM, with the latter showing a slower diffusion coefficient (Kleanthous et al., 2015; Ritchie et al., 2013). OMP have also been shown to be heterogeneously distributed through the bacterial surface, clustering in what have been called “OMP islands” of small size (~150 nm). These islands form around the BAM machinery situated near the mid-cell and move to the poles as bacteria grow, with an uniform distribution on the surface (8-10 per μm^2) (Mamou et al., 2022). Some studies point to promiscuous homologous and heterologous interactions between the β-barrels of the OMPs as the force keeping the islands tightly packed (Kleanthous et al., 2015; Rassam et al., 2015; Ursell et al., 2012). Interestingly, it has been recently

shown that the BAM machinery is regulated by the biosynthesis of PG (Mamou et al., 2022). The mature, tetrapeptide-rich PG is able to bind the BAM complex, blocking the folding of OMPs, while the new, pentapeptide-rich PG is not able to efficiently bind the BAM components, allowing its correct functioning. The different distribution of these types of PG, with the new one mainly found near the septa, controls the biosynthesis of OMPs, with reduced activity in the long axis of cells and little or no OMP insertion in the bacterial poles.

8. Chimeric receptors for detection of extracellular antigens and small molecules.

We have discussed how technology from our laboratory allows us to direct the specific adhesion of non-pathogenic *E. coli* strains to the surface of tumor cells, increasing the colonization of solid tumors where they could perform therapeutic and diagnostic tasks. It is known that bacteria alter their gene expression profile upon binding to surfaces, however, those changes are not specific to the recognition of a target cell or surface antigen and mostly detect changes in physicochemical conditions and mechanical stress (Kimkes and Heinemann, 2020). It would be very useful to connect the specific bacterial adhesion mediated by the synthetic adhesins to the tumor antigens with the triggering of a specific response in the bacterium (e.g., expression of a therapeutic cargo or diagnostic reporter). Such an antigen-binding biosensor system would increase the safety and specificity of the engineered synthetic bacterium by limiting its activity to the specific recognition of the target. The following response could be direct or integrated into a genetic circuit that would compute it together with other environmental signals for further discrimination. This approach has been previously explored only in mammalian cells, with the development of Chimeric Antigen Receptors T (CAR-T) cells. CAR-T cells are modified lymphocytes that display in their membrane a chimeric protein receptor comprising an antigen-binding domain, typically a single-chain variable fragment (scFv) or a Nb, connected to a transmembrane domain and a cytoplasmic signaling domain derived from natural T-cell receptors. These chimeric fusion proteins have been shown to detect binding to both membrane-bound and soluble antigens and initiate a signaling cascade that activates cytokine production, T-cell proliferation, and tumor-cell clearance (Z. L. Chang et al., 2018; Kalos et al., 2011). CAR-T signaling has increased in complexity through the different generations of these receptors, which were originally based on phosphatidylinositol and tyrosine kinase pathways (Sadelain et al., 2013). With similar principles, other antibody-based chimeric sensors have also been developed for

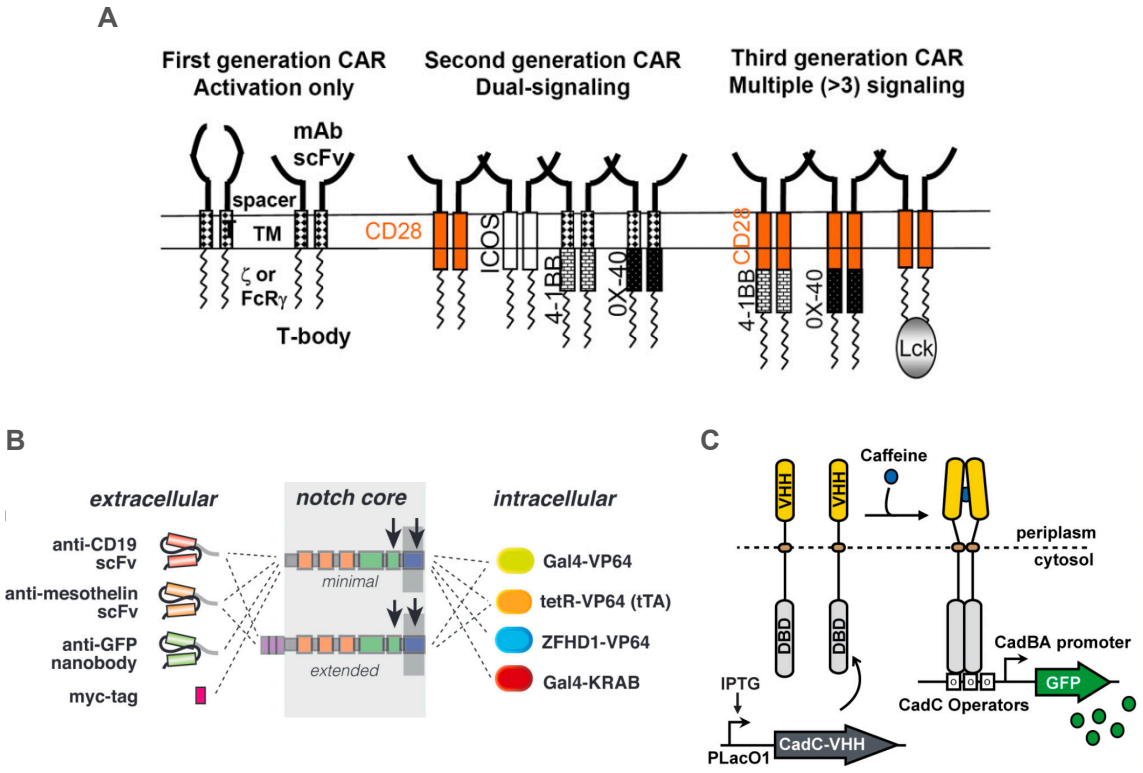

Figure 7. Examples of antibody-based synthetic membrane receptors. (**A**) Different CAR-T generations (Sadelain et al., 2013). (**B**) Examples of synthetic notch receptors (Morsut et al., 2016). (**C**) Synthetic inner membrane-bound caffeine receptor in *E. coli* (H.-J. Chang et al., 2018)

mammalian cells, in which release of a TF is triggered by proteolysis upon antigen binding. Examples include sensors based on Notch receptors, which naturally undergo proteolysis as a signaling response (Morsut et al., 2016), but also synthetic receptors pairs in which the members are connected to either a protease or a cleavable TF (Daringer et al., 2014; Schwarz et al., 2017). In this last example, binding to the cognate antigen forces dimerization between the two chimeric proteins, which allows the protease to release the TF into the cytoplasm.

To date, the development of an analogous extracellular antigen-sensing system for bacteria has not been reported. Gram-negative bacteria, in particular, pose a challenge for this specific design as the receptor signal must traverse through the periplasm and the IM to trigger transcription activation. In fact, two-component systems, which represent one of the main pathways of signal transduction in bacteria, are usually formed by a cytoplasmic response regulator activated by an inner membrane-bound histidine kinase receptor. While this design allows for the transduction of extra-cytoplasmic signals through the inner membrane, it limits the detection to small ligands that are able to access the periplasm (Hall et al., 2012; Zschiedrich et al., 2016). For this limitation, bacterial receptors based on two-components systems have been only used for

detection of small molecules (Lehning et al., 2017) and metabolites (Zúñiga et al., 2022). Interestingly, a modular chimeric IM sensor for *E. coli* has been reported based on the one-component IM protein CadC linked to a Nb binding caffeine in the periplasmic side (H.-J. Chang et al., 2018). In this sensor, the dimerization of the cytoplasmic DNA-binding domain of CadC (Schlundt et al., 2017) activate transcription of a target promoter having CadC DNA-binding sites, which can be coupled to expression of a reporter gene for detection.

Therefore, one of the objectives of this PhD thesis is to engineer in *E. coli* bacteria the ability to detect the presence of extracellular tumor associated-protein antigens, wether they are soluble or associated to the surface of the tumor cells.

OBJECTIVES

Objectives

1. To identify inducible promoters of *E. coli* that could respond to tumor associated metabolites and characterize their activity while integrated in the chromosome.

2. To evaluate the capacity of serine integrases for the development of genetic logic and memory circuits when both the integrases and their targets are integrated in the chromosome of *E. coli*.

3. To engineer chimeric T5SS proteins that simultaneously display nanobodies on the bacterial surface and peptides or enzyme fragments in the periplasm.

4. To test the capacity of the chimeric T5SS proteins as outer membrane sensors producing a quantifiable output signal when the specific antigen is present.

Objetivos

1. Identificar promotores inducibles de *E. coli* que respondan a metabolitos asociados a tumores y caracterizar su actividad estando integrados en el cromosoma.

2. Evaluar la capacidad de las serin-integrasas para desarrollar circuitos genéticos lógicos y de memoria cuando tanto las integrasas como sus secuencias diana se encuentran integradas en el cromosoma de *E. coli.*

3. Diseñar y construir proteínas del T5SS quiméricas que presenten simultáneamente nanoanticuerpos en la superficie bacteriana y péptidos o fragmentos de enzimas en el periplasma.

4. Examinar la capacidad de las proteínas del T5SS quiméricas para funcionar como sensores de membrana externa, produciendo una señal cuantificable cuando el antígeno específico está presente.

MATERIALS AND METHODS

1. Bacterial strains and growth conditions.

E. coli strains used in this work can be found in Table 1. Bacteria were grown in Lysogeny Broth (LB) liquid medium or LB-agar plates (1.5% w/v) at 37 ºC, unless otherwise specified. Antibiotics and inducers were added to the media at the following concentrations: kanamycin (Km) at 50 µg/mL, chloramphenicol (Cm) at 30 µg/mL, ampicillin (Amp) at 150 µg/mL, anhydrotetracycline (aTc) at 200 ng/mL, isopropyl-ß-D-thiogalactopyranoside (IPTG) at 0.1 mM and L-arabinose (L-ara) at 0.4% (w/v). Diaminopimelic acid (DAPA) at 0.3 mM was added to cultures of the *dapA* mutant *E. coli* MFDpir strain. Plasmids carrying the π-dependent R6K origin of replication (Stalker et al., 1982), such as pGE and pGEC derivatives, were cloned, propagated and isolated using *E. coli* BW25141. *E. coli* DH10BT1^R was used as a host for the rest of plasmids.

For expression of the different intimin, invasin and ATs constructs the *E. coli* EcM1 strain was freshly transformed with the corresponding plasmid and individual colonies harvested from plates were used to start pre-inoculate cultures. Pre-inoculums were grown at 30 ºC, with glucose 2% (w/v) for repression of the P_{lac} promoter and static conditions overnight (O/N). The next day, pre-inoculum cultures were centrifuged (3 minutes, 4000 g) and washed using fresh LB medium twice to remove the glucose and finally diluted to an O.D. of 0.5 at 600 nm (OD_{600}). The cultures were later induced using IPTG for 3 h at 30 ºC and 160 rpm.

For expression of GFP using the different tumor-induced promoter candidates, each promoter (P_{lldP}, P_{lldP}*, P_{uof} P_{hmp} and P_{norV},) controlling the GFP^{TCD} using the T7 ribosomal binding site (RBS) was integrated into the *csgCG* locus of EcM1. Two different clones from the resulting strains were grown O/N from individual colonies. After growth, cultures were diluted and grown up to 0.4 OD_{600} for their induction. For measuring fluorescence and absorbance using a microplate reader (Victor2, PerkinElmer, Shelton, CT, USA) cultures were diluted again to 0.2 OD_{600} using LB containing the specified concentrations of their respective inducer, sodium L-lactate (Sigma-Aldrich), H_2O_2 (Sigma Aldrich) or Spermine NONOate (SPER/NO) (Calbiochem) and grown for 22 h at 30 ºC, each condition with 6 technical replicates. Measurements for fluorescence (535 nm) and absorbance (OD_{600}) were taken every 15 minutes after a 30 s orbital shaking. For flow cytometry measuring of the candidate promoters' expression, inducers were directly added to the cultures and grown at 37 ºC with agitation at 200 rpm unless otherwise specified.

For expression of integrases, individual colonies of each EcM1 strains carrying the different targets in the *yhjY* locus and the integrases either in plasmid or integrated in the

ypjA or *ycgV* loci were used to inoculate 96-well plates containing LB medium. After O/N growth at 37 ºC and 200 rpm, cultures were serial diluted (1000-fold total dilution) with fresh medium containing the corresponding inducer and were grown again in the same conditions O/N.

2. Plasmids and DNA constructs.

Plasmids used in this work can be found in Table 2. DNA constructs were produced by standard methods of DNA manipulation, digestion, ligation and modification (Ausubel et al., 2002) or one-step isothermal Gibson assembly (Gibson et al., 2009). DNA synthesis of the tested promoters, the intimin sequence with the LysM deletion, and the LgBiT fragment was performed by ThermoFisher Scientific GeneArt. Oligonucleotides were purchased from Merck or Integrated DNA Technologies. Relevant oligonucleotides can be found in Table 3. Designs for integrase targets were kindly provided by Dr. Jérôme Bonnet based on previous works (Bonnet et al., 2012, 2013; Guiziou et al., 2019). For Polymerase Chain Reaction (PCR) either Taq DNA polymerase (NZYTaq II 2X Green Master Mix) for screening or high-fidelity DNA polymerase, Herculase II Fusion DNA polymerase (Agilent Technologies) for cloning were used. All DNA constructs were sequenced by Macrogen, Inc. or ACGT Inc.

3. *E. coli* transformation and chromosome modification.

Replicative plasmids and Gibson assembly reactions were transformed into the appropriate *E. coli* strains using the Transformation and Storage Solution (TSS) method (Chung et al., 1989). DNA ligations and suicide pGE plasmids were electroporated into electrocompetent bacteria. Conjugation of pGECs plasmids was performed using *E. coli* MFDpir as the donor strain.

Site-directed integration of DNA sequences into the *E. coli* chromosome was done following the marker-less I-*Sce*I endonuclease expression method (Pósfai et al., 1999, 2006), leaving no antibiotic resistance or recombination sequence in the chromosome of the modified strains. In short, the *E. coli* strain to be modified was previously transformed with the pACBSR plasmid (Cm^R) (Herring et al., 2003), which expresses the I-SceI and *λ* Red genes under control of the L-ara inducible promoter $P_{BAD,}$ and subsequently electroporated with the corresponding pGE-based suicide vector (Km^R). Co-integrants were selected using LB-Km-Cm plates grown at 37 ºC. Isolated colonies were used to inoculate LB cultures containing Cm and L-arabinose that were grown during up to 6 h

at 37 ºC with agitation (200 rpm). Approximately ~1 µL sample of the grown cultures was streaked on LB-Cm plates using an inoculating loop and incubated O/N. Individual colonies were replica-plated in LB-Cm and LB-Km-Cm plates to screen for the Km-sensitive colonies that had deleted the vector sequences after the endonuclease expression. Individual Km-sensitive colonies were checked by PCR using specific oligonucleotides to identify clones with the chromosomal integration in the targeted locus.

4. Flow cytometry.

Detection of chimeric proteins with Nb on the bacterial surface and binding to soluble antigen were analyzed by flow cytometry. After induction, a volume of the cultures equivalent to 1 OD_{600} was centrifuged (4000 g, 3 min), washed 3 times with 500 µl of phosphate-buffered saline (PBS) and resuspended in 400 µl of the same buffer. Next, 180 µl of the cell resuspension were incubated for 1 h at room temperature with 20 µl of the primary antibody (for display detection) or biotinylated EGFR fused to Fc (EGFR-Fc) (50 nM). For intimin and invasin constructs, the primary antibody used was a mouse anti-c-myc monoclonal antibody (mAb) (1:500; 9B11 clone; Cell Signaling, Ref: 2276) unless indicated. For AT constructs, a mouse anti-E-tag antibody (1:500; Phadia) was used. After incubation, bacteria were washed 3 times with PBS and incubated in the same manner with the secondary reagent: for display detection, a goat anti-mouse IgG-Alexa 488 conjugated polyclonal antibody (1:500; Life technologies, Ref: A11029), and for detection of the biotinylated antigen, Streptavidin-APC (1:100; Beckman Coulter, Ref: 733001). Finally, samples were washed 3 times with PBS and resuspended in 500 µl of the same buffer for analysis in a Gallios cytometer (Beckman Coulter, Inc).

For flow cytometry of bacteria expressing GFP under the control of tumor sensing promoters and integrases, grown cultures were diluted 1:100 and directly measured using either a Gallios cytometer (Beckman Coulter Inc.) or an Attune NxT flow cytometer (Thermo Fisher Scientific Inc.), respectively.

5. Protein electrophoresis and Western blots.

Electrophoresis in denaturing conditions using polyacrylamide gels containing SDS (SDS-PAGE) was performed following standard methods (Ausubel et al., 2002). A volume equivalent to 1 OD_{600} of an induced culture was centrifuged (4000 g, 3 min) and resuspended in 100 µL of Tris-HCl 10 mM pH 8. Next, 100 µL of SDS loading buffer 2x

(120 mM Tris-HCl pH 6.8, 2% (p/v) SDS, 2% (v/v) β-mercaptoethanol (2-ME), 10% glycerol and 0.01% (p/v) bromophenol blue) were added. Samples were either boiled (100 ºC, 10 min) or not, as specified, and centrifuged (21.000 g, 10 min) to eliminate any insoluble material (e.g., the PG). 100 µL of the supernatants were transferred to new tubes from which up to 20 µL were loaded into 8% polyacrylamide gels for intimin, invasin and flu constructs and 10% polyacrylamide gels for EhaA constructs. Electrophoresis was performed in a Miniprotean III chamber (Bio-Rad).

Due to the high resistance to denaturation of intimin and invasin, samples containing these proteins were prepared in 2x urea-SDS loading buffer (120 mM Tris-HCl pH 6.8, 4% (p/v) SDS, 10 mM EDTA, 8 M urea, 2% (v/v) 2-ME, 10% glycerol and 0.01% (p/v) bromophenol blue). When boiled, these samples were kept at 100 ºC for 30 min.

For Western blot analysis, gels were transferred to a polyvinylidene difluoride membrane (PVDF, Immobilon-P, Merck-Millipore) in semi-dry conditions as previously reported (Bodelon et al., 2009; Salema et al., 2013). Detection of protein constructs was achieved by incubating the membrane in PBS containing 3% (w/v) non-fat-milk and 1% (w/v) BSA, and the indicated primary antibodies: mouse anti-E-tag mAb (1:5000; Phadia, Thermo Fisher Scientific), mouse anti-c-myc mAb (1:2500; 9B11 clone; Cell Signaling, Ref: 2276). A goat anti-IgG mouse conjugated to peroxidase (POD) (1:5000; Sigma A2554) was used as a secondary antibody. Membranes were developed by measure of chemiluminescence using Clarity Western ECL Substrate (Bio-Rad ref. 1705061) by ChemiDoc Touch system (Bio-Rad). Precision Plus Protein Dual Color Standards (Bio-Rad) was used as molecular weight marker.

6. *In vivo* protein cross-linking.

Cross-linking of the intimin constructs was performed according to (Thanabalu *et al*., 1998). Induced cultures of *E. coli* EcM1 transformed with the different plasmids were centrifuged (4000 g, 3 min) and a 1:10 or 1:100 of the induction volume was resuspended in PBS with 2,5 mM of dithiobis(succinimidyl propionate) (DSP, Pierce) and incubated for 30 min at room temperature. Reaction was stopped using 50 mM Tris-HCl pH 7,5 and after 15 min bacteria were washed twice with 10 mM Tris-Cl pH 7,5 and finally resuspended in 200 µL of the same buffer. Samples were divided in two and the same volume of SDS loading buffer 2x, with or without 5% (v/v) 2-ME, was added. The 2-ME reduces the internal disulfide bond of DSP, breaking the covalent crosslinkings.

7. Outer membrane protein extraction.

Induced E. *coli* EcM1 cultures expressing intimin, invasin or ATs constructs were centrifuged (3000 g, 5 min) and pellets were air-dried and frozen at -80 ºC. After thawing in ice, the pellets were resuspended in 2 mL of TN buffer (20 mM Tris-HCl pH 8, 10 mM NaCl) supplemented with 0.1 mg/mL DNAse I (Roche), 0.1 mg/mL pancreatic RNAse A (Amresco), 0.1 mM phenylmethylsulfonyl fluoride (Sigma) and a protease inhibitor cocktail (Complete EDTA-free, Roche). The resuspended culture was then lysed by sonication (7 pulses of 30 sec, with the tip being cooled between pulses) and the resulting extract was centrifuged to eliminate non-lysed bacteria (1500 g, 10 min, 4 ºC). The supernatant was then ultracentrifuged (100.000 g, 1 h, 4 ºC, Beckman Optima-Max XP) and the pellet, corresponding to the totality of the membranes, was resuspended in 2 mL of TN Buffer with 1.5 % (v/v) Triton-X-100 (Sigma) (Schnaitman, 1971) in order to eliminate the fraction corresponding to the IM proteins. Resuspension was aided by using an ultrasonic bath for 10 sec. After a second ultracentrifugation the resulting pellet correspond to the OM and insoluble remains. To obtain the OMPs, the pellet was resuspended in 1 mL TN buffer with 1% (p/v) Zwittergent 3-14 (Calbiochem) by incubating at 4 ºC using a rotator for 1 h. A final ultracentrifugation results in the OMPs recovered in the supernatant.

8. Blue Native-PAGE.

In order to assess the oligomeric nature of the chimeric proteins generated in this work, the proteins extracted from the OM were subjected to non-denaturing electrophoresis in polyacrylamide gels using Coomassie Blue G-250 as a negative charge provider (Blue Native-PAGE). Glycerol (Merck) and Coomassie Blue G-250 (Bio-Rad) were added to the OMP extracts to a final concentration of 8.7% (v/v) and 0.5%, respectively, and 20 µL of each sample were loaded into a 4-20% polyacrylamide gradient, Tris-Glycine native gel (Invitrogen). The cathode buffer composition was 50 mM tricine (Fluka), 15 mM Bis/Tris/HCl pH 7 (Fluka) and 0.002% Coomassie Blue G-250, while the anode buffer was 50 mM Bis/Tris/HCl pH 7. Native molecular weight markers (66-669 kDa; GE Bioscience) were resuspended to a final concentration of 2.5 mg/ml in 50 mM Bis/Tris/HCl ph7 and 750 mM aminocaproic acid, and 5 µL were loaded into the gel. Using a Mini-Gel-Tank (Invitrogen), the electrophoresis was first run at 100 V for 45 min, until samples have successfully penetrated the gel, and later at 500 V until the dye front has reached the gel's border. For Western blot analysis, the gel is transferred to a PVDF membrane following standard methods. To unfold the proteins and facilitate antibody

access, after transferring the membrane was incubated in 8% acetic acid (Panreac) for 15 min, rinsed in de-ionized water and air dried, after which it was re-wet with methanol (MERCK) for 1 min to remove the excess of Coomassie, which helped visualizing the molecular weight markers. The membrane was rinsed in PBS with 0.05% (v/v) Tween 20 (PBS-Tween) before continuing with the standard Western blot protocol.

9. Luminescence assays.

For detection of luminescence variations due to the presence of EGFR-Fc bacteria were induced for expressing the protein constructs as above. A volume of the cultures equivalent to 1 OD_{600} was centrifuged (4000 g, 3 min), washed 3 times with 500 µl of PBS and resuspended in 200 µl of PBS and BSA 1% (w/v). A 100 µl volume of each resuspended culture was placed in a 96-well black plate with flat clear bottom (Corning). EGFR-Fc (0.5, 5, 50 or 200 nM) or PD-L1-Fc (50 nM) as a control were added to the wells and incubated at room temperature for 1 h. After incubation, the plate was placed in an orbital shaker at 37 ºC for 5 min and 25 µl of the Nano-Glo® Live Cell Reagent (Promega) were added to each well immediately before measuring luminescence (full spectrum, 2 sec integration time) and OD_{600} using a Spectramax iD5 Multi-mode Microplate Reader (Molecular Devices). Plate was shaken for 3 sec prior to the measurements.

10. Software and web tools.

In silico DNA visualization and analysis was done using DNASTAR Lasergene 17 and Benchling softwares. Schematic representation of circuits was based in the Synthetic Biology Open Language (SBOL) Visual Glyphs (Galdzicki et al., 2014). Secondary structure prediction for intimin helices was a consensus from the results of the web tools PsiPred (Bio.tools), GOR (Center for Informational Biology, Ochanomizu University) based on (Garnier et al., 1978), APSSP (Bioinformatics Centre Institute of Microbial Technology) and CFSSP (Ashok Kumar, 2013). Cytometry analysis of integrases experiments used Flow-Jo (Treestar, Inc.), while promoters and protein constructs experiments were analyzed using Kaluza (Beckman Coulter, Inc.). Statistical analysis was performed using GraphPad Prism 9.4 (GraphPad Software, LLC.). AlphaFold predictions were kindly provided by Dr. Florencio Pazos from the Computational Systems Biology group (CNB-CSIC), and the results were visualized using Mol* Viewer (Sehnal et al., 2021).

Table 1: Bacterial strains used in this work.

Strain	Genotype	Reference
MG1655	K-12 (F- λ-)	(Blattner et al., 1997)
EcM1	MG1655Δ*fimA-H*	(Salema et al., 2013)
BW25141	(F- λ-) Δ(*araD-araB*)567, Δ*lacZ4787*(::*rrnB-3*), Δ(*phoB-phoR*)580, *galU95*, Δ*uidA3::pir*, *recA1*, *endA9(del-ins)::FRT*, *rph-1*, Δ(*rhaD-rhaB*)568, *hsdR51*	(Datsenko & Wanner, 2000)
DH10B-T1R	(F- λ-) *mcrA* Δ*mrr-hsdRMS-mcrBC φ80lacZDM15* Δ*lacX74 recA1 endA1 araD139* Δ(*ara, leu*)7697 *galU galK rpsL (StrR) nupG tonA*	(Durfee et al., 2008)
MFDpir	MG1655 RP4-2-Tc::[*Mu1::aac(3)IV-DaphA-Dnic35-DMu2::zeo*] *DdapA:: (erm-pir) DrecA*	(Ferrières et al., 2010)
EcM1ΔypjA::Ptac GFP	EcM1Δ*ypjA*::P_{tac}-*gfp*	Laboratory collection
EcM1ΔcsgCG::pIldP-GFP	EcM1Δ*csgCG*::P_{IldP}-*gfp*	This work
EcM1ΔcsgCG::pIldP*-GFP	EcM1Δ*csgCG*::P_{IldP}*-*gfp*	This work
EcM1ΔcsgCG::puof-GFP	EcM1Δ*csgCG*::P_{uof}-*gfp*	This work
EcM1ΔcsgCG::phmp-GFP	EcM1Δ*csgCG*::P_{hmp}-*gfp*	This work
EcM1ΔcsgCG::pnorV-GFP	EcM1Δ*csgCG*::P_{norV}-*gfp*	This work
EcM1 InvBxb1	EcM1 with an inversion target for Bxb1 integrated in place of the *yhjY* locus	This work
EcM1 InvTp901	EcM1 with an inversion target for Tp901 integrated in place of the *yhjY* locus	This work
EcM1 InvInt7	EcM1 with an inversion target for Int7 integrated in place of the *yhjY* locus	This work
EcM1 InvAND	EcM1 with the inversion AND gate integrated in place of the *yhjY* locus	This work
EcM1 ExcBxb1	EcM1 with an excision target for Bxb1 integrated in place of the *yhjY* locus	This work
EcM1 ExcTp901	EcM1 with an excision target for Tp901 integrated in place of the *yhjY* locus	This work
EcM1 ExcInt7	EcM1 with an excision target for Int7 integrated in place of the *yhjY* locus	This work
EcM1 ExcAND	EcM1 with the excision AND gate integrated in place of the *yhjY* locus	This work
EcM1 PtetBxb1	EcM1 ExcBxb1 Δ*ypjA*::*tetR*-P_{tet}-*bxb1*	This work
EcM1 PtetTp901	EcM1 ExcTp901 Δ*ycgV*::*tetR*-P_{tet}-*tp901*	This work
EcM1 PhmpBxb1	EcM1 ExcBxb1 Δ*ypjA*::P_{hmp}-*bxb1*	This work

Table 2: Plasmids used in this work.

Name	Features	Reference
pGE	KmR; R6K ori, suicide vector for integration/deletion.	(Piñero-Lambea et al., 2015)
pGEC	pGE with oriTRP4.	(Seco & Fernández, 2021)
pACBSR	CmR, p15A ori, *araC*, P_{BAD}, *I-SceI* and λ *Red* genes.	(Herring et al., 2003)
pGECyhjY	pGE with homology regions flanking the *yhjY* locus of MG1655.	Laboratory collection
pGEcsgCG	pGE with homology regions flanking the *csgC* and *csgG* loci of MG1655.	Laboratory collection
pGEypjA	pGE with homology regions flanking the *ypjA* locus of MG1655.	Laboratory collection
pGECycgV	pGEC with homology regions flanking the *ycgV* locus of MG1655.	Laboratory collection
pGEcsgCGplldP-GFP	pGEcsgCG for integration of the P_{lldP}-*gfp.*	This work
pGEcsgCGplldP*-GFP	pGEcsgCG for integration of P_{lldP}*-*gfp.*	This work
pGEcsgCGpuof-GFP	pGEcsgCG for integration of P_{uof}-*gfp.*	This work
pGEcsgCGpnorV-GFP	pGEcsgCG for integration of P_{norV}-*gfp.*	This work
pGEcsgCGphmp-GFP	pGEcsgCG for integration of P_{hmp}-*gfp.*	This work
pGEypjA-tetRPtetgfp	pGEypjA for the integration of *tetR*-P_{tet}-*gfp.*	This work
pGECyhjY_Bp_target_Bxb1	pGECyhjY for the integration of the Bxb1 inversion target	This work
pGECyhjY_BP_target_Tp901	pGECyhjY for the integration of the Tp901 inversion target.	This work
pGECyhjY_BP_target_Int7	pGECyhjY for the integration of the Int7 inversion target.	This work
pGECyhjY_AND_00	pGECyhjY for the integration of the inversion AND gate.	This work
pGECyhjY_B12	pGECyhjY for the integration of the Bxb1 excision target.	This work
pGECyhjY_31_Tp901_ID	pGECyhjY for the integration of the Tp901 excision target	This work
pGECyhjY_7_12	pGECyhjY for the integration of the Int7 excision target.	This work
pGECyhjY_AND_LD_32	pGECyhjY for the integration of the excision AND gate.	This work
pGEypjA-tetRPtet-Bxb1	pGEypjA for the integration of tetR-Ptet-bxb1.	This work
pGECycgV-tetRPtet-Tp901	pGEycgV for the integration of tetR-Ptet-Tp901.	This work
pGEypjA_phmp_Bxb1	pGEypjA for the integration of Phmp-bxb1.	This work
pBL_Const1	AmpR plasmid that constitutively expresses Bxb1.	(Bonnet et al., 2013)
pBL_Const2	AmpR plasmid that constitutively expresses Tp901.	(Bonnet et al., 2013)
pBL_Const4	AmpR plasmid that constitutively expresses Int7.	(Bonnet et al., 2013)
pBL_Const15	AmpR plasmid that constitutively expresses multiple integrases, including Bxb1 and Tp901.	(Bonnet et al., 2013)
pAK-Not (pAK)	CmR, pBR322 ori, lacIQ-Plac, empty vector used as a parental for all protein constructs plasmids.	(Veiga et al., 1999)
pNeae2	pAK vector expressinga fusion of EHEC intimin residues 1-654, E-tag, 6xHis tag and c-myc-tag.	(Salema et al., 2013)
pNVEGFR2	pNeae2 with a VHH anti-EGFR substituting the 6xHis tag	(Salema et al., 2016)
pNDVe	pNVEGFR2 with a deletion of the LysM domain and spacer (Δ54-153).	This work
pNDHVe	pNVEGFR2 with a deletion of the LysM domain and periplasmic helices (Δ54-206).	This work
pND	pNeae2 with a deletion of the LysM domain and spacer (Δ54-153)	This work
pNDVeSB	pNDVe with the SmBiT fragment fused between amino acids 43 and 154.	This work
pNDVeLB	pNDVe with the LgBiT fragment fused between amino acids 43 and 154.	This work
pNDVeSpy	pNDVe with the Spytag fused between amino acids 43 and 154.	This work
pNDVeSnoop	pNDVe with the SnoopTag fused between amino acids 43 and 154.	This work
pVgfpA	pAK vector expressing a fusion of the pelB signal peptide, a VHH anti-GFP, the E-tag and EhaA residues 989-1327.	(Salema et al., 2013)
pVeA	pVgfpA with a VHH against EGFR instead of a VHH against GFP.	This work

pVeASB	pVeA with the SmBiT fragment fused to the C terminal end using the first three amino acids of the OmpA linker (residues 192-194).	This work
pVeALB	pVeA with the LgBiT fragment fused to the C terminal end using the first three amino acids of the OmpA linker (residues 192-194).	This work
pVeALOA	pVeA with the complete OmpA linker (residues 192-208) fused to the C terminal end.	This work
pVeALOALB	pEVe with the LgBiT fragment fused to the C-terminal through the complete OmpA linker (residues 192-208)	This work
pF330Ve	pAK vector expressing a fusion of the pelB pignal peptide, a VHH anti-GFP, the E-tag and the flu (Ag43) residues 710-1039.	This work
pF330VeSB	pF330Ve with the LgBiT fragment fused to the C-terminal end through the complete OmpA linker (residues 192-208).	This work
pF330VeLB	pF330Ve with the SmBiT fragment fused to the C-terminal end through the complete OmpA linker (residues 192-208).	This work
pF487Ve	pAK vector expressing a fusion of the pelB signal peptide, a VHH anti-GFP, the E-tag and flu (Ag43) residues 553-1039.	This work
pF487VeSB	pF487Ve with the LgBiT fragment fused to the C-terminal end through the complete OmpA linker (residues 192-208).	This work
pF487VeLB	pF487Ve with the SmBiT fragment fused to the C-terminal end through the complete OmpA linker (residues 192-208).	This work
pIVe	pAK vector expressing a fusion of invasin residues 1-596, E-tag, a VHH anti-EGFR and c-myc-tag.	This work
pIFVe	pIVe with the L352F mutation.	This work
pIFDVe	pIFVe without the D1 Ig-like domain (residues 503-596).	This work
pIFDVeSB	pIFDVe with the SmBiT fragment fused between invasin residues 51 and 52.	This work
pIFDVeLB	pIFDVe with the LgBiT fragment fused between invasin residues 51 and 52.	This work
pIFDVeSpy	pIFDVe with the SpyTag fused between invasin residues 51 and 52.	This work
pIFDVeSnoop	pIFDVe with the SnoopTag fused between invasin residues 51 and 52.	This work
pAK-pelB-Nanoluc	pAK vector for expression of the full length Nanoluc with an N-terminal pelB signal for periplasmic secretion.	This work
pSEVA221	KmR, RK2-origin	(Silva-Rocha et al., 2013)
pSEVA221-Ptet-NDVe	pSEVA221 with a P_{tet} promoter for expressing the NDVe construct.	This work
pSEVA221-Ptet-NDVeSB	pSEVA221 with a P_{tet} promoter for expressing the NDVeSB construct.	This work
pSEVA221-Ptet-IFDVe	pSEVA221 with a P_{tet} promoter for expressing the IFDVe construct.	This work
pSEVA221-Ptet-IFDVeSB	pSEVA221 with a P_{tet} promoter for expressing the IFDVeSB construct.	This work

Table 3: Oligonucleotides used in this work.

Sequence (5'-3')	Use
CCATTCATTGTCATTATCCCTACACA	Check cloning of PlldP promoter in pGEcsgCG
GTTAACCATTCATTGTTCATGAACTAATACG	Check cloning of PlldP* promoter pGEcsgCG
AATGTCCCGGTGTTCAAGTGG	Check cloning of Puof promoter pGEcsgCG
TGGCACGCAATCTGCAATTAGC	Check cloning of PnorV promoter pGEcsgCG
CCAAAGAACCATTTACATTGCAGG	Check cloning of Phmp promoter pGEcsgCG
GTCAGTTTGCCGTACGTGGCGTC	Check cloning of promoters in pGEcsgCG
CACAACAGGCATTCTCTCCGGTATC	5' check of the integration in *csgCG*
ATTCGGCTCTTCCCTGGAGGAGCTCGGATACCCTTACTC TGTTGAAAACGAATAGATAGGTTCGCGGCCGCTTCTAGA GTTA	Cloning of inversion targets in pGECyhjY
TCTGCGTTTATATACTAGTAGCGGCCATTATTGACCACTT CCGAGTAGAATCGTGCTTCAGTAAGAAGCGACTATCTGT ATACGATGGGGGTTAG	Cloning of inversion targets in pGECyhjY
ATTCGGCTCTTCCCTGGAGGAGCTCGGATACCCTTACTC TGTTGAAAAC	Cloning of AND gates and excision targets in pGECyhjY
CCGAGTAGAATCGTGCTTCAGTAAGAAGCGACTATCTGT ATACGATGGGGGTTAG	Cloning of AND gates and excision targets in pGECyhjY
CCCACATGCCTGCATAAAGG	5' check of the integration in *yhjY*
TCCAAGAAGGAGATATACATATGAGAGCCCTGGTAGTCA T	Cloning of Bxb1 in pGEypjA-tetR-Ptet vector
ATGACTACCAGGGCTCTCATATGTATATCTCCTTCTTGGA TCC	Cloning of Bxb1 in pGEypjA-tetR-Ptet vector
CGCTCCTGATGCACCCATACACTAGTGTATGGAAGTTGA GC	Cloning of Bxb1 in pGEypjA-tetR-Ptet vector
CTCAACTTCCATACACTAGTGTATGGGTGCATCAGGAGC G	Cloning of Bxb1 in pGEypjA-tetR-Ptet vector
AAAAACAACTTAAATGTGAAAGTGG	Check cloning in vectors with tetR-Ptet
GTTGTTAAACCTTCGATTCCGACC	Check cloning in vectors with tetR-Ptet
GCTGCCTTCACTACGAGCTCTGTGATGCAAATTTTTCACT TCATCAC	Cloning of Phmp in pGEypjA-Phmp-Bxb1
ATGTATATCTCCTTCTTGGAGGATCCTCTAGATTTTTTGC ATCTTAATTG	Cloning of Phmp in pGEypjA-Phmp-Bxb1
AAAAACTGGTCAGGACATCATCG	5' check of the integration in *ypjA*
GTGCTTATTGCCTATAGTGAACCACG	5' check of the integration in *ycgV*
CATTTTTCACTTCACAGGTCAAGCTT	Cloning in pAK-Not derived vectors
CCGATTCATTAATGCAGCTGGC	Check cloning in pAK-Not derived vectors
GGTAATAAGAAGTCCAGTGAACTACCG	Check cloning of intimin constructs
CCGCGGTTACAACATTATGGAACGGCAGAGG	Cloning of pNDHVe
AATTCGGTGGGGGAAGCGTGACCGGCTACCGGCTGTTC GAGGAGATTCTGGGCGGAGGGTCTCCGC	Cloning of SmBiT in pNDVe

GGAGACCCTCCGCCCAGAATCTCCTCGAACAGCCGGTAGCCGGTCACGCTTCCCCCACCG	Cloning of SmBiT in pNDVe
ACTCGGAACAGCATGGAGCC	Check cloning of LgBiT
GCGCATATTGTGATGGTTGATGCCTATAAACCGACCAAGGGCGGAGGGTCTCCGCGGAAAAGC	Cloning of SpyTag in pNDVe
CTTGGTCGGTTTATAGGCATCAACCATCACAATATGCGCGCTTCCCCCACCGAATTCATTTTCACC	Cloning of SpyTag in pNdVe
AAACTGGGCGATATTGAATTTATCAAGGTGAACAAAGGCGGAGGGTCTCCGCGGAAAAGC	Cloning of SnoopTag in pNdVe
TTTGTTCACCTTGATAAATTCAATATCGCCCAGTTTGCTTCCCCCACCGAATTCATTTTCACC	Cloning of SnoopTag in pNdVe
CATAGTGGTTTGTTTCTGCTCACC	Check cloning in pEVe vectors
GGGTAGCTACATTGCGAACCTTGC	Check cloning in pEVe vectors
GCTTCCCCCACCGCCCTGTCCGAATTGCCACTTAATGCCAACC	Cloning of short linker in pEVeLB
GGTCAAGCTTTTACAGAATCTCCTCGAACAGCCGGTAGCCGGTCACGCTTCCCCCACCGCCCTGTC	Cloning of SmBiT in pEVeLOA
CGGACAGGGCGGTGGGGGAAGCGTCTTCACACTCGAAGATTTCGTTGG	Cloning of LgBiT in pEVeLB
CAAGCTTTTAGCTGTTGATGGTTACTCGGAACAGC	Cloning of LgBiT in pEVe vectors
ACCTGTGGTTGCGCCTGCACCGGCTCCTGCACCATAAAAGCTTGACCTGTGAAGTGAAAAATGGC	Cloning of LOA in pEVeLOA
AGCCGGTGCAGGCGCAACCACAGGTGCTGCTTCTCCTTGACCGAATTGCCACTTAATGCC	Cloning of LgBiT in pEVeLOALB
ACCTGTGGTTGCGCCTGCACCGGCTCCTGCACCAGTCTTCACACTCGAAGATTTCGTTGG	Cloning of LOA in pEVeLOA
CACGTCCACCAACACCGCGGGTCCCCCTGTATGCCTCCAT	Cloning of *flu*330 constructs in pAK-Not vectors
ATGGAGGCATACAGGGGGACCCGCGGTGTTGGTGGACGTG	Cloning of *flu*330 constructs in pAK-Not vectors
CACGTCCACCAACACCGCGGACGAATGTCACTCTCGCCTC	Cloning of *flu*487 constructs in pAK-Not vectors
GAGGCGAGAGTGACATTCGTCCGCGGTGTTGGTGGACGTG	Cloning of *flu*487 constructs in pAK-Not vectors
CACTTCACAGGTCAAGCTTTTAGAAGGTCACATTCAGTGTGGCC	Cloning of flu constructs without fusions in pAK-Not vectors.
GGCCACACTGAATGTGACCTTCTAAAAGCTTGACCTGTGAAGTG	Cloning of flu constructs without fusions in pAK-Not vectors.
CCACACTGAATGTGACCTTCGGTCAAGGAGAAGCAGCACCT	Cloning of LOA-LgBiT in flu constructs
GGTGCTGCTTCTCCTTGACCGAAGGTCACATTCAGTGTGG	Cloning of LOA-LgBiT in flu constructs
CTGCACCGGCTCCTGCACCAGTGACCGGCTACCGGCTGTT	Cloning of LOA-SmBiT in flu constructs
AACAGCCGGTAGCCGGTCACTGGTGCAGGAGCCGGTGCAG	Cloning of LOA-SmBiT in flu constructs
ATCTCTAGAATGATGGTTTTCCAGCCAATCAGTG	Cloning of invasin constructs
ATCGTCGACCTTAACAAAGTGGGTATCAACACTTTGCC	Cloning of invasin constructs maintaining the D1 domain
TTTCTTGATTAACCGCATCGCC	Check cloning of invasin constructs
AAATGAACTATCGCTTTGGCGAGAG	Mutation of invasin leucine 352 to phenylalanine

TCGCCAAAGCGATAGTTCATTTGG	Mutation of invasin leucine 352 to phenylalanine
ACTGGTCGACCTGAGGCTGCTGAACG	Cloning of invasin constructs without the D1 domain
GTGACCGGCTACCGGCTGTTCGAGGAGATTCTGGGCGGAGGGTCTAAATATGATGCTAACGCACCGCAACAG	Cloning of SmBiT in pIFDVeSB
CAGAATCTCCTCGAACAGCCGGTAGCCGGTCACGCTTCCCCCACCTTCTGAAGCCCCAGCCATGAAC	Cloning of SmBiT in pIFDVeSB
TCATGGCTGGGGCTTCAGAAGGTGGGGGAAGCGTCTTCAC	Cloning of LgBiT in pIFDVeLB
GTGAAGACGCTTCCCCCACCTTCTGAAGCCCCAGCCATGAAC	Cloning of LgBiT in pIFDVeLB
TCAACAGCGGCGGAGGGTCTAAATATGATGCTAACGCACCGCAACAG	Cloning of LgBiT in pIFDVeLB
GGTGCGTTAGCATCATATTTAGACCCTCCGCCGCTGTTGA	Cloning of LgBiT in pIFDVeLB
GCGCATATTGTGATGGTTGATGCCTATAAACCGACCAAGGGCGGAGGGTCTAAATATGATGCTAACGCACCGCAACAG	Cloning of SpyTag in pIFDVeSpy
CTTGGTCGGTTTATAGGCATCAACCATCACAATATGCGCGCTTCCCCCACCTTCTGAAGCCCCAGCCATGAAC	Cloning of SpyTag in pIFDVeSpy
AAACTGGGCGATATTGAATTTATCAAGGTGAACAAAGGCGGAGGGTCTAAATATGATGCTAACGCACCGCAACAG	Cloning of SnoopTag in pIFDVeSnoop
TTTGTTCACCTTGATAAATTCAATATCGCCCAGTTTGCTTCCCCCACCTTCTGAAGCCCCAGCCATGAAC	Cloning of SnoopTag in pIFDVeSnoop

RESULTS

1. Development of a Tumor Sensing Memory Circuit in *E. coli*.

In this first chapter we are going to focus on the creation of a memory circuit in the chromosome of *E. coli* that permanently registers the presence of characteristic tumor metabolites. For this purpose, we initially characterized promoters that respond to specific compounds of the TME looking for sensitivity, minimum basal transcription and a good dynamic range. Next, we investigated the viability of using serine integrases to create memory circuits within the chromosome of *E. coli*. Finally, we combined the findings from both parts to create a memory circuit that is triggered by tumor metabolites. This was achieved by controlling the expression of a serine integrase using one of the previously characterized promoters.

1.1. Screening and characterization of chromosome-integrated promoters for tumor specific induction.

We first aimed to characterize the activity of promoters whose induction depend on metabolites with high presence in the TME while in the context of the *E. coli* EcM1 strain. In order to avoid the need for antibiotics to maintain plasmids, all the promoters were tested in single copy while integrated in the chromosome of *E. coli* replacing the *csgCG* locus. The codon-optimized gfp^{TCD} gene (Corcoran et al., 2010) was used as a reporter.

1.1.1. Detection of L-lactate.

E. coli naturally possesses the ability to detect and metabolize L-lactate through the *lldPRD* operon (Aguilera et al., 2008). Here, we selected the wild type (WT) promoter of this operon, P_{lldP}, and a mutated version in which one binding site of the anoxic regulator ArcA (Iuchi & Lin, 1988), placed downstream the -35 and -10 boxes, had been substituted by a randomized sequence (GCATGAACTAATACG). This promoter was denominated P_{lldP}* and was expected to have higher expression than the WT at lower oxygen concentrations.

First, we measured the activity of the two promoters with different concentrations of L-lactate during 22 h using microplate cultures (Figure 8). L-lactate concentration in healthy tissue is described to be 1.5-3 mM, while tumor tissue has been described to present concentrations up to 40 mM (Brizel et al., 2001; Walenta et al., 2000). We decided to test for increasing concentrations of L-lactate up to 10 mM. For lower L-lactate concentrations (0, 0.1 and 1 mM) both promoters showed a similar behavior in terms of changes in GFP signal over time, with an initial expression during the first 6-8 h, a signal

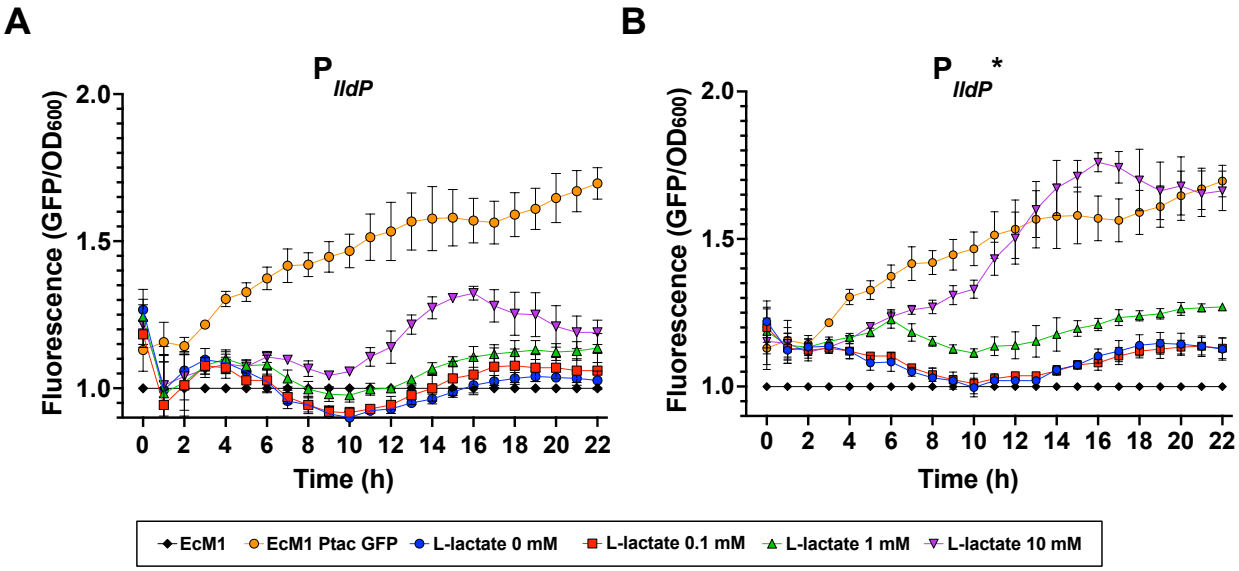

Figure 8. GFP expression by the L-lactate sensing promoters at 30 ºC. Fluorescence of cultures of *E. coli* bacteria carrying *gfp*^{TCD} reporter under P$_{lldP}$ (**A**) and P$_{lldP}$* (**B**) promoters and grown in microplate wells at 30 ºC for 22 h with different concentrations of L-lactate in the media. Measurement of the GFP fluorescence is divided by the OD_{600} of the corresponding well and normalized to the parental EcM1 strain used as a negative control. An EcM1 strain with a P_{tac} promoter expressing *gfp*^{TCD} in the same *csgCG* locus was used as a positive control by inducing with 0.1 mM IPTG. Each value is the mean of 3 biological replicates, with 6 technical replicates each.

decay during the 8-14 h, and a rise in induction after that point. The GFP levels were, however, higher for the mutated P$_{lldP}$* promoter, with the 1 mM condition showing an induction difference with the lower concentrations that was not as noticeable in the case of the WT promoter. Regarding the 10 mM condition, both promoters showed a clear induction, especially after the 10 h, with the mutated promoter reaching a 2-fold higher GFP signal than the WT.

As the microplate assay had to be performed at 30 ºC, below the human body temperature of 37 ºC, we also tested the promoters by growing the strains in agitated flasks at 37 ºC and measured their fluorescence by flow cytometry (Figure 9). Similar results were found for both the WT and the mutated promoter. In both cases the promoters produced levels of GFP higher than the negative control even without any inducer present, pointing out to an important promoter leakage. Increased GFP fluorescence was observed at 3 h only for a L-lactate concentration of 10 mM, but values were only ~2 times higher. Contrary to what had been observed at 30 ºC, GFP signal started to decay for both promoters after 3 h, with values close to the negative control at 16 h.

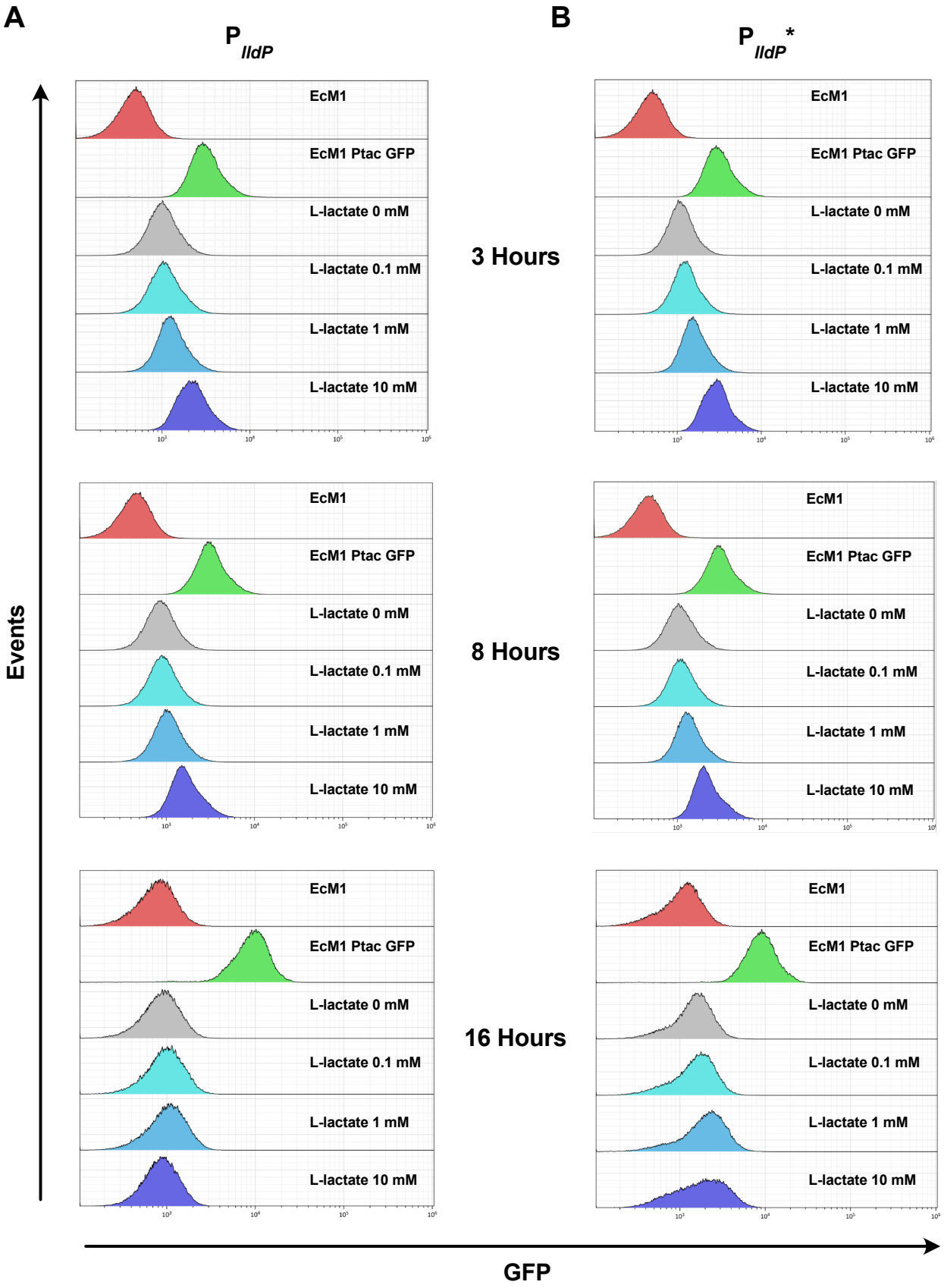

Figure 9. GFP expression by the L-lactate sensing promoters at 37 ºC. Flow cytometry analysis of the expression of GFP under the P_{lldP} (**A**) and P_{lldP}* (**B**) promoters at 37 ºC after 3, 8 and 16 h of induction with different concentrations of L-lactate, as indicated. The parental EcM1 strain was used as negative control, and EcM1 carrying a P_{tac}-*gfp*^{TCD} cassette in the *csgCG* locus was used as a positive control by inducing it with 0.1 mM IPTG.

Summarizing, both promoters presented a low dynamic range and a measurable expression with no L-lactate present in the media (promoter leakage). These characteristics make it difficult to use them in the memory circuit, as their sensitivity would be very low and auto induction could activate them, producing a false positive.

1.1.2. Detection of Reactive Oxygen Species.

In *E coli*, several TFs are capable of sensing the oxidative stress produced by ROS, activating or repressing genes. The literature shows that the regulatory sequence of the promoter controlling the expression of the genes *uof* and *fur*, P_{uof}, is activated by two of these TF, SoxS and OxyR (Zheng et al., 1999). Therefore, we selected this promoter to test its capability as a biosensor for ROS.

ROS encompass several different molecules of high reactivity, making it difficult to establish specific concentrations to emulate the TME (Liou & Storz, 2010; Weinberg et al., 2019). Here, we used increasing concentrations of H_2O_2 (0, 0.05, 0.5 and 5 mM) as the inducer, as this molecule can be maintained in relatively stable conditions and its production by a 1 cm^3 epithelial tumor could be roughly estimated at 0.55-1.38 µM/s (Del Monte, 2009; Szatrowski & Nathan, 1991). As before, we first performed a 22 h microplate assay (Figure 10A). No changes in GFP signal were detected after 6 h and

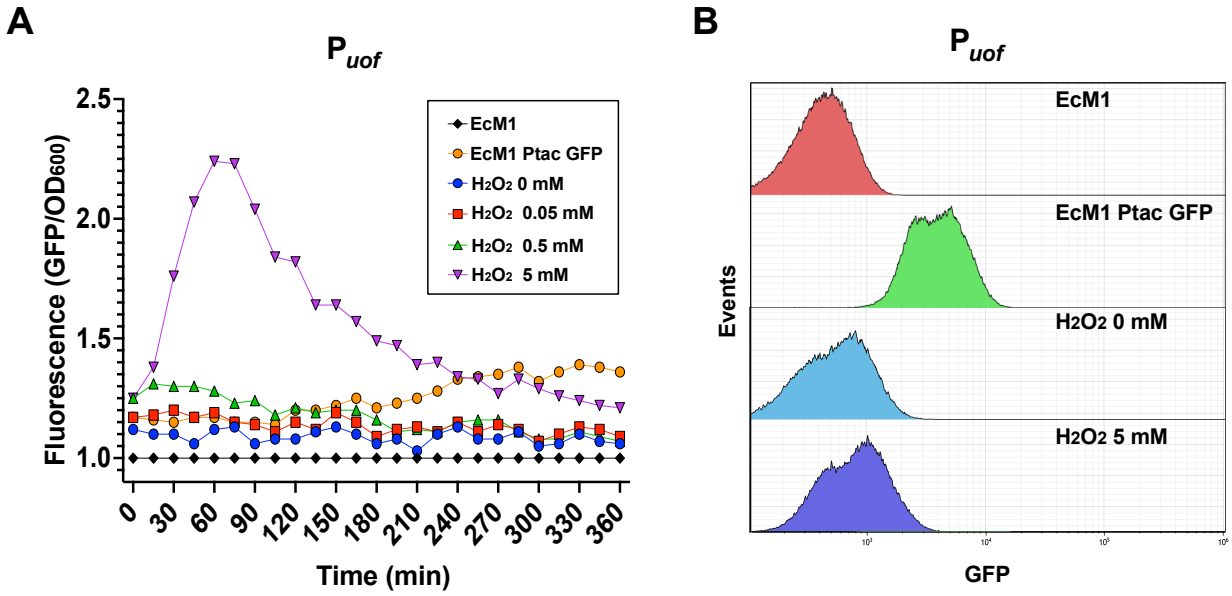

Figure 10. GFP expression by the ROS sensing promoter P_{uof}. (A) Fluorescence of cultures of *E. coli* bacteria carrying gfp^{TCD} reporter under P_{uof} promoter and grown in microplate wells at 30 ºC for 6 h with different concentrations of of H_2O_2 in the media, as indicated. Measurement of the GFP fluorescence, normalization and controls as in Figure 8. **(B)** Flow cytometry analysis of the expression of GFP driven by P_{uof} promoter at 37 ºC after 2 h of induction with the indicated concentrations of H_2O_2. Cultures were grown in static conditions to avoid any possible oxidative stress due to agitation. Same controls as in **(A)**.

therefore, we focused hereafter in this initial period. Results showed detectable basal levels of GFP even with no H_2O_2 present in the media, with similar values for low concentrations of the inducer. Only the 5 mM condition showed a high spike in GFP signal after 1 h of induction, followed by a constant reduction of fluorescence afterwards, until basal levels of expression were reached.

Next, we evaluated the expression of the promoter at 37 ºC as before. However, cytometry showed high basal expression levels and we suspected that the flask agitation and the consequent oxygenation of the culture might have been causing oxidative stress in the culture. To avoid this possibility, we repeated the experiment in static conditions (Figure 10B). Nevertheless, even with no agitation, the non-induced culture still presented a basal GFP signal. Moreover, the 5 mM condition showed an induction only slightly higher than the non-induced, far from the GFP signal differences observed in the microplate reader at 30 ºC.

The poor dynamic range of this promoter coupled with its autoinduction are two undesirable traits that make P_{uof} a non-viable choice for our desired memory circuit.

1.1.3. Detection of Nitric Oxide.

Nitric oxide is a highly reactive molecule that is used by mammalian cells to attack pathogens. Therefore, it is not surprising that *E. coli* naturally present multiple mechanisms to detoxify it (Robinson & Brynildsen, 2013). In this study, we selected as candidates the promoters controlling the *norVW* operon and the *hmp* gene, P_{norV} and P_{hmp}, as their regulatory regions are controlled by TF that respond to the presence of NO. The concentration of this molecule changes through the evolution of the tumor. Diazeniumdiolates, also known as NONOates, which spontaneously release NO, have been successfully used *in vitro* to emulate the natural flux of this molecule *in vivo*. Here, we chose SPER/NO, whose activity can emulate the TME when used at concentrations up to 200 µM (Somasundaram et al., 2019; Thomas et al., 2006, 2008).

In a similar fashion to the previous promoter, the microplate reader assay (Figure 11) showed that both the P_{norV} and the P_{hmp} strains presented an induction spike during the first hour, with a gradual decrease in fluorescence after that point until reaching the fluorescence levels of the no inducer condition after 6 h for P_{norV}. On the contrary, P_{hmp} kept the fluorescence signal from the 2.5 h point throughout the rest of the experiment. Both promoters showed expression in a dosage-dependent manner, with sensitivity for

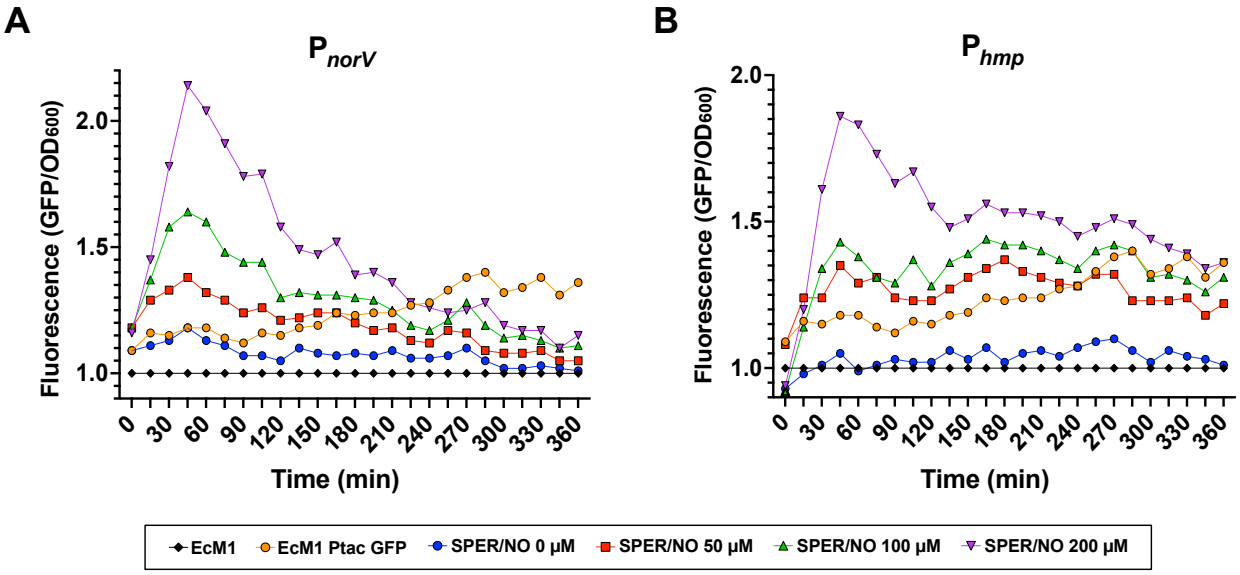

Figure 11. GFP expression by the NO sensing promoters at 30 ºC. Fluorescence of cultures of *E. coli* bacteria carrying *gfp*^{TCD} reporter under P*norV* **(A)** and P*hmp* **(B)** promoters at 30 ºC for 6 h with different concentrations of SPER/NO in the media, as indicated. Measurement of the GFP fluorescence, normalization and controls as in Figure 8.

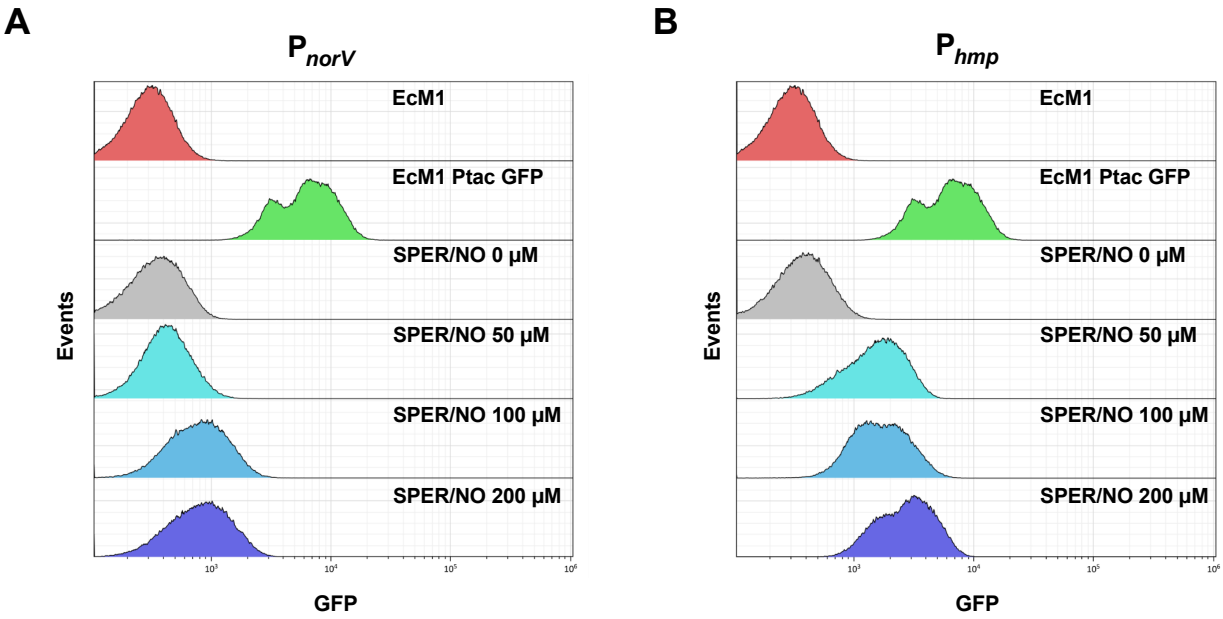

Figure 12. GFP expression by the NO sensing promoters at 37 ºC. Flow cytometry analysis of the expression of the P*norV* **(A)** and P*hmp* **(B)** promoters at 37 ºC after 2 h of induction with the indicated concentrations of SPER/NO. The parental EcM1 strain was used as negative control, and a EcM1 carrying a P$_{tac}$-*gfp*^{TCD} cassette integrated in the csgCG locus was used as a positive control by inducing it with 0.1 mM IPTG.

concentrations as low as 50 µM. Basal expression of P*hmp* was surprisingly low, with a GFP signal similar to that of the parental strain used as a negative control.

The flow cytometry analysis of the strains induced at 37 ºC (Figure 12) showed a very tight control of the expression from both promoters, with their strains exhibiting no fluorescence in the absence of SPER/NO. From the two of them, P*hmp* displayed the

highest induction levels of both promoters, with a good dynamic range from 50 to 200 µM.

After analyzing the results of all the different promoters assayed in this section, we concluded that the sensitivity, minimum basal expression and wide dynamic range of P_{hmp} make it the best candidate for the construction of our tumor sensing memory circuit.

1.2. Construction of a chromosome-integrated memory circuit in *E. coli* using serine integrases.

Serine integrases have been extensively employed in synthetic biology to generate genetic circuits, including logic gates and memory circuits. However, most of these constructs are usually designed for and implemented in plasmids or Bacterial Artificial Chromosomes (BACs) (Rubens et al., 2016; Siuti et al., 2013; Zúñiga et al., 2020). Applications involving the integrase targets in the chromosome are rare and involve expression of the integrases from plasmids (Bonnet et al., 2012; Hsiao et al., 2016). In this work, we first tested the feasibility of using these genetic devices to both invert and excise target sequences in the chromosome of the *E. coli* EcM1 strain. Next, we aimed to control the expression of integrases using inducible promoters also integrated into the chromosome. Finally, we used our previously identified P_{hmp} promoter to control their expression and create a NO-sensing memory circuit.

1.2.1. Inversion of chromosome-integrated sequences using serine integrases.

Inversion targets for integrases Bxb1, Tp901 and Int7 were integrated in the *yhjY* chromosome locus. The design of targets for both Bxb1 and Tp901 placed a strong constitutive promoter (Part:BBa_J23119) insulated by a transcriptional terminator (Part: BBa_B0010) between the inversely oriented *attB* and *attP* sites of one of these integrases. A graphic representation of the constructs can be found in Figure 13.

In this initial configuration, the promoter drives expression of the *gfp* reporter gene and the resulting strains, named EcM1 InvBxb1 and EcM1 InvTp901, should exhibit green fluorescence. Once the corresponding integrase is present in the cell, the enzyme is expected to invert the DNA sequence (and promoter) between the *attB* and *attP* sites, making transcription of the reporter gene by the promoter impossible. In a different

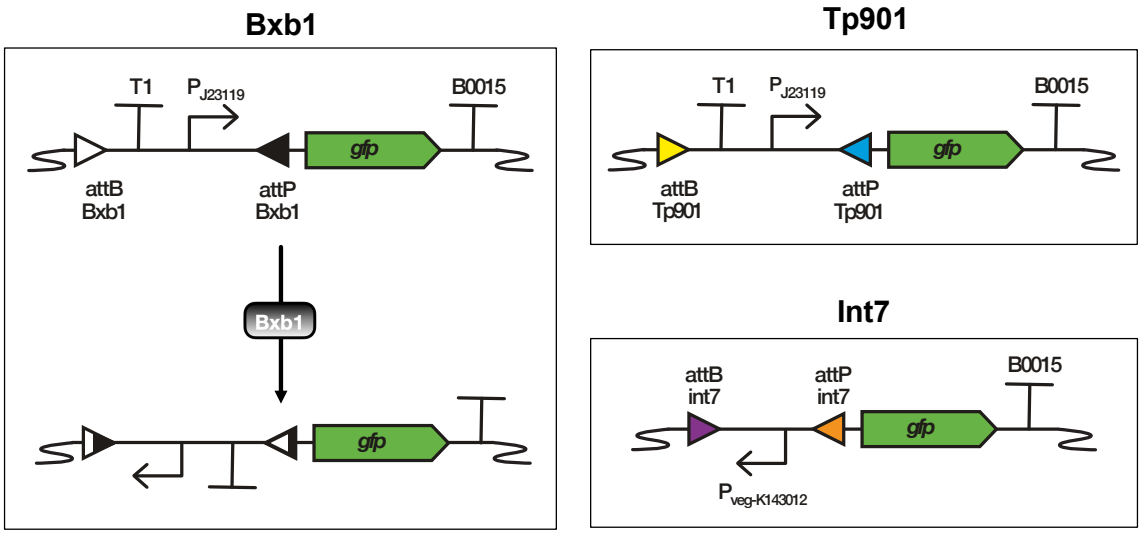

Figure 13. Inversion targets for Bxb1, Tp901 and Int7. Schematic representation of the genetic components employed in the inversion targets used for the Bxb1, Tp901 and Int7 serine integrases. Symbols are based on the SBOL Visual Glyphs (Galdzicki et al., 2014). An example of the result of the inversion is shown in the Bxb1 target.

approach, the target for Int7 placed a constitutive promoter (Part:BBa_K143012) between the inversely oriented *att* sites in an initial state where transcriptional activation activity is directed to the opposite direction of the *gfp* gene and thus it is not expressed in the resulting EcM1 InvInt7 strain. In this case, inversion of the sequence between *attB* and *attP* places the promoter in a functional configuration and the reporter is expressed.

The three resulting strains were transformed with a plasmid constitutively expressing the integrase corresponding to their targets and their GFP fluorescence levels were analyzed by flow cytometry while compared to the non-transformed counterparts (Figure 14). As expected, prior to transformation, the strains EcM1 InvBxb1 and EcM1 InvTp901 showed green fluorescence in the majority of the analyzed population (71.5% and 96.5% respectively). Despite the identical configuration and parts used, EcM1 InvTp901 presented higher fluorescence, which could be attributed to the difference of *att* sequences, as they have been reported to affect transcription (Guiziou et al., 2019). Once transformed with the plasmids, green fluorescence dropped for both strains, with EcM1 InvBxb1 reaching almost 0% and EcM1 InvTp901 presenting just a 23% GFP positive population. On the other hand, EcM1 InvInt7 displayed no GFP signal in almost 100% of the population before transformation. Once Int7 was expressed from the plasmid, almost 48% of the population showed green fluorescence. These results showed that the three integrases are able to invert sequences integrated in the chromosome of the EcM1 strain and allowed us to estimate an efficiency of inversion for chromosome-integrated targets of 71.5% for Bxb1, 73.5% for Tp901 and 48% for Int7.

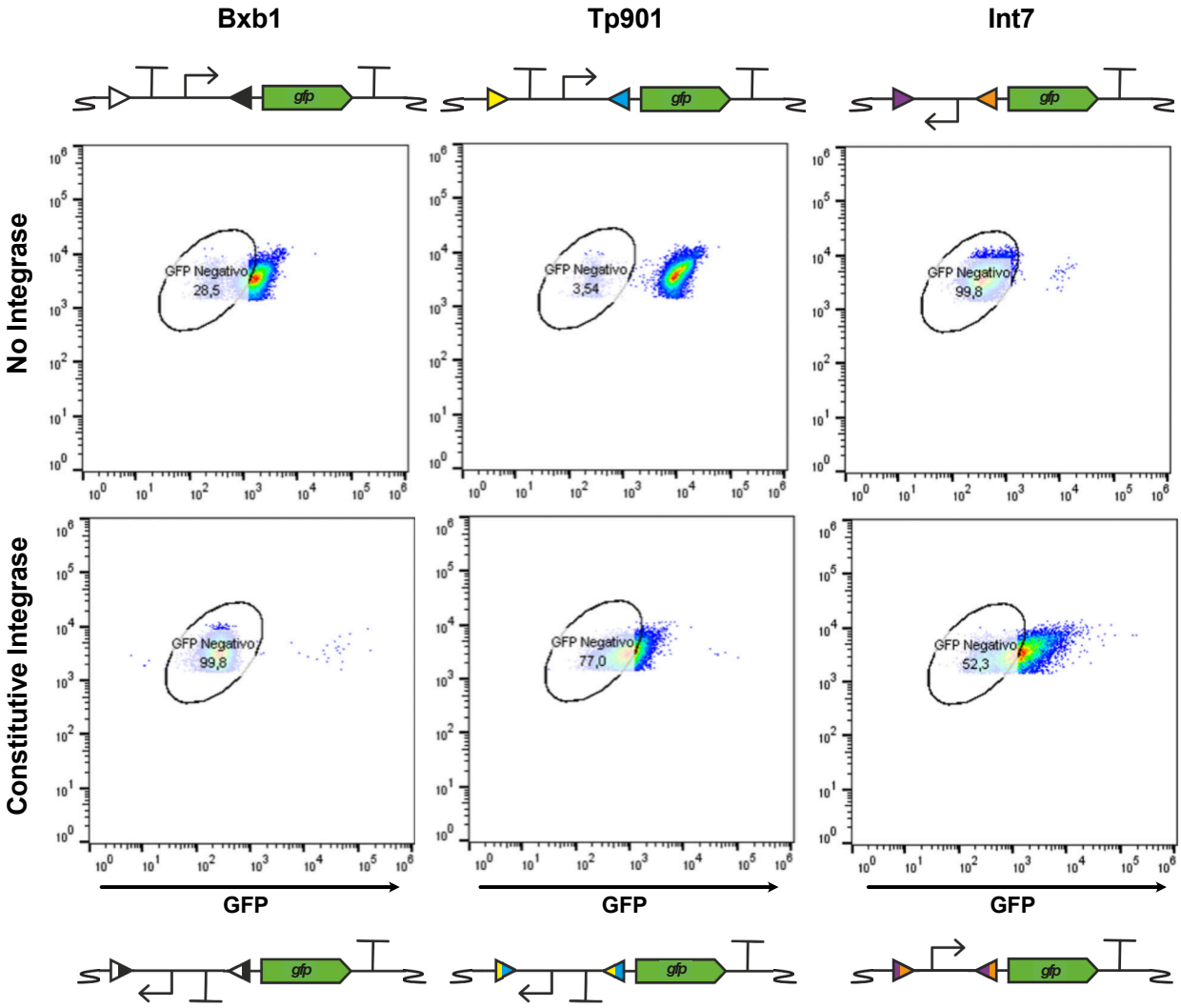

Figure 14. Inversion of chromosome-integrated targets by serine integrases. Flow cytometry analysis of the GFP fluorescence of the EcM1 strains carrying the integrated inversion targets when no integrase is present in the cells (upper row) or transformed with a plasmid constitutively expressing the indicated serine integrase (lower row). Circular gates mark the fluorescence values for the parental strain EcM1 used as negative control, the number represents the percentage of the population inside the gate. Schematic representations of the targets in each state can be found above and under the flow cytometry charts.

Next, we tested the feasibility of using multiple integrases to generate an integrated genetic logic circuit. We placed in the *yhjY* locus an AND logic gate which required the inversion activity of both the Bxb1 and Tp901 integrases in order to start the transcription of a reporter *gfp* gene. The design of the construct placed a constitutive promoter (Part:BBa_K3606016) between the inversely oriented *att* sites of Tp901, with its transcription blocked by a following double terminator (Part:BBa_B0015) situated outside the Tp901 sites. This whole sequence is nested between the two inversely oriented Bxb1 att sites and followed by the RiboJ insulator (Clifton et al., 2018), a bicistronic RBS

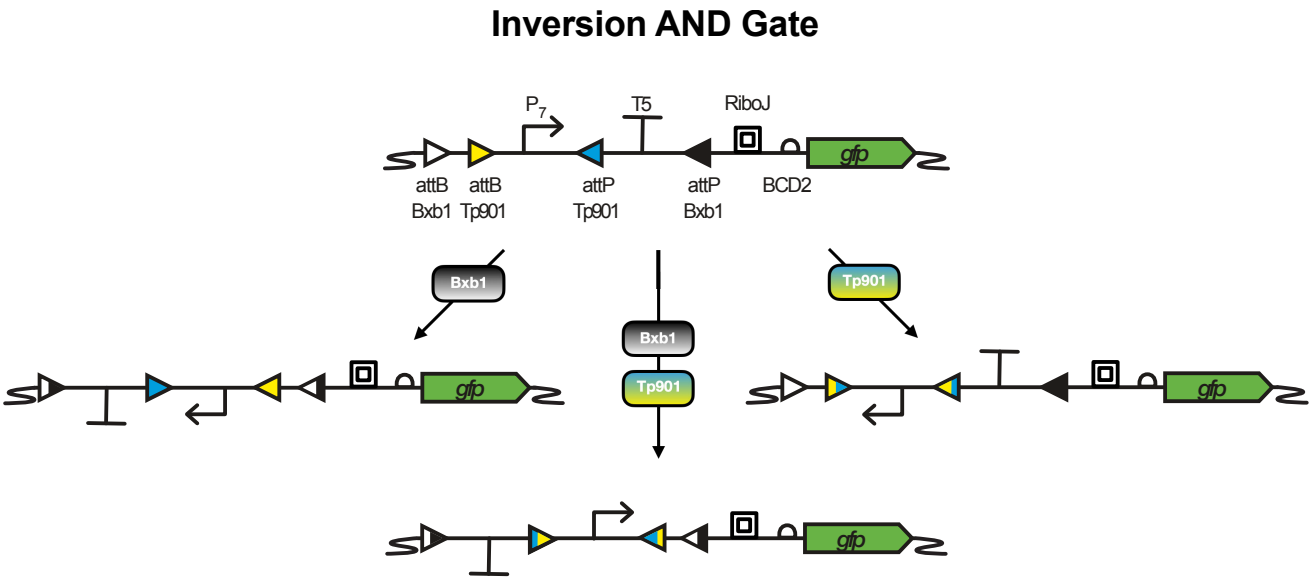

Figure 15. Inversion AND gate using targets for Bxb1 and Tp901. Schematic representation of the genetic components employed in the inversion AND gate and the results of the activity of Bxb1, Tp901 or both. The independent inversion by only one of the integrases is not enough to allow the promoter to express the reporter *gfp* gene. Symbols are based on the SBOL Visual Glyphs.

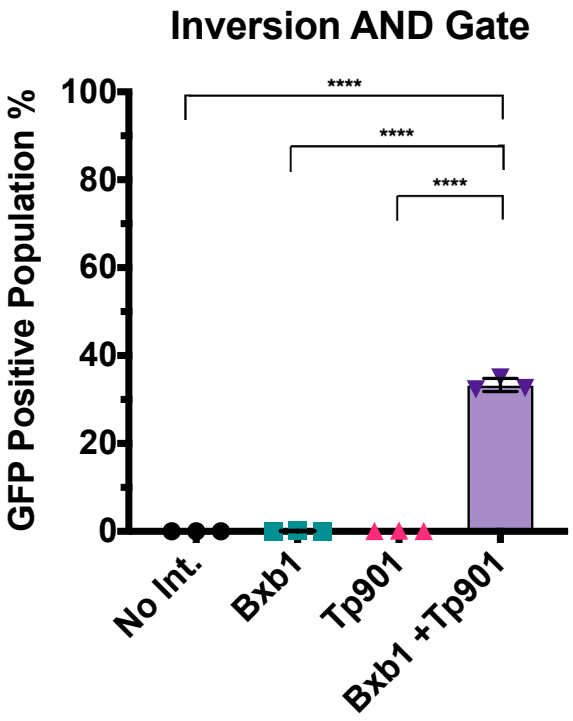

Figure 16. Flow cytometry analysis of the Inversion AND gate. Flow cytometry analysis of the EcM InvAND strain with no integrase (negative control) or with a plasmid expressing constitutively either Bxb1, Tp901 or both of them. Points represent the percentage of the bacteria population showing a higher GFP signal than the negative control. Error bars represent the standard deviation. Statistical significance inferred by unpaired t-test analysis. (****) p-value < 0.0001.

(Mutalik et al., 2013) and the *gfp* gene. The target and its possible configurations depending on integrase activity can be found in Figure 15.

We integrated the target into our parental strain generating the EcM1 InvAND strain. To test it, the strain was transformed with plasmids constitutively expressing either Bxb1, Tp901, or both integrases, and the resulting bacteria were subjected to flow cytometry to compare green fluorescence levels to the non-transformed counterparts (Figure 16). The results showed no difference in fluorescence levels between populations expressing no integrase or just one of them. However, 33% of bacteria expressing both Bxb1 and Tp901 were positive for GFP fluorescence, indicating that the inversion AND gate is functional.

In conclusion, we demonstrated the possibility of integrating targets into the chromosome of E. coli using various integrases with varying efficiencies, and successfully implemented genetic AND gates based on inversion.

1.2.2. Excision of chromosome-integrated sequences using serine integrases.

Excision targets for Bxb1, Tp901 and Int7 were also integrated into the *yhjY* locus. The design of the constructs consisted in a constitutive promoter (Part:BBa_K3606016) blocked by a transcription terminator placed between the equally oriented *att* sites of each recombinase. Following the second *att* site, the RiboJ insulator and the bicistronic RBS preceded the reporter *gfp* gene. In the initial configuration the terminator blocked the transcription in the three different targets and only the excision activity of the corresponding integrase is able to cleave the terminator and restore the expression of the *gfp* gene. Therefore, the resulting strains, named EcM1 ExcBxb1, EcM1 ExcTp901 and EcM1 ExcInt7, were expected to present no green fluorescence unless transformed with their corresponding integrases. Constructs and their configurations are shown in Figure 17.

We subjected the three strains to the same experiment performed with the inversion targets (Figure 18). Without integrase expressing plasmids, the three strains presented no differences in GFP fluorescence to the parental strain in almost 100% of the screened population. Once transformed, the population showing GFP fluorescence rose to 99% for EcM1 ExcBxb1, 76.6% for EcM1 ExcTp901 and 80.5% for EcM1 ExcInt7. Both EcM1 ExcTp901 and EcM1 ExcInt7 displayed fluorescence levels up to 1 order of magnitude higher than EcM1 ExcBxb1, which could probably be attributed again to the effect of the

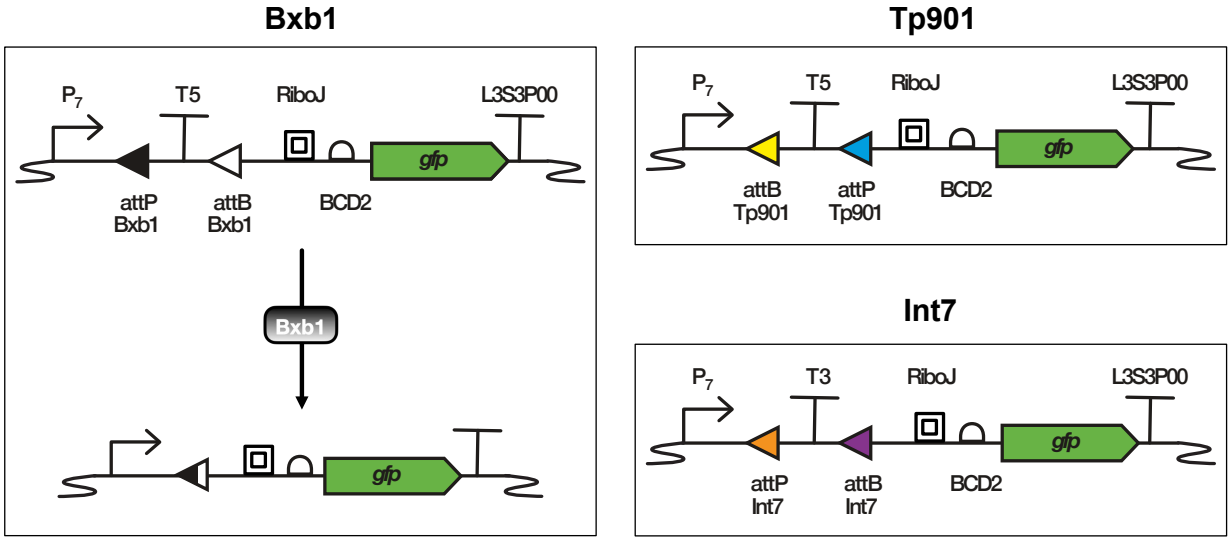

Figure 17. Excision targets for Bxb1, Tp901 and Int7. Schematic representation of the genetic components employed in the excision targets used for the Bxb1, Tp901 and Int7 serine integrases. Symbols are based on the SBOL Visual Glyphs. An example of the result of the excision is shown in the Bxb1 target.

different *att* sites to the transcriptional activity. Interestingly, a small part of the GFP expressing population of the strains with the Tp901 and Int7 targets showed lower fluorescence levels, similar to the GFP positive EcM1 ExcBxb1 population. These results showed that using excision targets in the chromosome of *E. coli* EcM1 is possible and even more efficient than using inversion targets.

With these good results, we proceeded to test the possibility of using multiple excision targets to create a genetic AND gate in the chromosome. The design of the construct was based on the previous Bxb1 excision target but placed a second transcription terminator between the excision-oriented *att* sites of Tp901 (Figure 19). Once again, we transformed the resulting strain, EcM1 ExcAND, with plasmids expressing constitutively either Bxb1, Tp901, or both integrases and compared the transformed strains to the one not expressing an integrase by flow cytometry (Figure 20). In a similar manner to the inversion AND gate, the strains expressing one or none of the integrases showed no differences in the fluorescence of their population; however, the strain expressing both Bxb1 and Tp901 showed excellent results with 93% of its population being GFP positive, almost tripling the percentage obtained using the inversion AND gate.

In conclusion, we have determined that the use of excision by serine integrases to modify both simple targets and genetic AND gates integrated into the chromosome of *E. coli* is possible, and even more efficient than using inversion targets.

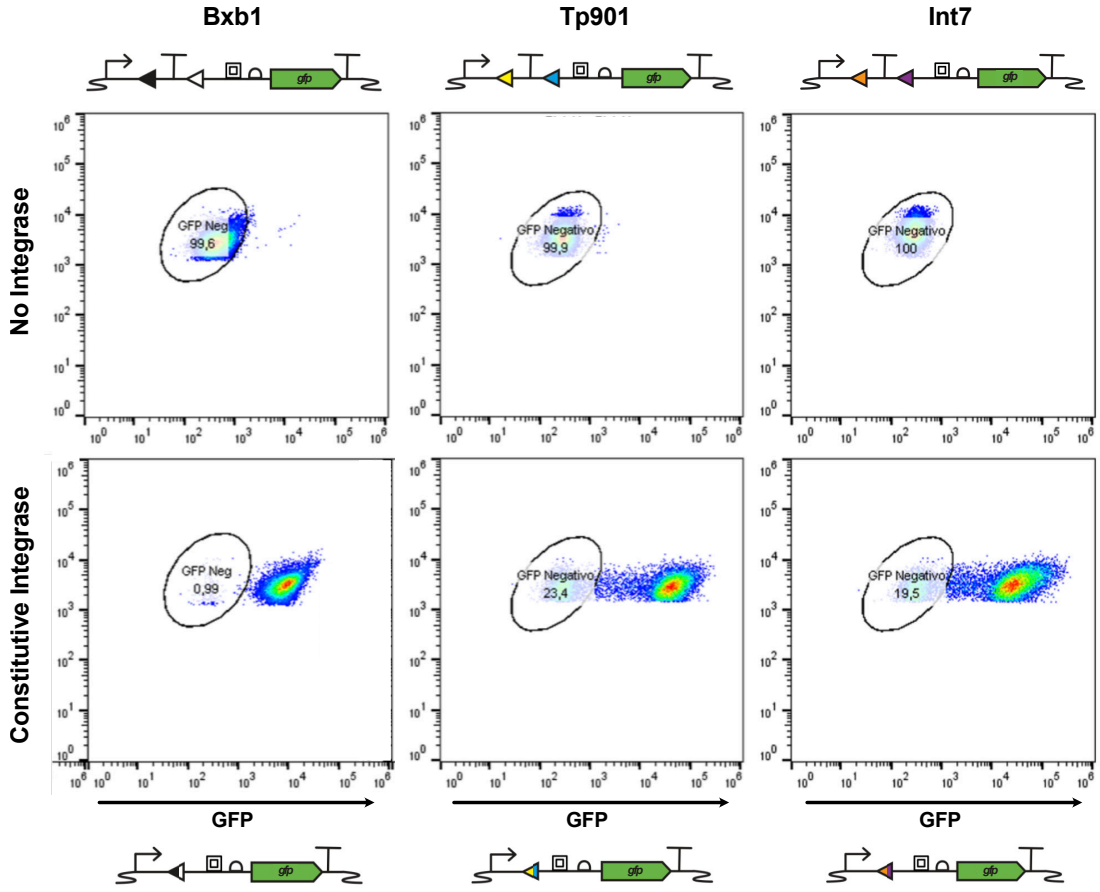

Figure 18. Excision of chromosome-integrated targets by serine integrases. Flow cytometry analysis of the GFP fluorescence of the EcM1 strains carrying the integrated excision targets when no integrase is present in the cells (upper row) or when they are transformed with a plasmid constitutively expressing its corresponding serine integrase (lower row). Circular gates label the fluorescence values for the EcM1 parental strain used as negative control; the number represents the percentage of the population inside the gate. Schematic representations of the targets in each state can be found above and under the flow cytometry charts.

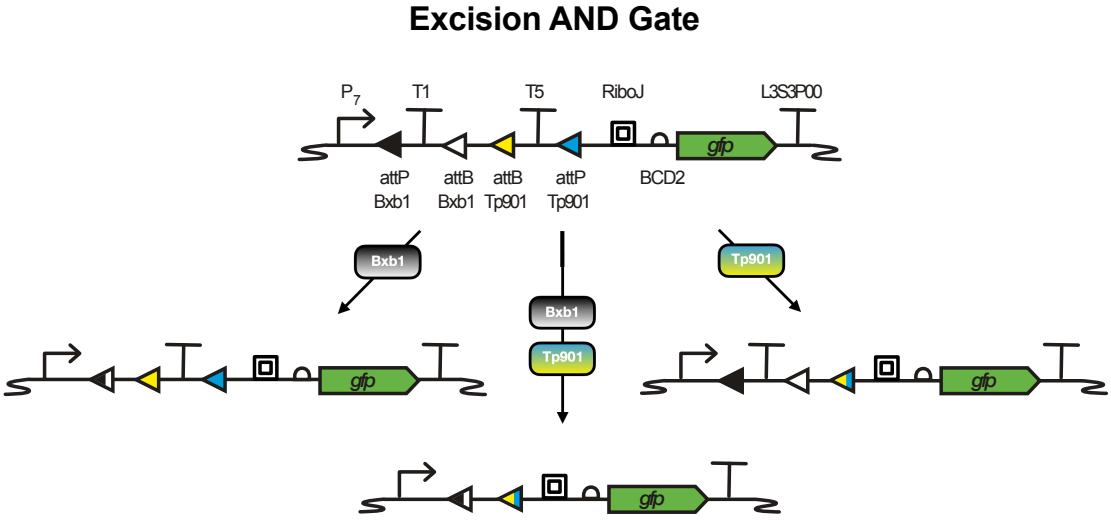

Figure 19. Excision AND gate using targets for Bxb1 and Tp901. Schematic representation of the genetic components employed in the excision AND gate and the results of the activity of Bxb1, Tp901 or both. The independent excision by only one of the integrases is not enough to allow the promoter to express the reporter *gfp* gene. Symbols are based on the SBOL Visual Glyphs.

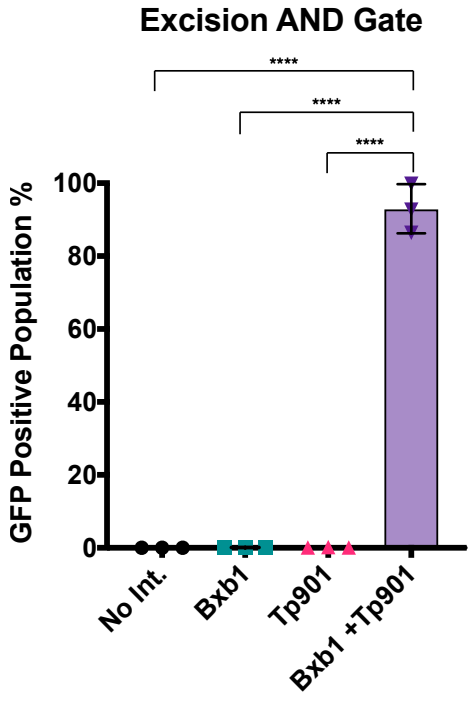

Figure 20. Flow cytometry analysis of the excision AND gate. Flow cytometry analysis of the EcM ExcAND strain with no integrase (negative control) or with a plasmid expressing constitutively either Bxb1, Tp901 or both of them. Points represent the percentage of the bacteria population showing a higher GFP signal than the negative control. Error bars represent the standard deviation. Statistical significance inferred by unpaired t-test analysis. (****) p-value < 0.0001.

1.2.3. Implementation of chromosome-integrated genetic cassettes to control the expression of serine integrases using inducible promoters.

In the following experiments, we aimed to move from using plasmids that constitutively expressed serine integrases to integrating those integrases into the *E. coli* chromosome and controlling their expression using inducible promoters. Since moving from constitutive to inducible expression was expected to reduce the concentration of the integrases in the cell, we selected the strains carrying excision targets as parental strains because of their better efficiency compared to inversion targets.

Our first approach relied on using the IPTG-inducible P_{tac}, a commonly used promoter in synthetic biology, to express the *bxb1* gene. The construct was integrated in the *ychO* locus of the EcM1 ExcBxb1 strain. A successfully integrated strain; however, could not be obtained. Through the several steps of the integration process (see Material and methods: *E. coli* transformation and chromosome modification) most colonies presented a strong green fluorescence. The few non-fluorescent colonies resulting after the resolution of cointegrants were analyzed through PCR to look for the integrated P_{tac}-*bxb1*

cassette; however, this sequence could not be detected. These results suggested that the non-induced basal activity of P_{tac} was able to generate enough Bxb1 to activate the excision of the target. Therefore, only those bacteria that had reverted to the WT and lost the expression of the integrase remained non-fluorescent. This idea matches our former experience with this promoter in our laboratory, which had shown strong leaky expression of P_{tac} fusions without inducer (Ruano-Gallego et al., 2015).

In a second attempt, we selected the tetracycline promoter P_{tet} and the *ypjA* locus, as previous results using GFP as a reporter showed this combination to have a tight control of the expression, while also reaching high expression levels when the inducer aTc is present. This time, the colonies presenting green fluorescence were a small percentage and were easily discarded for the target conserving ones. PCR confirmed the successful integration of the cassette and the strain was termed EcM1 PtetBxb1. We tested the strain by measuring its fluorescence after growing with or without aTc and compared it to both the parental strain without a recombinase, and the parental strain carrying the plasmid constitutively expressing Bxb1 from previous experiments (Figure 21A). When exposed to aTc, a 97% of the bacterial population showed GFP fluorescence, a comparable result to the 99% reached by strain with a constitutive expression of Bxb1. Without aTc, a 14% of the population still showed positive fluorescence levels, which correlates with the small percentage of fluorescent colonies obtained during the integration process.

Aiming to replicate the success with Bxb1, we integrated Tp901 under control of P_{tet} in EcM1 ExcTp901, this time in the *ycgV* locus. We conducted a similar integration process, producing the strain EcM1 PtetTp901. Figure 21B shows the results from testing the strain in the same manner as its Bxb1 counterpart. The induction of P_{tet} with aTc produced an 80% of the population showing GFP fluorescence, lower, but comparable, to the strain carrying the constitutive plasmid (84-97%). Only 10% of this bacterial population manifested fluorescence levels without aTc present in the media.

Taking together these results, we have demonstrated that the chromosome of *E. coli* can be used to place genetic circuits relying on the excision or the inversion activity of serine integrases, with both the integrases and the targets integrated. We have also demonstrated that the integrases can be expressed to functioning levels using inducible promoters when their encoding genes are integrated in the chromosome.

For the final part of this chapter, we combined the results of the previous experiments to create an EcM1 strain carrying in its chromosome a genetic memory circuit capable of

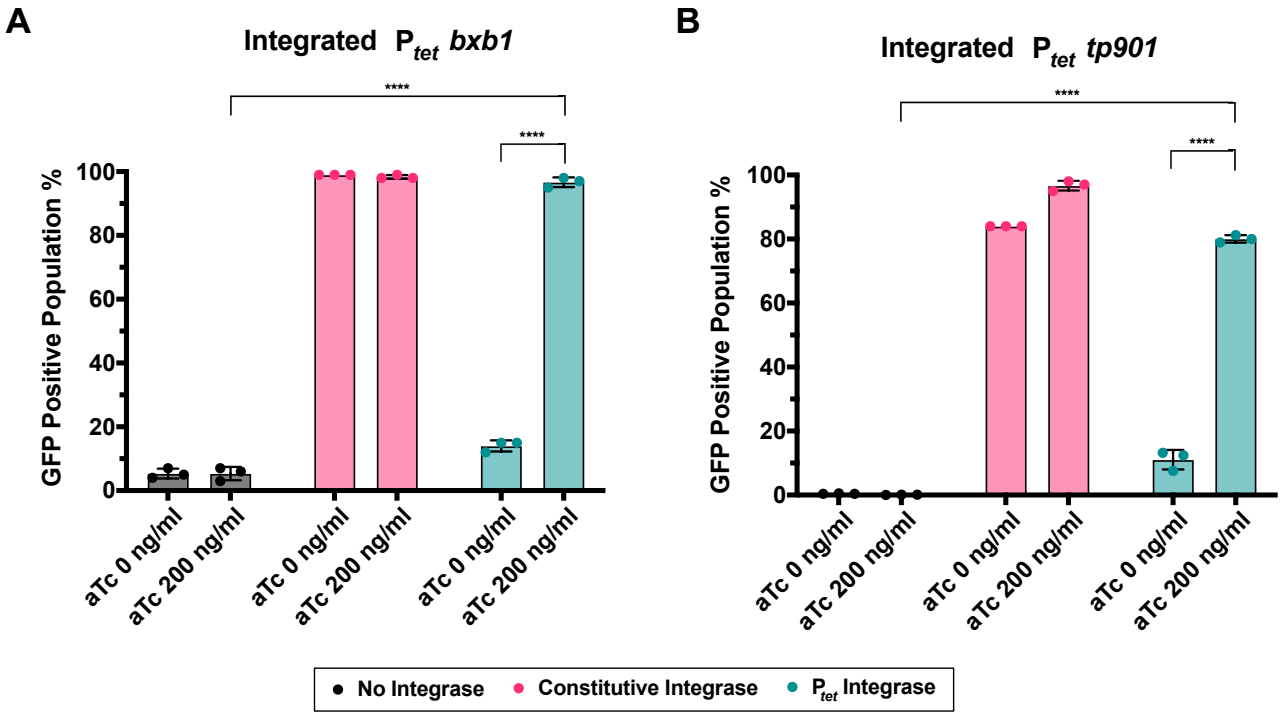

Figure 21. Excision of targets by serine integrases integrated in the chromosome. Flow cytometry analysis of the GFP fluorescence presented by **(A)** EcM1 PtetBxb1 and **(B)** EcM1 PtetTp901 with or without aTC and either no integrase (black), a plasmid expressing the constitutive integrase (pink) or the integrase under control of the P_{tet} promoter integrated in the chromosome (green). Points represent the percentage of the bacterial population showing a higher GFP signal than the parental EcM1 strain. Error bars represent the standard deviation. Statistical significance inferred by unpaired (when comparing to the strain without integrase) or paired (when comparing effects of aTc concentration) t-test analysis. (****) p-value < 0.0001.

detecting specific metabolic conditions in the tumor microenvironment. As a parental strain, we selected EcM1 ExcBxb1, due to the previous good results of the excision target.

In our first attempt, we aimed to use L-lactate as activator of the memory circuit, and so we used the P_{lldP}* promoter to control the transcription of Bxb1 in the *ypjA* locus. Unfortunately, in a similar manner to the P_{tac} promoter, through the process of integration it was not possible to find non-fluorescent colonies that maintained the construct in the chromosome. Considering promoter leakage as the limiting condition, we tried the weaker P_{lldP} WT promoter, but obtained the same results. In an effort to reduce this basal expression, we tried integrating the WT promoter cassette using a less rich growth medium (M9 minimal medium supplemented with 0.4% of glycerol), without success. As a last attempt, we changed the RBS of the construct for a weaker variant (Part:BBa_B0030). While this change allowed the integration of the construct, the resulting clones did not show any fluorescence when exposed to L-lactate.

Next, we focused in triggering our memory circuit by detecting the NO presence in the tumor microenvironment. We generated a cassette with P_{hmp} controlling the expression of the *bxb1* gene and integrated it in the *ypjA* locus of EcM1 ExcBxb1, successfully generating the strain EcM1 PhmpBxb1. This new strain was tested by comparing its fluorescence levels by flow cytometry after being exposed to a SPER/NO concentration used to emulate *in vivo* NO conditions (Figure 22A). After exposure to the inducer, 43% of the bacterial population showed positive levels of green fluorescence. While this is far from the 96% presented by the P_{tet} equivalent strain used as a positive control, the EcM1 PhmpBxb1 strain presented a negligible percentage of the population with GFP expression when not exposed to SPER/NO. This clear differentiation between the exposed and not exposed population demonstrates that this strain functions as a biosensor for for NO. Moreover, when the cultures from the end of the experiment were used to inoculate a fresh LB plate, most of the resulting colonies showed GFP expression if they came from the SPER/NO exposed cultures but only a few were GFP positive when coming from the non-exposed cultures (Figure 22B). This result demonstrated that bacteria were able to maintain the activated state of the genetic circuit through the following generations, confirming the functionality of the genetic memory circuit.

In conclusion, we have developed a biosensor *E. coli* strain, EcM1 PhmpBxb1, with the capacity to sense NO at concentrations present in human tumors and activate a chromosomally integrated genetic memory circuit, expressing a reporter gene in a permanent and heritable manner.

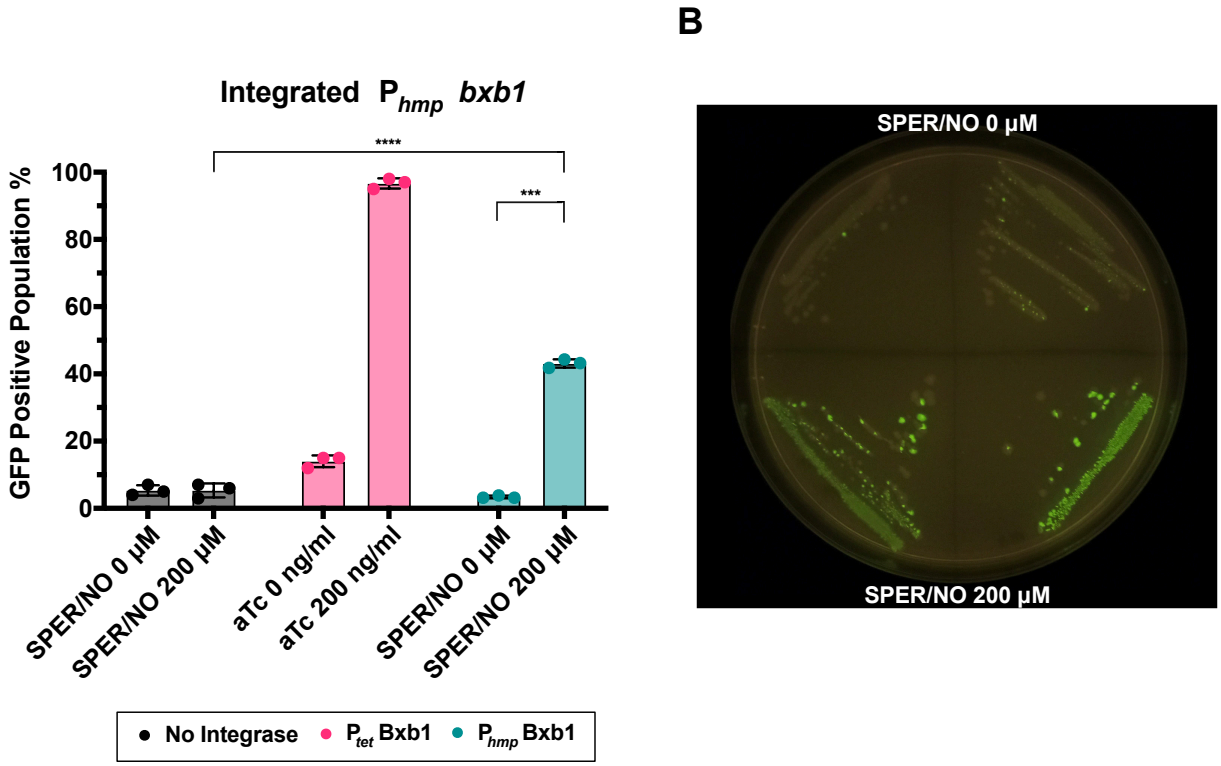

Figure 22. Nitric oxide activated memory circuit. **(A)** Flow cytometry analysis of the GFP fluorescence presented by EcM1 PhmpBxb1 with or without SPER/NO 200 µM and either no integrase (black), a plasmid expressing the constitutive integrase (pink) or the integrase under control of the P_{hmp} promoter integrated in the chromosome (green). Points represent the percentage of the bacterial population showing a higher GFP signal than the parental EcM1 strain. Error bars represent the standard deviation. Statistical significance inferred by unpaired (when comparing to the strain without integrase) or paired (when comparing effects of aTc concentration) t-test analysis. (***) p-value < 0.001, (****) p-value < 0.0001. **(B)** LB-Agar plate inoculated with the cultures used in the flow cytometry experiment and grown overnight. A blue light transilluminator was used to excite GFP. Cultures belonged to two different clones of EcM1 PhmpBxb1 exposed to either 200 µM SPER/NO (down) or none (up).

2. Development of an antigen sensing *E. coli* strain based on nanobody-displaying outer membrane proteins.

Another potential way for bacteria to sense their localization in a tumor could be the detection of tumor-associated protein antigens. Through this second chapter, we aimed to create a system of bacterial receptors in the OM that would enable the binding of an extracellular target antigen and the generation of a signal upon recognition. Our approach relied in the hypothesis that Nb-displaying OMPs may dimerize if they became attached to an antigen (Figure 23). The recognized antigens could be dimeric in nature or multimeric due to their cell-surface association. Monomeric antigens could be detected as well if two non-overlapping epitopes of the antigen could be bound simultaneously by two receptors. Thus, antigen interaction might allow the dimerization of two components of a reporter system attached to the periplasmic side of these chimeric OMP receptors, activating the signal. In order to create such a system, we required OMPs that simultaneously presented three characteristics: the capacity to display functional, antigen-binding Nbs in the OM, the capacity to support peptide

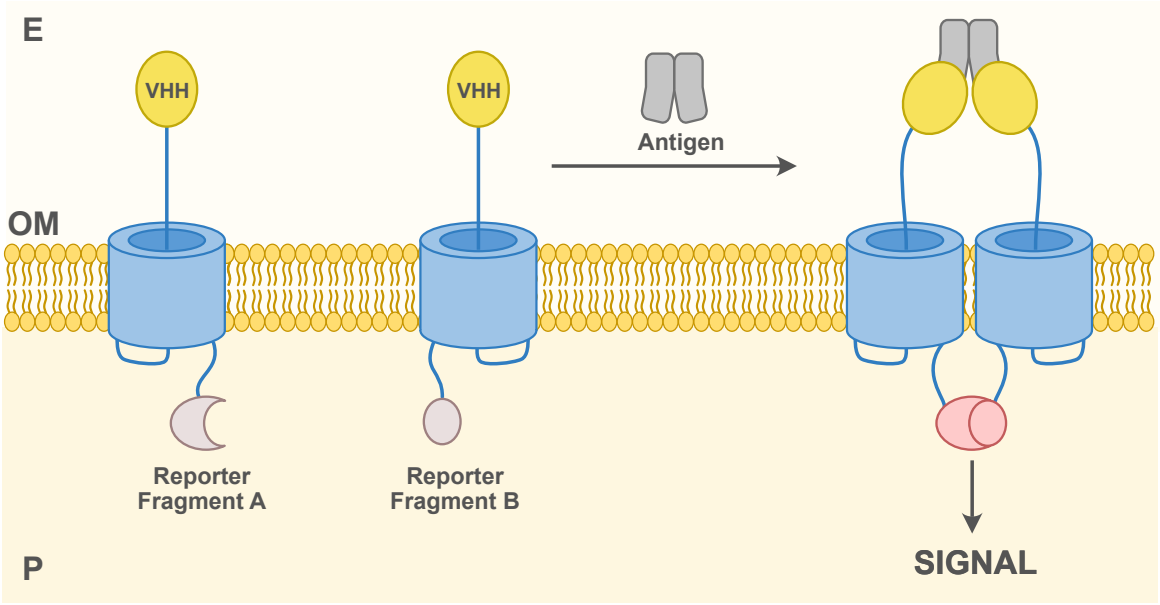

Figure 23. Concept of a bacterial antigen receptor in the outer membrane. Bacterial antigen receptors could be based on fusion proteins composed of: 1) a Nb (yellow) displayed on the bacterial surface and able to bind specifically to a target antigen; 2) a β-barrel domain (blue) inserted in the outer membrane that can be derived from a T5SS protein; and 3) periplasmic signaling domains that are part of a split enzyme (light brown) or that could be linked to a split enzyme in the periplasm. Bacterial antigen receptors might behave as monomers in the absence of the antigen. The presence of the antigen (grey) was expected to trigger dimerization of these receptors in the OM and of the linked periplasmic domains, which would then reconstitute the enzyme activity and generate a detectable output signal. E: Extracellular space, OM: Outer Membrane, P: Periplasm.

and/or protein fusions in the periplasmic side, and a monomeric nature in the absence of antigen. In the following sections we engineered different proteins belonging to the T5SS in an attempt to obtain these desired characteristics.

2.1. Engineering intimin for outer membrane sensors.

2.1.1. Modification of the periplasmic domain of intimin.

The OM anchoring fragment of a synthetic adhesin is based on the protein intimin, from its N-terminus up to the D0 Ig-like domain (Piñero-Lambea et al., 2015). Intimin has been reported to form homodimers (Touzé et al., 2003) and the formation of this dimers has been attributed to the periplasmic segment containing the LysM domain followed by a short peptide spacer (Leo, Oberhettinger, Chaubey, et al., 2015). We first evaluated whether the deletion of the LysM and spacer region enabled the production of a monomeric intimin-Nb fusion. As a model, we used the plasmid pNVEGFR2, encoding a synthetic adhesin with a Nb binding the human EGFR. The LysM domain includes residues 63 to 112 of intimin (Leo, Oberhettinger, Chaubey, et al., 2015) and our deletion comprised residues 54 through 153 to also delete the spacer. In addition, in order to facilitate future modifications, an EcoRI restriction site was placed at position 44 and a SacII site at position 54 of intimin. The resulting plasmid was termed pNDVe. Following the LysM and spacer region, we noticed that the periplasmic region of intimin also contains two α-helices that are connected to the β-barrel. The role of these α-helices in dimerization and/or folding of intimin has not been reported. Thus, we also generated a second construct deleting the LysM domain, the spacer and these two α-helices. As the α-helices had not been determined experimentally, we used four different secondary structure prediction algorithms (PsiPred, GOR, APSSP and CFSSP) to determine their more likely position, selecting the amino acids 154 through 206 as consensus. Therefore, this second deletion comprised amino acids 54 through 206 and the plasmid was named pNDHVe. A graphic representation of the different aforementioned constructs can be found in Figure 24.

The above intimin-Nb constructs were tested for their capacity to be displayed on the bacteria surface, as well as for the functionality of the Nb to bind its antigen (i.e., EGFR-Fc) (Figure 25). Flow cytometry analysis of the transformed bacteria showed that the deletion of LysM-spacer in pNDVe did not affect the display nor the binding of the Nb, with values almost identical to the non-modified construct pNVEGFR2. On the other hand, deletion comprising LysM-spacer and the α-helices severely hindered the capacity

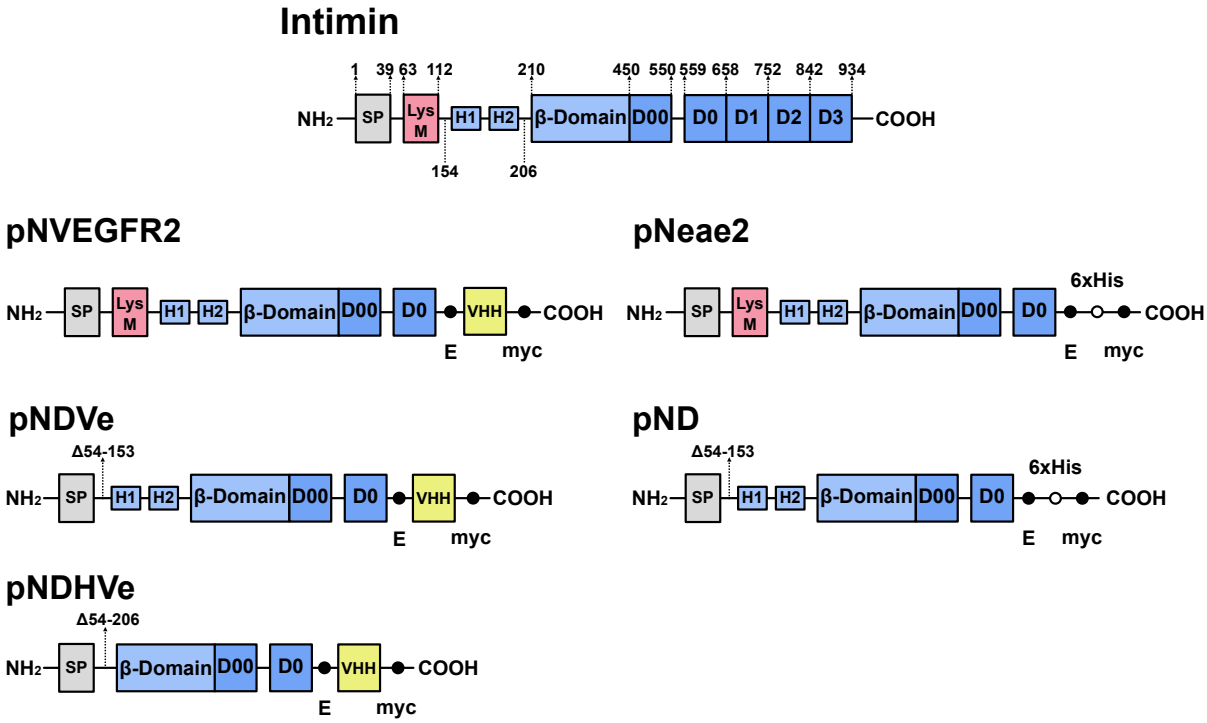

Figure 24. **Schematic representation of the full-length WT intimin and intimin constructs.** Each box delimits a different protein domain. Numbers relate to the corresponding amino acid in the EHEC intimin WT protein based on its crystal (Fairman *et al.,* 2012). The periplasmic helices region was predicted using secondary structure algorithms. Deletions are marked with the Δ symbol followed by the amino acid range deleted. SP = Signal Peptide, H = helix, D = Ig-like domain (D00, D0, etc.), E = E-tag, myc = c-myc-tag, 6xHIs = chain of six histidines. Schemes are not at scale to maintain visual clarity.

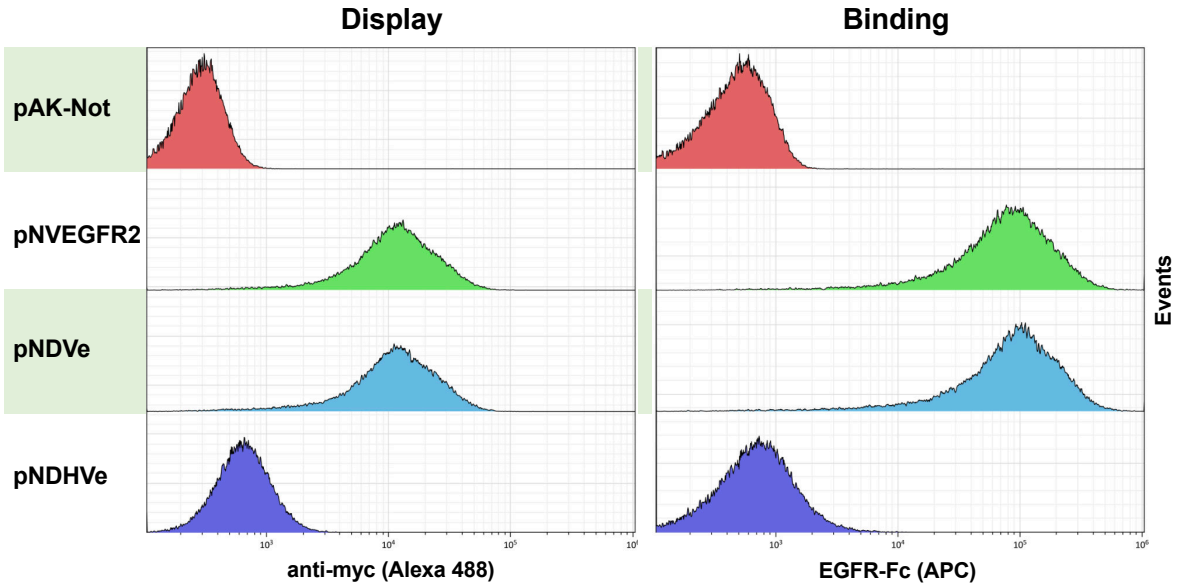

Figure 25. Surface display and antigen binding capabilities of the intimin-nanobody constructs with periplasmic deletions. Flow cytometry analysis of induced *E. coli* EcM1 bacteria carrying the empty vector (pAK-Not), the unmodified intimin-Nb fusion (pNVEGFR2), the LysM-deletion derivative (pNDVe) or the construct lacking the LysM and α-helices (pNDHVe). Left, display of the intimin proteins on the outer membrane. Histogram shows fluorescence intensity of bacteria stained with anti-myc tag mAb and secondary anti-mouse IgG-Alexa488. Right, binding of antigen by the surface displayed Nb. Histogram shows fluorescence intensity of bacteria incubated with 50 nM of biotinylated EGFR-Fc and secondary streptavidin-APC.

for both display and antigen-binding of the bacteria, which were close to the negative control (pAK-Not).

We subjected whole-cell protein samples from the above cultures to a Western blot analysis with anti-myc mAb (Figure 26). The Western blot showed that the three proteins were expressed, with protein bands having mobilities of the expected size for the full-length proteins, and of different mass according to their deletions in the N-terminal. However, deletions seemed to increase the proteolysis of the fusions *in vivo*, especially for the longer deletion, with a reduced intensity for the full-length protein band and a significant higher intensity of a band of smaller mass corresponding to a proteolytic fragment of ~40 kDa.

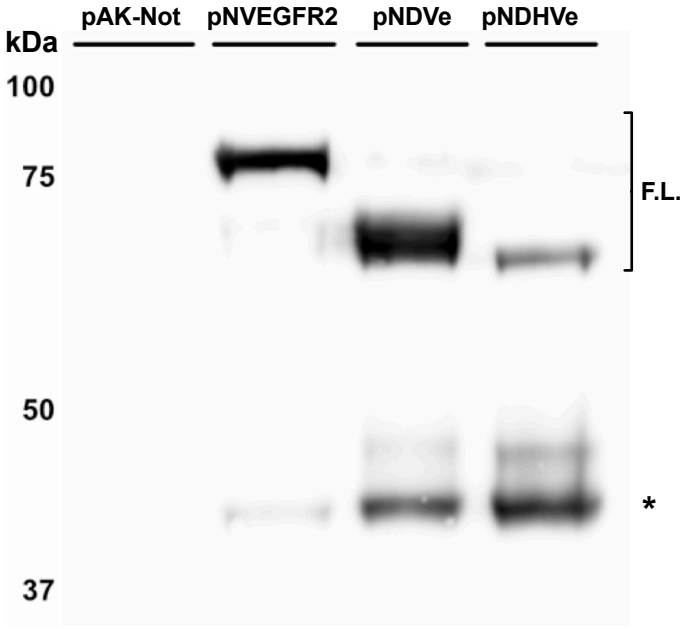

Figure 26. Western blot analysis of the expression for intimin constructs with periplasmic modifications. Samples analyzed contained whole-cell protein extracts from induced *E. coli* EcM1 cultures carrying the indicated plasmids. After electrophoresis, proteins were transferred to a membrane and incubated with anti-c-myc mouse mAb and secondary goat anti-mouse polyclonal serum conjugated with peroxidase (POD). The empty vector (pAK-Not) was used as a negative control. Molecular weights in kDa are indicated on the left. Bands corresponding to the full-length proteins are indicated as F.L. Main proteolytic fragments are indicated with an asterisk.

Taken together, the flow cytometry and Western blot results indicated that deletion of both α-helices was severely affecting the stability of intimin, suggesting an impaired folding and/or insertion in the outer membrane. At this point, we wondered whether the lack of the LysM-spacer region (LysM-deletion hereafter) may also affect the stability of the protein. We used Western blot to compare the mobility shift on SDS-PAGE of the β-barrels from unmodified intimin and the LysM-deletion mutant under denaturing (i.e., boiled in SDS-urea buffer) and non-denaturing conditions (i.e., samples in SDS-urea

buffer at room temperature) (Figure 27A). Without boiling, the unmodified intimin-Nb fusion showed an intense band of high mobility and a faint band of low mobility on SDS-PAGE. When boiled, the only band present for this parental fusion was the one with low mobility, which corresponds to the fully denatured polypeptide. These mobility shift is characteristic of OMPs containing stable β-barrels (Schnaitman, 1973) and indicate that, without boiling, the intimin β-barrel remains folded even in the presence of SDS-urea. On the other hand, the unboiled sample of the LysM-deletion mutant presented additional protein bands between those of high and low mobility, which indicated the presence of some partial unfolded states of the β-barrel. This partial unfolding in the presence of SDS-urea suggests a lower stability of the β-barrel in the LysM-deletion mutant. To rule out an effect of the Nb on the folding of the β-barrel, we performed this mobility-shift assay with constructs having a hexa histidine-tag (6xHis) instead of the Nb fused to the parental intimin fragment (pNeae2) or the LysM-deletion mutant (pND) (Figure 27B). Results were similar to those observed with the fusions having the Nb, showing that the lower stability of the β-barrel of the LysM-deletion mutant is not due to the Nb. Interestingly, the proteolytic bands of ~40 kDa were not present here, which suggested that they may result from cleavage of a C-terminal fragment containing the Nb and myc-tag. We also examined the effect of the presence of 2-ME in these samples, but this reducing agent of disulfide bridges did not affect differently the protein samples. Therefore, these results suggested a role of the periplasmic LysM in the stability of the OM β-barrel of intimin. Although we cannot exclude a direct interaction between these different domains, it is more likely that LysM plays an indirect role due to its binding to the PG (Leo, Oberhettinger, Chaubey, et al., 2015). LysM's binding to the PG could stabilize intimin in the bacterial envelope and in the SDS-urea sample buffer.

Next, we tested whether lack of the LysM and spacer region could prevent formation of intimin homodimers. Thus, we investigated the oligomerization state of intimin constructs with and without the LysM-deletion. To avoid any potential interference of the Nb in the oligomerization state, we used the constructs having the 6xHis peptide tag. In our first approach we performed a crosslinking assay using bacteria expressing these intimin fusions. We used different concentrations of the dithiobis(succinimidyl propionate) (DSP) crosslinker agent on the intact bacteria, and the resulting samples were subjected to SDS-PAGE and Western blot. We found that both wild-type and LysM-deletion constructs presented crosslinking bands with an apparent size close to the expected size of the corresponding protein dimers (Figure 28A). These bands were absent in the crosslinked samples treated with the reducing agent 2-ME, which reduces the disulfide bridge present in the DSP reagent, cleaving the protein crosslinks (Figure 28B).

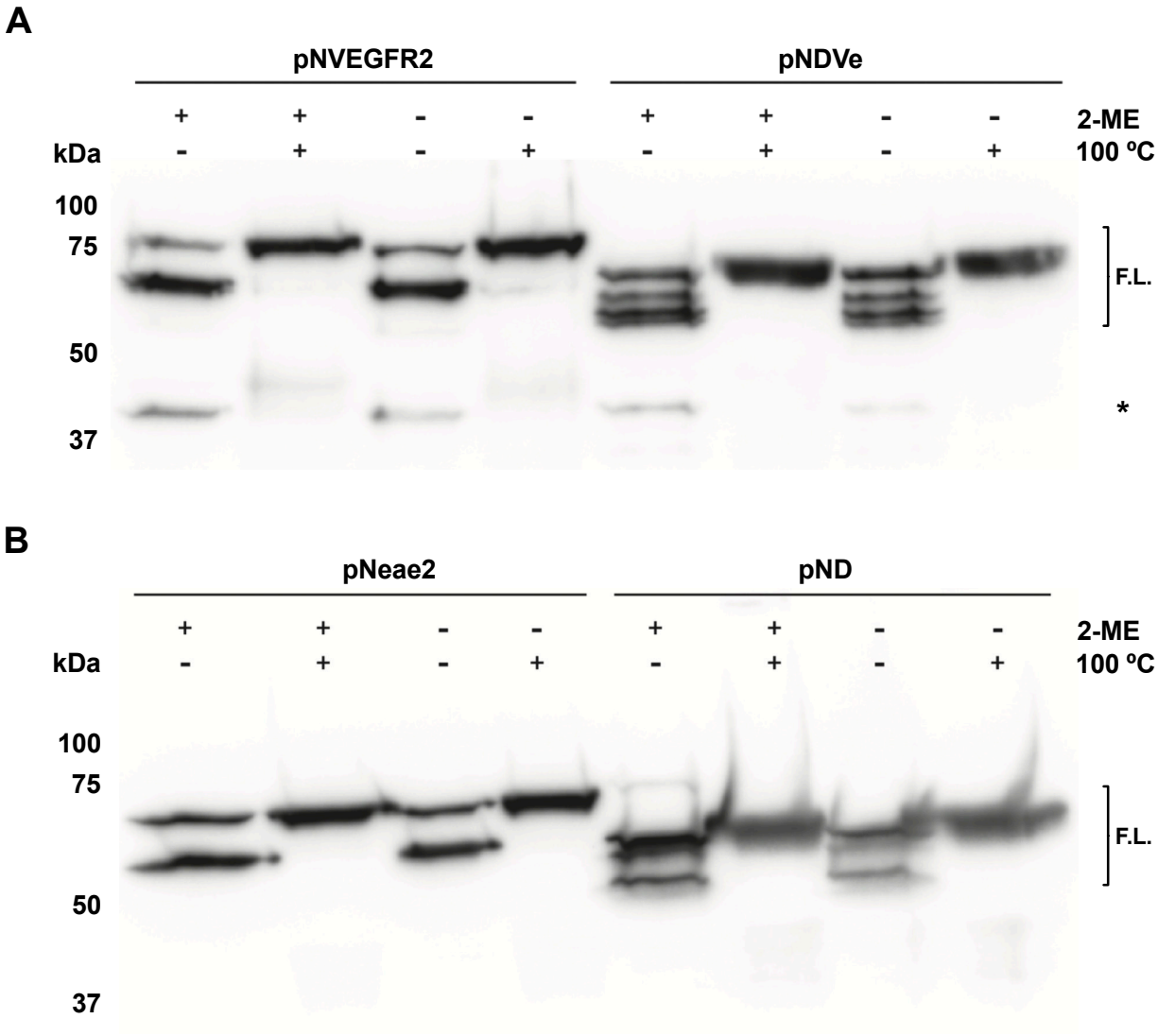

Figure 27. Western blot analysis of the effect of the LysM-deletion on the stability of the intimin β-barrel. Western blot analysis of whole-cell protein extracts from induced *E. coli* EcM1 cultures carrying **(A)** plasmids with parental intimin-Nb fusion (pNVEGFR2) and lacking the LysM domain and spacer (pNDVe) **(B)** intimin constructs with a C-terminal 6xHis peptide from parental (pNeae2) and LysM-deletion mutant (pND). Samples were boiled or not in an SDS-urea loading buffer with or without β-mercaptoethanol (2-ME)**.** After electrophoresis, proteins were transferred to a membrane and incubated with anti-c-myc mouse mAb and secondary goat anti-mouse polyclonal serum conjugated with peroxidase (POD). Molecular weight markers are indicated on the left (in kDa). Bands corresponding to the full-length proteins are indicated as F.L. Main proteolytic fragments are indicated with an asterisk.

This result was compatible with the formation of homodimers by both the WT and the LysM mutant.

To confirm this result, we extracted the proteins from the OM fractions (Materials and methods: Outer membrane protein extraction) of induced bacteria having pNeae2 or pND constructs. Samples were run in native conditions by BN-PAGE and transferred to

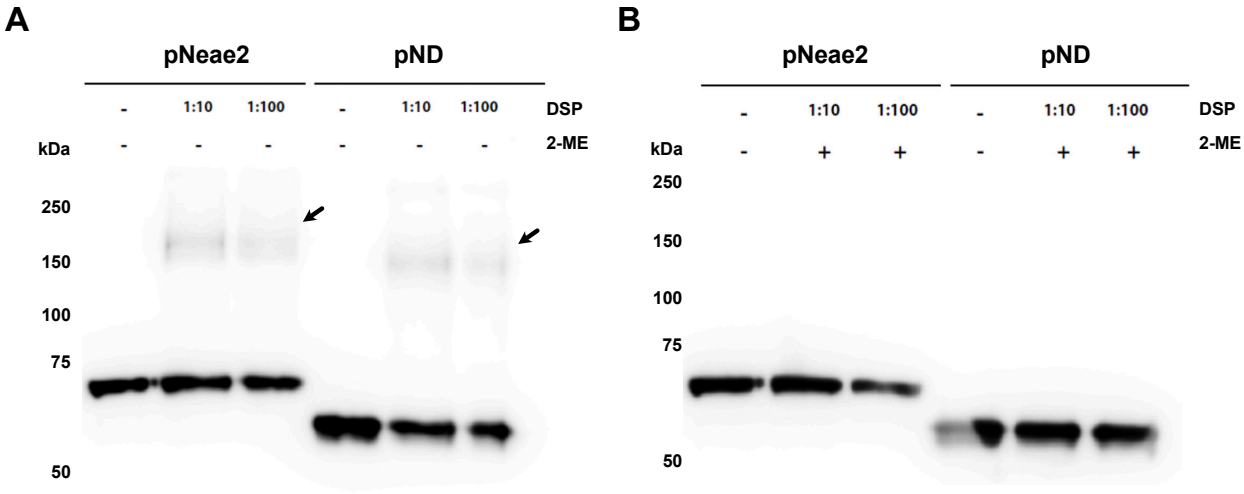

Figure 28. Crosslinking of intimin constructs with and without the LysM-deletion using DSP. Western blot analysis of whole-cell protein extracts from induced *E. coli* EcM1 cultures carrying plasmids expressing intimin constructs with a C-terminal 6xHis peptide from parental (pNeae2) and LysM-deletion mutant (pND). **(A)** Samples of whole-cell bacteria treated with increasing concentrations of DSP and no 2-ME in the loading buffer. **(B)** Samples of whole-cell bacteria treated with increasing concentrations of DSP and 2-ME in the loading buffer**.** After electrophoresis, proteins were transferred to a membrane and incubated with anti-c-myc mouse mAb and secondary goat anti-mouse polyclonal serum conjugated with peroxidase (POD). Molecular weight standards are indicated on the left (in kDa). Arrows indicate bands of a molecular weight compatible with the formation of homodimers.

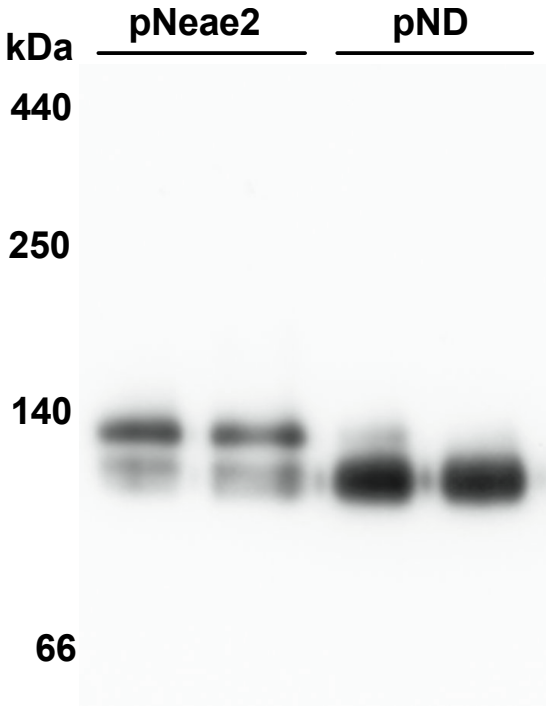

Figure 29. BN-PAGE analysis of the quaternary structure of intimin constructs with or without the LysM-deletion. Protein samples were extracted from the OM of cultures of *E. coli* EcM1 carrying the intimin-6xHis constructs with (pNeae2) and without (pND) LysM. Extraction was performed using the zwitterionic detergent Zwittergent 3-14 (see Material and methods: Outer membrane protein extraction). Samples were analyzed by electrophoresis in native conditions to maintain any oligomeric interaction (BN-PAGE). For Western blot, the resulting gel was transferred to a membrane and incubated with anti-c-myc mouse mAb and secondary goat anti-mouse polyclonal serum conjugated with peroxidase (POD). Native molecular weights in kDa are indicated on the left.

a membrane for Western blot developed with anti-myc mAb (Figure 29). This analysis revealed that both intimin constructs produced protein bands with apparent molecular masses that are consistent to the formation of homodimers. Taking together protein crosslink and mobility on native BN-PAGE, our data indicated that the LysM-deletion in intimin did not prevent its dimerization in the outer membrane. This conclusion meant that we could not use intimin-based proteins as the only components of an OM sensor relying on antigen-driven dimerization, as the endogenous dimer formation of intimin would trigger a constant activation of the system. However, intimin constructs could potentially be used in combination with other OMPs capable of displaying Nbs.

2.1.2. Modification of the periplasmic region of the intimin LysM-deletion mutant with protein fragments of a reporter system.

Before exploring the use of intimin constructs in combination with other OMPs, we still needed to test its capacity to tolerate the fusion in its periplasmic side of proteins fragments that could be employed in the generation of a periplasmic signal. Since deletion of LysM may improve the diffusion of the protein in the outer membrane, and thus, its possibility to interact with other OMPs, we chose the intimin-Nb construct lacking LysM (pNDVe) as the basis of our future sensor constructs. It is important to note that the LysM-deletion did not have any impact on the surface display of the intimin construct or the antigen binding activity of the Nb.

Next, we chose a protein reporter for testing dimerization of periplasmic domains linked to intimin. We selected the NanoBiT system (Dixon et al., 2016) as a reporter candidate. NanoBiT is a protein complementation assay based on a split NanoLuc luciferase with two protein fragments: the small SmBiT, a 1.3 kDa-peptide, and the large LgBiT, an 18 kDa-polypeptide. NanoBiT is able to emit light once the two protein fragments interact to reconstitute the NanoLuc luciferase. However, this association *in vivo* is neglectable unless these fragments are linked to a pair of interacting proteins, constituting an excellent reporter for protein-protein interactions. Furthermore, the bioluminescence assay of NanoLuc is reported to be very sensitive, simple, fast, and robust at different temperatures (England et al., 2016). In addition, NanoLuc has been fused to recombinant antibodies expressed in the periplasm of *E. coli* (Boute et al., 2016), which indicates the proper folding of this luciferase in the bacterial periplasm. For all these reasons, we selected SmBiT and LgBiT fragments as candidates to be fused to the periplasmic side of the intimin construct.

Both SmBiT and LgBiT were cloned into the pNDVe plasmid in frame between the amino acids 43 and 154 of intimin, using the inserted EcoRI and SacII restriction sites. These fusions placed the NanoBiT fragments in the periplasmic domain of the intimin-Nb fusion, between the N-terminal SP and the periplasmic α-helices. Two Gly-Ser flexible peptide linkers (GGGS) were placed at both ends of the NanoBiT fragments. The plasmid carrying the SmBiT was named pNDVeSB and the one carrying the LgBiT was named pNDVeLB (Figure 30).

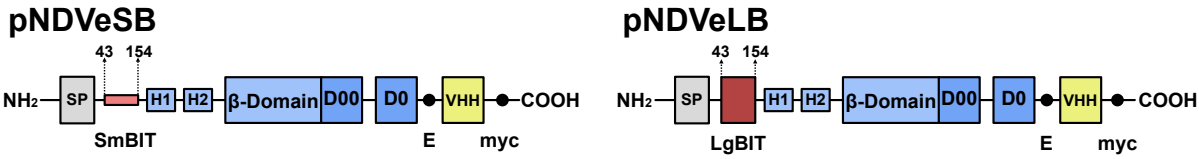

Figure 30. **Schematic representation of the intimin-nanobody constructs with the LysM-deletion fused to the NanoBiT fragments.** Each box delimits a different protein domain. Numbers relate to the corresponding amino acid in the intimin WT protein based on its crystal (Fairman *et al.,* 2012). SP = Signal Peptide, H = helix, D = Ig-like domain, E = E-tag, myc = c-myc-tag. Size is not proportional to maintain visual clarity

We used flow cytometry to test the display and antigen binding capabilities of these constructs (Figure 31). The protein fusion to the SmBiT fragment showed display and antigen binding values almost identical to the parental fusion NVDe, indicating that the presence of the SmBiT fragment did not affect insertion into the outer membrane or the functionality of the displayed Nb. However, on contrast, the protein fusion to LgBiT showed a significant reduction in the surface display levels, with values of ~35% of the parental, and even a higher difference in antigen binding activity (~20% of the parental). Western blot analysis of whole-cell protein extracts from these cultures (Figure 32) showed similar expression levels of NDVe and NDVeSB fusions, with the small difference in size (11 aas) not detectable by SDS-PAGE. The protein sample from bacteria carrying pNDVeLB presented a main protein band of larger size, as expected for the insertion of the LgBiT 158 residues, and a faint band of lower size, similar to parental fusion, suggesting some proteolysis of the LgBiT fragment. Attempts to extend the induction time resulted in a loss of display and binding for this large fusion, as well as increased proteolysis (data not shown).

We used the deep-learning algorithm AlphaFold (Jumper et al., 2021) to predict the structure of the protein fusion to the LgBiT fragment. The prediction estimated a correct folding of all the domains, including the LgBiT, which was placed in the periplasm and linked to the β-barrel of the construct through highly flexible helices (Figure 33).

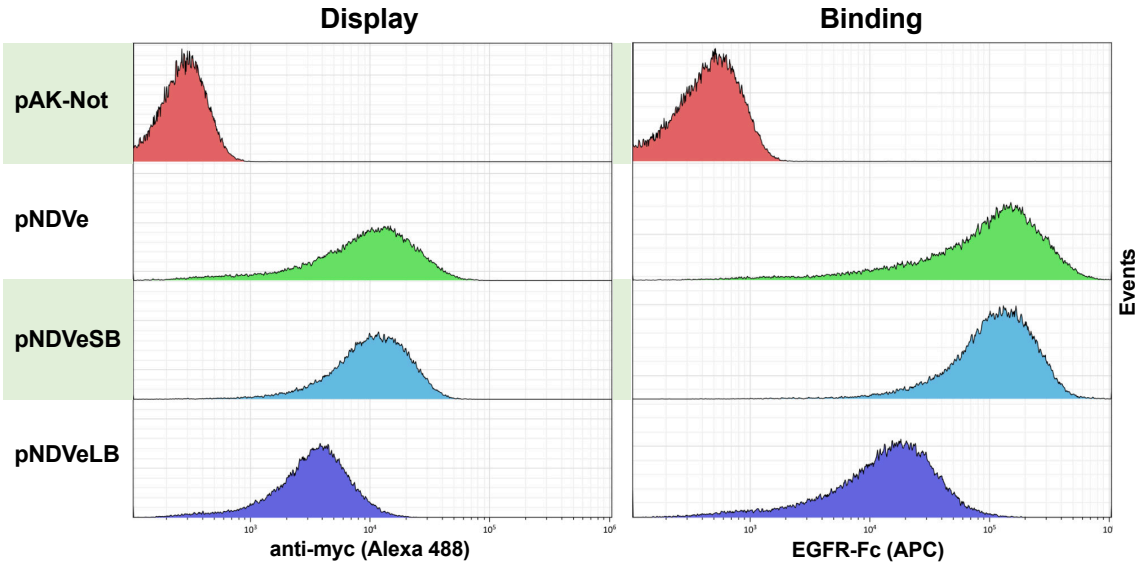

Figure 31. Display and antigen binding capabilities of intimin-nanobody constructs with the LysM-deletion fused to the NanoBiT fragments. Flow cytometry analysis of induced *E. coli* EcM1 bacteria carrying the empty vector (pAK-Not) or the intimin construct lacking LysM with no fusion (pNDVe) with the SmBiT fragment (pNDVeSB) or the LgBiT fragment (pNDVeLB). Left, display of the constructs in the outer membrane. Histogram shows fluorescence intensity of bacteria stained with anti-myc tag mAb and secondary anti-mouse IgG-Alexa488. Right**,** binding of antigen by the displayed Nb. Histogram shows fluorescence intensity of bacteria incubated with 50 nM of biotinylated EGFR-Fc and secondary streptavidin-APC.

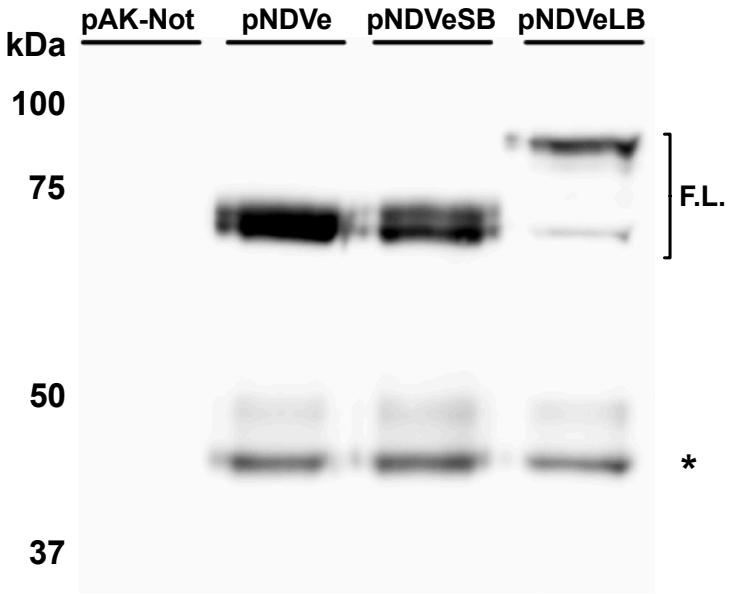

Figure 32. Western blot analysis of the expression of intimin-nanobody constructs lacking LysM and spacer with periplasmic fusions to the NanoBiT fragments. Samples analyzed contain whole-cell protein extracts from induced *E. coli* EcM1 cultures carrying the empty vector (pAK-Not) or the intimin construct with the LysM-deletion and either no fusion (pNDVe), the SmBiT fragment (pNDVeSB) or the LgBiT fragment (pNDVeLB). After electrophoresis, proteins were transferred to a membrane and incubated with anti-c-myc mouse mAb and secondary goat anti-mouse polyclonal serum conjugated with peroxidase (POD). The empty vector (pAK-Not) was used as a negative control. Molecular weight markers in kDa are indicated on the left. Bands corresponding to the full-length proteins are indicated as F.L. Main proteolytic fragments are indicated with an asterisk.

The above results suggested that the LysM-deleted intimin-Nb construct NDVe can be fused to small peptides in its periplasmic region without alterations in surface display or antigen-binding levels, but larger polypeptide fragments are not well tolerated and reduce the expression levels and binding activity of the fusion. The presence of large folded fragments in the periplasm might be interfering with the process of insertion of the β-barrel in the outer membrane through the BAM complex (Tomasek et al., 2020) and/or the translocation of its passenger (Nb) (Doyle & Bernstein, 2021). Therefore, we thought of an alternative that could allow the covalent linkage of large protein reporters once the protein fusion was already correctly inserted in the outer membrane. The SpyTag-SpyCatcher and SnoopTag-SnoopCatcher are homologous but orthogonal systems that allow the post-translational fusion of proteins (Hatlem et al., 2019). Both are derived from fimbrial subunits from *Streptococcus* species with an intradomain isopeptide bond. These fimbrial domains can be split into a small peptide (the Tag) that forms a covalent isopeptide bond with the large fragment of the domain (the Catcher), which is catalytically active. Each of these components of a pair can be fused to different proteins to covalently link them through an isopeptide bond. This strategy has been previously used in the production of vaccines and the stabilization of multiprotein complexes (Hatlem et al., 2019).

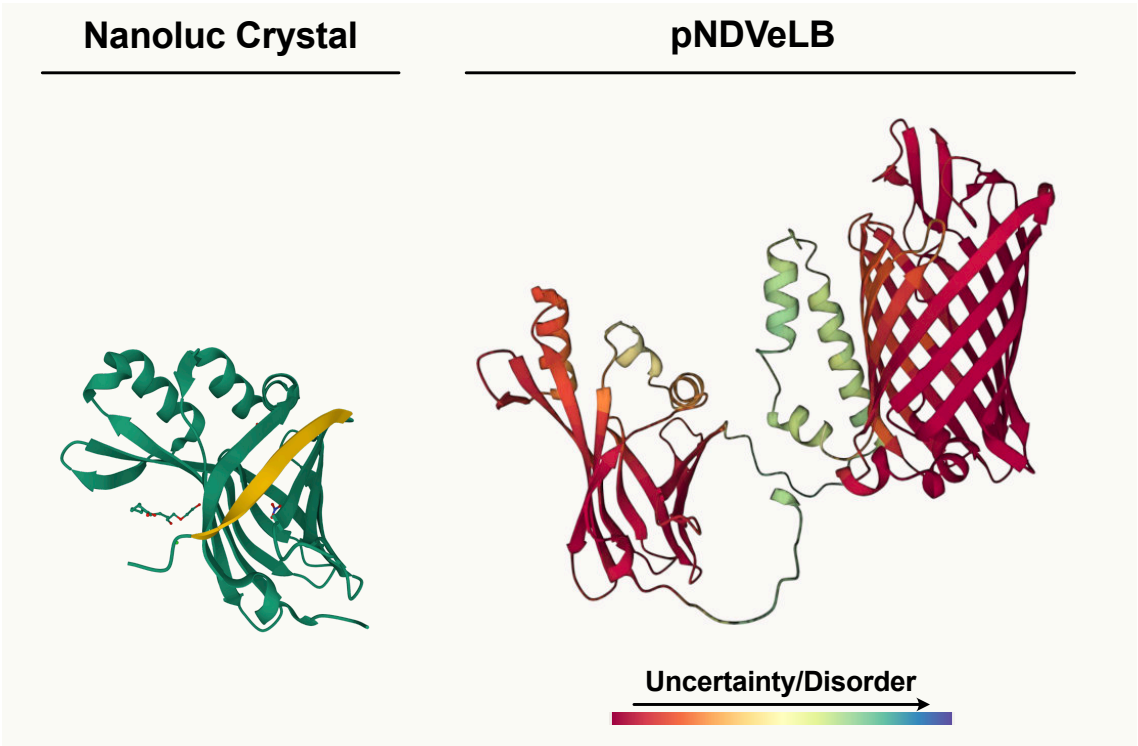

Figure 33. AlphaFold prediction of the structure of the intimin-nanobody construct lacking LysM and spacer with the periplasmic fusion to the LgBiT fragment. Detail of the β-barrel, periplasmic helices and LgBiT domain (right). The full-length NanoLuc crystal (PDB 7MJB) is shown in the left, with the β-strand corresponding to the SmBiT colored in yellow.

In our system, the Tag-Catcher partners could be used to covalently attach a large fragment of a reporter enzyme in the periplasm, fused to a Catcher domain, if a small Tag peptide is placed in the periplasmic domain of intimin. Thus, we decided to test the tolerance of the NVDe fusion to both SpyTag and SnoopTag peptides, generating similar plasmid constructs pNDVeSpy and pNDVeSnoop, respectively (Figure 34). As could be expected from the results with SmBiT fusion, these small peptide tags did not affect the surface display nor the antigen binding activity of the protein fusions as determined by flow cytometry (Figure 35). Also, the expression levels of these protein fusions were found similar to the parental NVDe construct in Western blot (Figure 36).

Therefore, through this section we have developed a new set of intimin-Nb fusions that, although maintain the dimeric nature of intimin after deletion of the LysM domain, were able to simultaneously display a functional Nb on the bacterial surface and a peptide or polypeptide fragment in the periplasm. These constructs show great potential for the development of an outer membrane sensor. However, before proceeding, it was necessary to identify a suitable partner that would not undergo spontaneous dimerization with intimin.

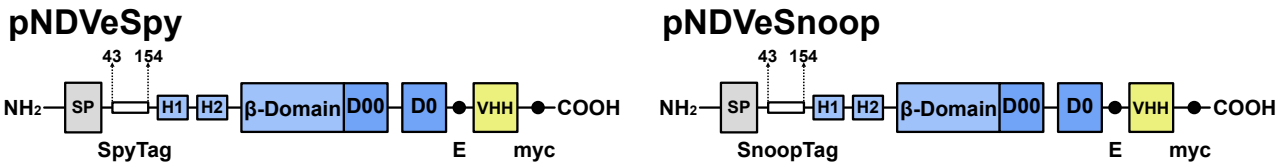

Figure 34. **Schematic representation of the intimin-nanobody constructs with the LysM-deletion fused to SpyTag or SnoopTag.** Each box delimits a different protein domain. Numbers relate to the corresponding amino acid in the intimin WT protein based on its crystal (Fairman *et al.,* 2012). SP = Signal Peptide, H = helix, D = Ig-like domain, E = E-tag, myc = c-myc-tag, Schemes not in scale to maintain visual clarity.

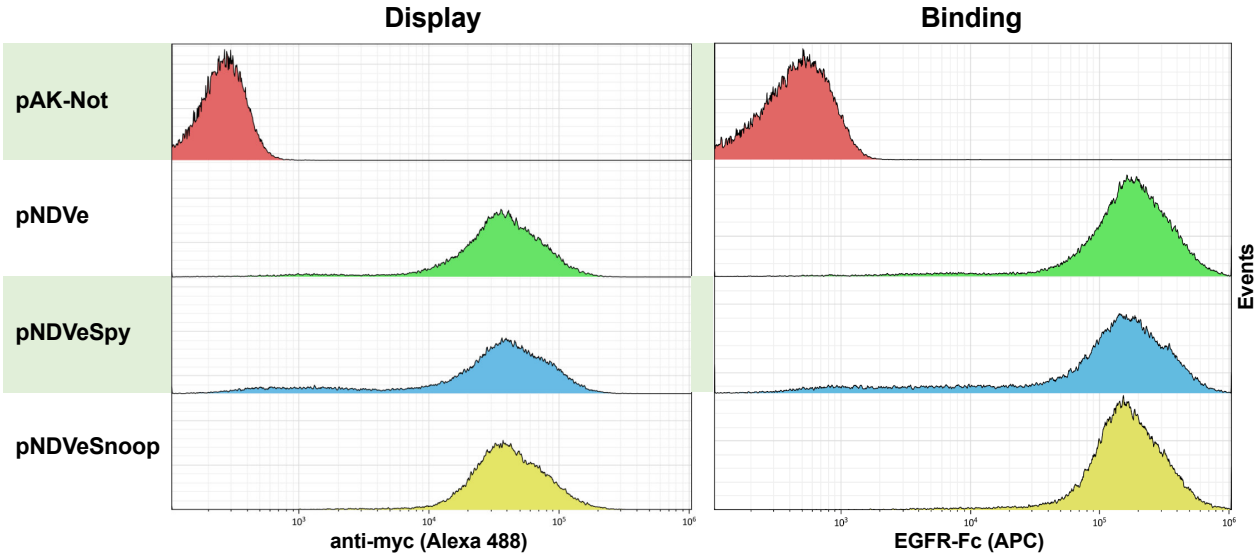

Figure 35. Display and antigen binding capabilities of intimin-nanobody constructs with the LysM-deletion fused to the Spy and Snoop tags. Flow cytometry analysis of induced *E. coli* EcM1 bacteria carrying the empty vector (pAK-Not) or the intimin construct lacking LysM with no tag (pNDVe), with the SpyTag (pNDVeSpy), or the SnoopTag (pNDVeSnoop). Left, display of the constructs in the outer membrane. Histogram shows fluorescence intensity of bacteria stained with anti-myc tag mAb and secondary anti-mouse IgG-Alexa488. Right, binding of antigen by the displayed Nb. Histogram shows fluorescence intensity of bacteria incubated with 50 nM of biotinylated EGFR-Fc and secondary streptavidin-APC.

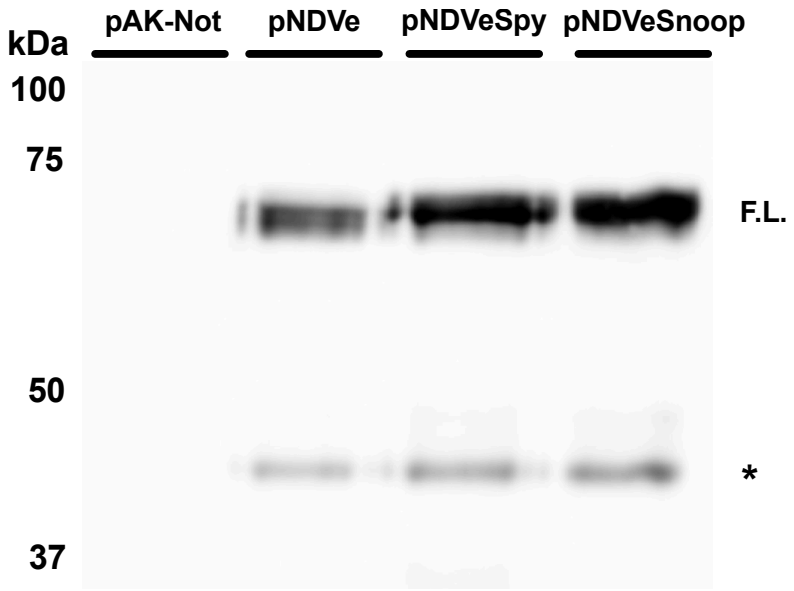

Figure 36. Western blot analysis of the expression of intimin-nanobody constructs with the LysM-deletion and periplasmic fusions to the Spy and Snoop tags. Samples analyzed contain whole-cell protein extracts from induced *E. coli* EcM1 cultures carrying the empty vector (pAK-Not) or the intimin construct lacking LysM with no fusion (pNDVe) with the SpyTag (pNDVeSpy) or with the SnoopTag (pNDVeSnoop). After electrophoresis, proteins were transferred to a membrane and incubated with anti-c-myc mouse mAb and secondary goat anti-mouse polyclonal serum conjugated with peroxidase (POD). The empty vector (pAK-Not) was used as a negative control. Molecular weights in kDa are indicated on the left. Bands corresponding to the full-length proteins are indicated as F.L. Main proteolytic fragments are indicated with an asterisk.

2.2. Engineering autotransporters for outer membrane sensors.

2.2.1. Engineering the EhaA autotransporter.

Our laboratory reported that Nbs can be displayed on the bacterial surface with the N-terminal fragment of intimin, Neae, but also with the C-terminal β-barrel domain of the EhaA AT from the EHEC O157:H7 strain (Salema et al., 2013). Despite showing lower display levels than intimin Neae, the EhaA β-barrel domain presented monomeric behavior (Marin et al., 2010), which could be advantageous for the development of our outer membrane sensors.

Hence, we first cloned the Nb binding human EGFR fused to the C-terminal β-barrel domain of EhaA (C-EhaA). To this end, we replaced the anti-GFP Nb found in a similar fusion, encoded by pVgfpA (Salema et al., 2013), generating the plasmid derivative pVeA. In agreement with previous data, surface display and antigen binding levels of this construct were found to be low when compared to those of pNDVe (compare Figure 25 with Figure 38).

EhaA, as all classical ATs, does not present a periplasmic domain (Meuskens et al., 2019; Wells et al., 2008). The C-terminal amino acid of the last β-strand is an aromatic phenylalanine (F) that faces the periplasm and is expected to be in contact with the phospholipids in the inner leaflet of the outer membrane. The β-strands of OMPs frequently contain aromatic residues (F or W - tryptophane) whose sidechains point to the polar head groups of phospholipids and which have been proposed to anchor the protein in the membrane (Koebnik et al., 2000). The C-terminal β-strand of all OMPs ends with an aromatic residue, and its mutagenesis reduces, but not completely abrogates, membrane insertion (Koebnik, 1999). We speculated that a direct link of a large protein domain to this last aromatic amino acid could disturb the stability of the β-barrel and searched for peptide linkers found in natural OMPs having a globular periplasmic domain.

The OMP OmpA from *E. coli* is composed of an N-terminal β-barrel embedded in the outer membrane, with a terminal F residue in the last β-strand, followed by a C-terminal periplasmic domain (Ortiz-Suarez et al., 2016). These two domains are connected through an unstructured 17-aa linker (GQGEAAPVVAPAPAPAP) that functions as a PG clamp (Samsudin et al., 2016). We chose the first three aa of the linker (GQG) and used them to connect the C-terminal end of EhaA β-barrel to the NanoBit domains preceded by a flexible GGGS linker, obtaining the plasmids pVeASB and pVeALB (Figure 37). Flow cytometry analysis of these constructs showed that, in a similar situation to

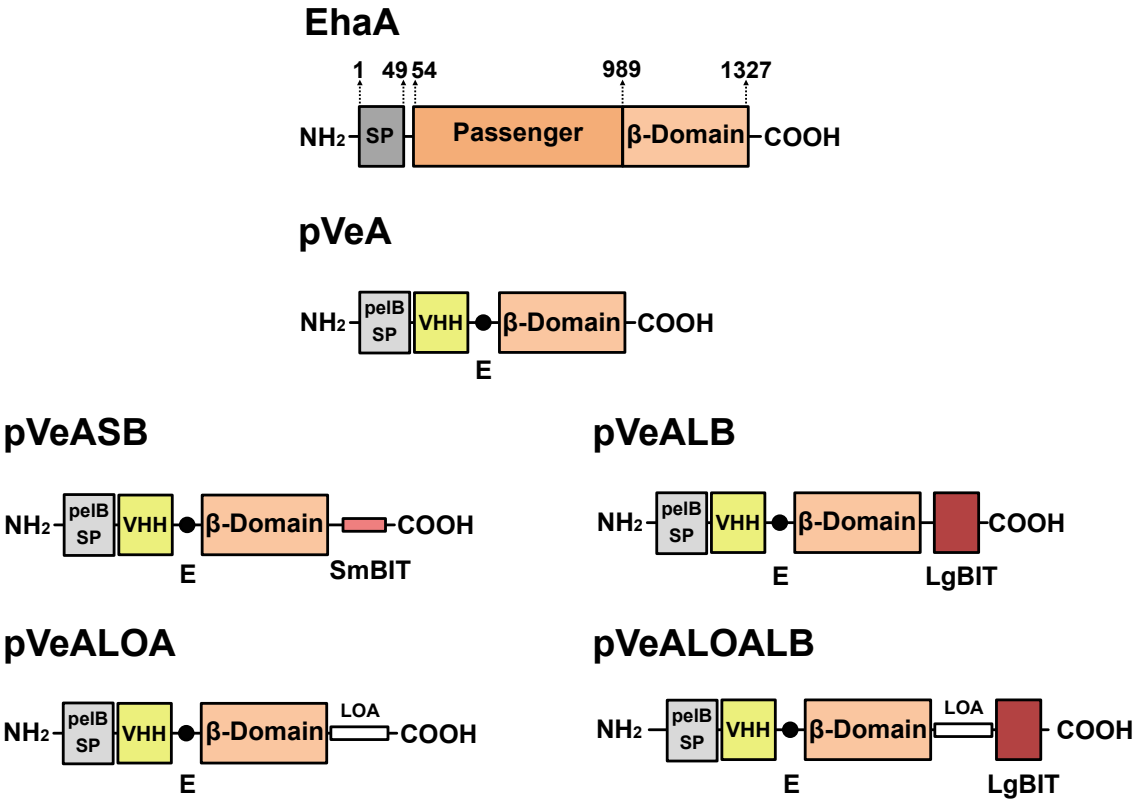

Figure 37. **Schematic representation of the full-length WT EhaA and EhaA-nanobody constructs.** Each box delimits a different protein domain. Numbers relate to the corresponding amino acid in the EhaA WT protein. SP = Signal Peptide, E = E-tag, LOA= Linker OmpA full-length. Size is not proportional to maintain visual clarity.

intimin-based fusions, the small peptide SmBiT did not hinder the display nor the antigen binding of the Nb, whereas the LgBiT fragment made the display and binding signals drop to values close to the negative control. Western blot analysis of whole-cell protein extracts from the induced cultures showed that both constructs were expressed, with the LgBiT chimera even being expressed at higher levels than the SmBiT fusion.

We suspected then that the close presence of a large, folded domain could be affecting the insertion and folding of the EhaA β-barrel despite the presence of the short peptide linkers connecting them. To increase the distance between these protein domains, we tested the full-length linker of OmpA (LOA) to directly attach the LgBiT domain to the β-barrel, creating the plasmid pVeALOALB. As a control, we fused the LOA to the barrel without LgBiT, generating pVeALOA. Flow cytometry of induced bacteria with these constructs revealed that the LOA did not affect the surface display or antigen binding signals of pVeA (Figure 38). Moreover, the presence of LOA was capable of restoring the surface display and antigen binding activity to the fusion carrying LgBiT, showing values similar to the positive control pVeA. Western blot analysis of bacteria from these

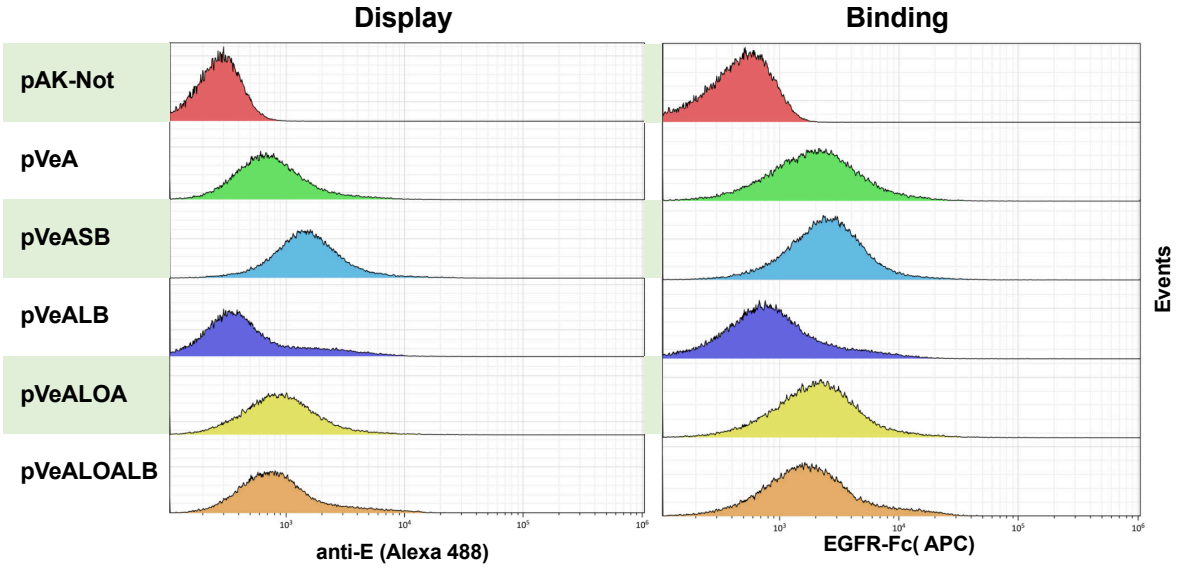

Figure 38. Display and antigen binding capabilities of EhaA-nanobody constructs with and without periplasmic fusions. Flow cytometry analysis of induced *E. coli* EcM1 bacteria carrying the empty vector (pAK-Not) or the EhaA-Nb constructs with either no periplasmic fusion (pVeA), or a fusion to either the SmBIT fragment (pVeASB), the LgBiT domain (pVeALB), the full linker of OmpA (pVeALOA) or the full linker of OmpA and the LgBiT domain (pVeALOALB). Left, display of the constructs in the outer membrane. Histogram shows fluorescence intensity of bacteria stained with anti-E tag mAb and secondary anti-mouse IgG-Alexa488. Right, binding of antigen by the displayed Nb. Histogram shows fluorescence intensity of bacteria incubated with 50 nM of biotinylated EGFR-Fc and secondary streptavidin-APC.

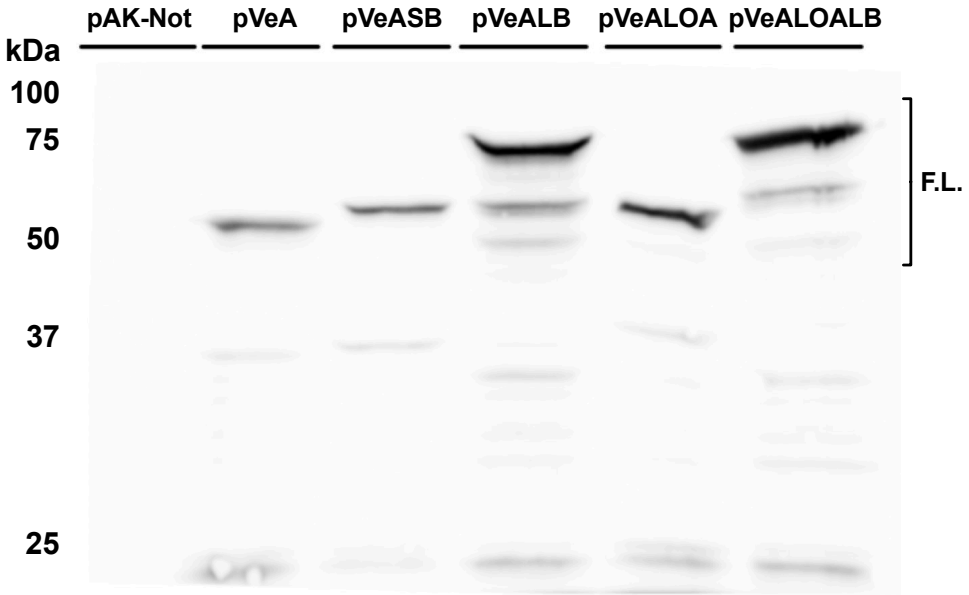

Figure 39. Western blot analysis of the expression of EhaA-nanobody constructs with or without periplasmic fusions. Samples analyzed contain whole-cell protein extracts from induced *E. coli* EcM1 cultures carrying the empty vector (pAK-Not) or EhaA-Nb constructs with either no periplasmic fusion (pVeA), the SmBIT fragment (pVeASB), the LgBiT fragment (pVeALB), the full linker of OmpA (pVeALOA) or the full linker of OmpA and the LgBiT fragment (pVeALOALB) After electrophoresis, proteins were transferred to a membrane and incubated with anti-E mouse mAb and secondary goat anti-mouse polyclonal serum conjugated with peroxidase (POD). The empty vector (pAK-Not) was used as a negative control. Molecular weights in kDa are indicated on the left. Bands corresponding to the full-length proteins are indicated as F.L.

cultures showed the expected pattern of protein bands for these constructs according to their mass, with no signs of higher proteolysis (Figure 39). In fact, we observed higher expression levels in the protein fusions carrying both LgBiT and LOA.

We used AlphaFold to predict the structure of these constructs. The algorithm predicted that the β-barrel is correctly folded in all constructs and expected a flexible unstructured region for the peptides SmBiT and LOA. Interestingly, AlphaFold predicted a highly disorganized LgBiT domain in the case of pVeALB, with limited confidence in the result. The prediction of a folded LgBiT domain improved once the LOA was used to increase the distance between the β-barrel and the LgBiT fragment (Figure 40).

At this point, we had generated a potential partner for the intimin-based constructs with SmBiT and LgBiT reporter system. EhaA-based fusions could be engineered to display a Nb while simultaneously carrying a periplasmic reporter. However, as the expression levels of these constructs remained relatively low compared to intimin fusions, we made the decision to explore other AT proteins that could be modified in a similar manner but expressed at higher levels.

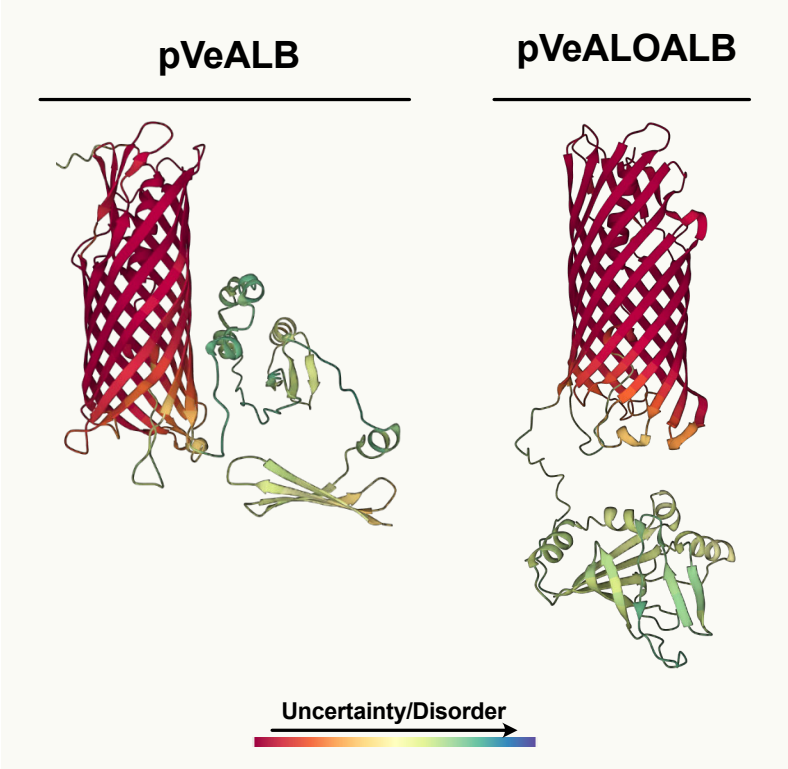

Figure 40. AlphaFold prediction of the structures of the EhaA-nanobody constructs with fusions to the LgBiT fragment or the LOA and LgBiT fragment. Detail of the β-barrel and the periplasmic LgBiT and LOA-LgBiT fusions.

2.2.2. Engineering of other autotransporters.

In an effort to expand our chimeric OMP repertoire, we selected different monomeric AT proteins from *E. coli* that had been previously reported to allow the surface display of protein fusions. We chose the pVeALOALB construct, having the EhaA β-barrel, LOA and LgBiT, and replaced the EhaA fragments for homologous fragments from the AIDA-I AT (residues 793 through 1286) (Gustavsson et al., 2011) and the EspP AT (residues 999 through 1300, with a D1120N mutation to avoid the autoproteolytic cleavage of the passenger domain) (Binder et al., 2010). However, these constructs failed to display the Nb in the OM for unknown reasons and were discarded (data not shown).

We then tested the *flu* AT, also known as Antigen43 (Ag43), as our next candidate β-barrel. Following the results of Jong et al., 2018, we selected the last 330 aa of Ag43 and used it as the β-barrel for the chimeric protein fusions with the Nb EGFR and either no periplasmic fusion (pVeF330), the LOA-SmBiT fusion (pVeF330SB), or the LOA-LgBiT fusion (pVeF330LB) (Figure 41). Flow cytometry analysis of surface display and antigen binding of these new constructs is shown in Figure 42. These constructs showed

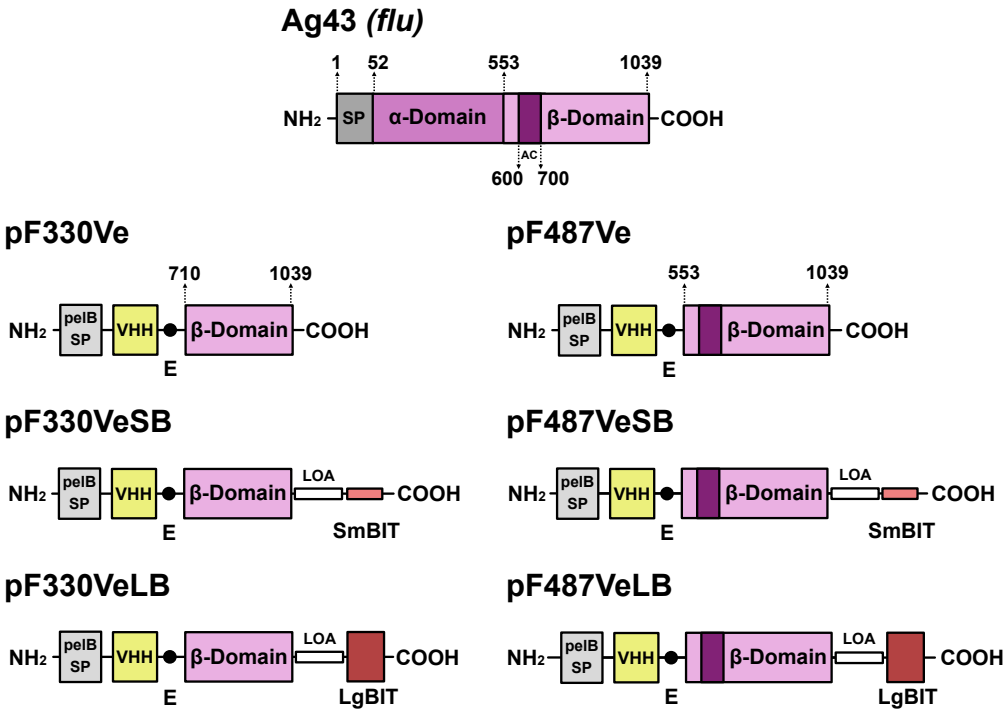

Figure 41. Schematic representation of the full-length WT Ag43 and Ag43-nanobody constructs using the last 330 or 487 Ag43 residues. Each box delimits a different protein domain. Numbers relate to the corresponding amino acid in the Ag43 WT protein. SP = Signal Peptide, AC = Autochaperone domain, E = E-tag, LOA= Linker OmpA full-length. Schemes are not at scale to maintain visual clarity.

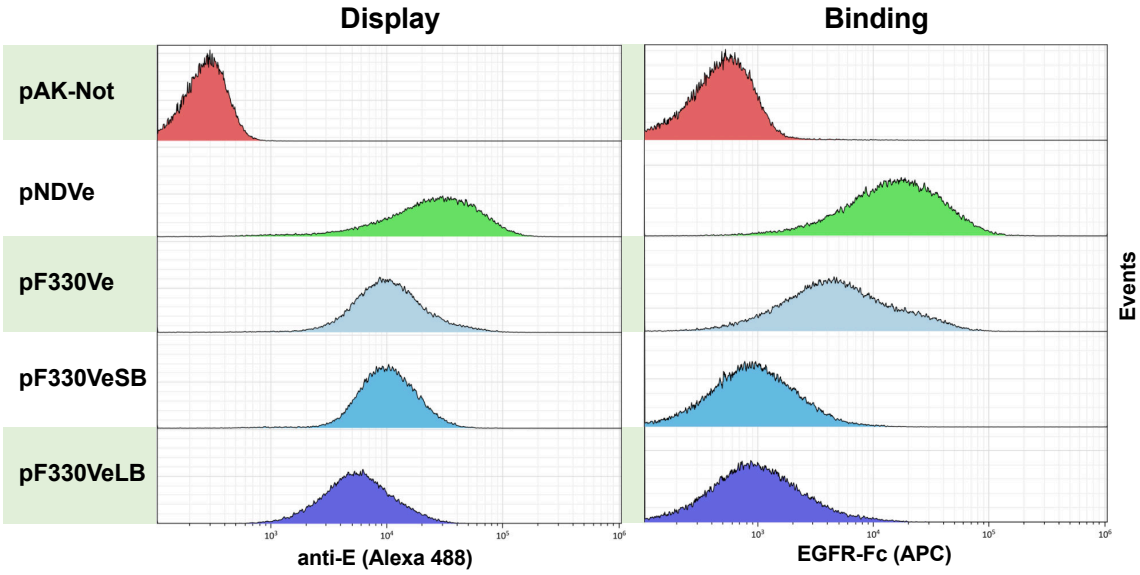

Figure 42. Display and antigen binding capabilities of the constructs combining the last 330 residues of Ag43 with a nanobody and periplasmic fusions to NanoBiT fragments. Flow cytometry analysis of induced *E. coli* EcM1 bacteria carrying the empty vector (pAK-Not) or the flu330-Nb construct with either no periplasmic fusion (pF330Ve), the LOA-SmBIT fusion (pF330VeSB) or the LOA-LgBiT fusion (pF330VeLB). The intimin construct pNDVe was used as a positive control. Left, display of the constructs in the outer membrane. Histogram shows fluorescence intensity of bacteria stained with anti-E tag mAb and secondary anti-mouse IgG-Alexa488. Right, binding of antigen by the displayed Nb. Histogram shows fluorescence intensity of bacteria incubated with 50 nM of biotinylated EGFR-Fc and secondary streptavidin-APC.

higher display levels than those with the EhaA β-barrel, with values close to the intimin fusions. However, surprisingly for us, the antigen binding capabilities of the fusions did not correlate with their display levels, with the constructs having either of the periplasmic fusions, SmBiT or LgBiT, showing very low binding signals.

We wondered whether the binding activity of the Nb in these constructs could be suffering from steric hindrance due to its close location to the extracellular part of the Ag43 β-barrel (Figure 43). To test this hypothesis, we generated a longer version of the *flu* β-barrel for these constructs using the last 487 amino acids (Dvořák et al., 2020; Muñoz-Gutiérrez et al., 2014). The new plasmids, named pVeF487, pVeF487SB and pVeF487LB, were also analyzed by flow cytometry for surface display and antigen binding. Once again, results showed that surface display was high, similar to the intimin control, but binding of antigen was not happening, with values equivalent to the negative control strain even for the strain having no periplasmic fusion (Figure 44). The molecular explanation of this behavior of the *flu* β-barrel remains unclear to us, but regardless of the reason behind the lack of antigen binding, this excluded *flu* (Ag43) for our purposes.

After these attempts to obtain different ATs as partners for the development of an OM sensor system, our data only confirmed the potential EhaA β-barrel as a viable option.

Nevertheless, the low surface display and antigen binding activity of EhaA constructs promoted us to consider the β-barrel of other OMPs.

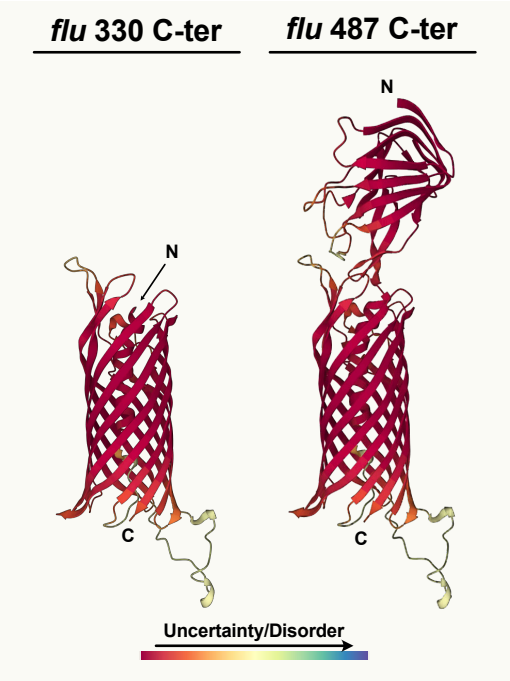

Figure 43. Predicted structure of the last 330 and 487 amino acids of Ag43. AlphaFold prediction of the structure used as a backbone for the pFV330Ve and pFV487Ve chimeric proteins. In our constructs, E-tag and VHH fusions would occur at the marked N-terminal residues. Modified from Uniprot P39180.

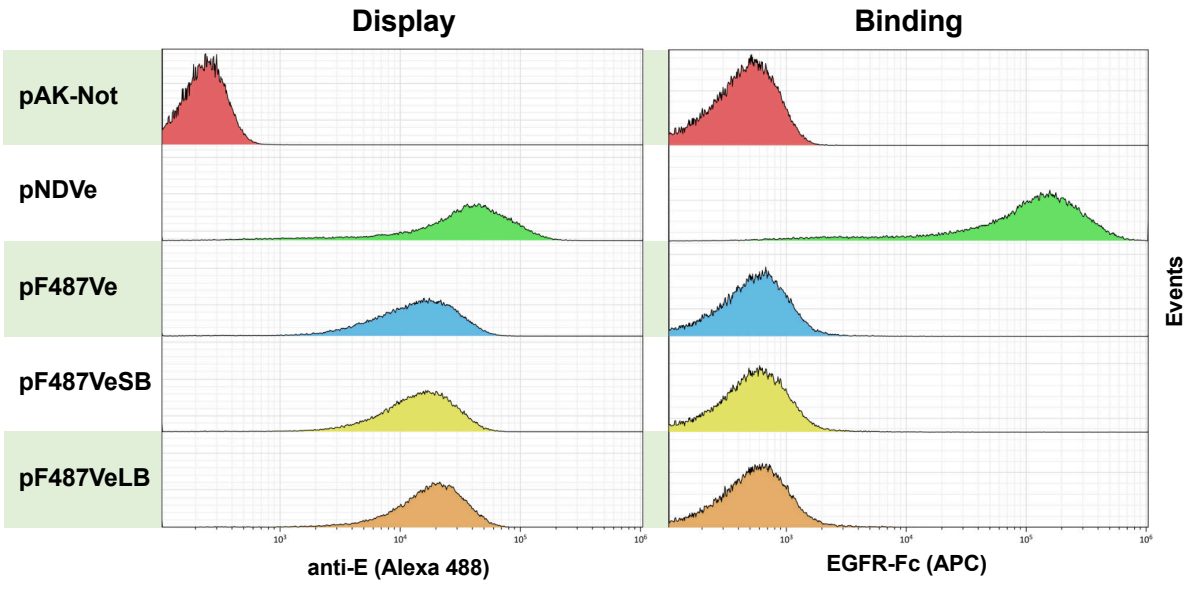

Figure 44. Display and antigen binding capabilities of the constructs combining the last 487 residues of Ag43 with a nanobody and periplasmic fusions to NanoBiT fragments. Flow cytometry analysis of induced *E. coli* EcM1 bacteria carrying the empty vector (pAK-Not) or the flu487-Nb construct with either no periplasmic fusion (pF487Ve), the LOA-SmBIT fusion (pF330VeSB) or the LOA-LgBiT fusion (pF330VeLB). Left, display of the constructs in the outer membrane. Right, binding of antigen by the displayed Nb. Same controls and staining as in Figure 42.

2.3. Engineering of invasin for outer membrane sensors.

Invasins are inverted ATs proteins found in *Yersinia* species that present a high homology to intimin in their overall structure and β-domains (Fairman et al., 2012; Leo, Oberhettinger, Schutz, et al., 2015; Palumbo & Wang, 2006, 2006). In most cases, invasins do not present a periplasmic LysM domain. We chose the invasin (*invA*) from *Yersinia pseudotuberculosis* to generate a new set of constructs by replacing the intimin Neae fragment encoding the β-domain. The crystal structure of the β-barrel of this invasin has been solved and was reported to be monomeric (Fairman et al., 2012). We selected the N-terminal 595 residues of invasin, from its SP to the D1 Ig-like domain, in an equivalent structure to the Neae fragment used in the intimin fusions lacking the LysM domain. We excluded the D2 domain of invasin, which had been suggested to be responsible for the oligomerization of the full-length invasin of *Y. pseudotuberculosis*, in contrast to other monomeric invasins such as the one from *Y. enterocolitica* (Dersch & Isberg, 2000).

By replacing the intimin backbone in pNVEGFR2 with the aforementioned 1-595 fragment from invasin, we generated the construct pIVe (Figure 45). Flow cytometry analysis comparing the surface display and antigen binding of bacteria expressing the pIVe construct revealed lower fluorescence signals compared to bacteria expressing pNVEGFR2 (Figure 46), with values close to those of EhaA constructs. Western blot analysis of the protein samples from these bacteria revealed that the invasin-Nb fusion presented a major band, with a similar size and intensity to that of the intimin-Nb fusion, but also showed a large amount of proteolysis (Figure 47).

These results were not surprising. It had been previously reported (Fairman et al., 2012) that the BAM sequence from invasin (Q_{343}WNLQMNYR**L**$_{352}$) lacks the canonical aromatic residue in the last position of the β-barrels in *E. coli*, and so attempts at expressing its β-barrel in this bacteria usually produced low yields of functional protein. The authors restored high expression levels of functional protein by generating the L352F mutation. We replicated this L352F mutation in our construct generating pIFVe. Using this mutated version, we also evaluated the possibility of removing the extracellular D1 domain and generated the plasmid pIFDVe. Flow cytometry experiments with these new constructs revealed that the L352F mutation greatly increased surface display and antigen-binding signals by ~10-fold (Figure 48). Furthermore, the simultaneous L352F mutation and D1 removal was able to increase display and binding even more, reaching values comparable to the intimin construct.

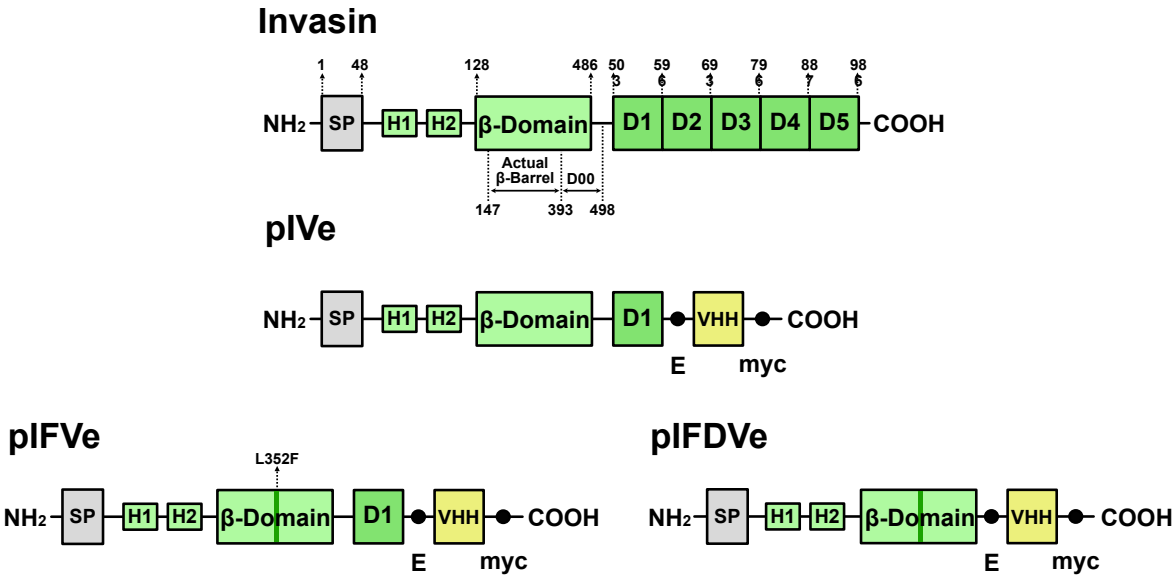

Figure 45. Schematic representation of the full-length invasin and invasin-nanobody constructs. Each box represents a different feature. Numbers relate to the corresponding amino acid in the intimin WT protein based on its crystal (Fairman *et al.,* 2012). The D00 domain was predicted by AlphaFold. SP = Signal Peptide, H = helix, D = Ig-like domain, L352F = Leucine 352 to phenylalanine mutation, E = E-tag, myc = c-myc-tag. Size is not proportional to maintain visual clarity.

Next, we tested the oligomerization state of the IFDVe construct. We extracted the OMPs from induced *E. coli* bacteria carrying pIFVDVe and subjected the samples to BN-PAGE and Western blot with anti-myc mAb (Figure 49). Migration of this fusion protein produced a protein band of ~140 kDa, which is roughly double the expected size for the monomer. This observation suggests that the invasin-based construct was also behaving as a dimer, similar to intimin. Due to its dimeric nature, for its functioning in a dimerization sensor this fusion would likely require its co-expression with the intimin or EhaA partners.

Finally, we tested whether peptide and protein domains could be attached to the periplasmic side of the IFDVe protein without affecting its functionality. We generated several fusions between residues 51 and 52 of IFDVe having the SmBiT (pIFDVeSB), the LgBiT (pIFDVeLB), the SpyTag (pIFDVeSpy) or the SnoopTag (pIFDVeSnoop) (Figure 50). Flow cytometry analysis showed that these fusions did not affect the display nor the antigen binding of the Nb, with values almost identical to the parental protein fusion without periplasmic modifications (Figure 51). Western blot of the protein samples from these bacteria showed major bands with the expected size for the full-length proteins of all constructs, with just some increased proteolysis for one of the fusions with LgBIT (Figure 52).

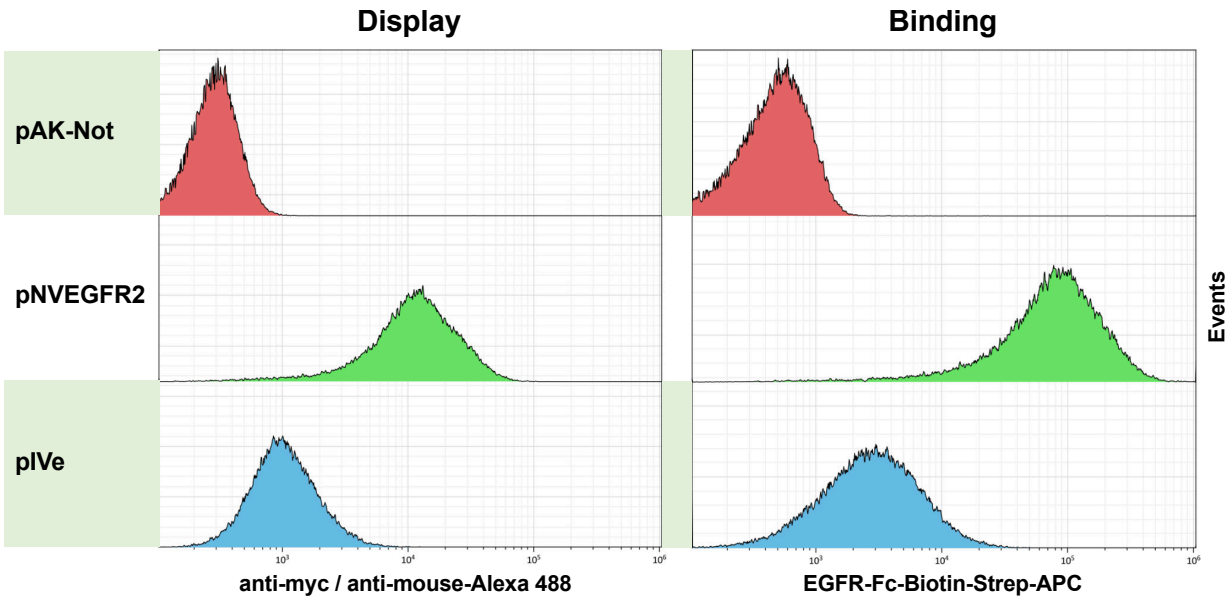

Figure 46. Display and antigen binding capabilities of the invasin-nanobody construct. Flow cytometry analysis of *E. coli* EcM1 bacteria transformed with plasmids expressing either no construct (pAK-Not), the invasin-Nb construct (pIVe) or the original intimin-Nb construct with LysM (pNVEGFR2) as positive control. Left, display of the constructs in the outer membrane. Histogram shows fluorescence intensity of bacteria stained with anti-myc tag mAb and secondary anti-mouse IgG-Alexa488. Right, binding of antigen by the displayed Nb. Histogram shows fluorescence intensity of bacteria incubated with 50 nM of biotinylated EGFR-Fc and secondary streptavidin-APC.

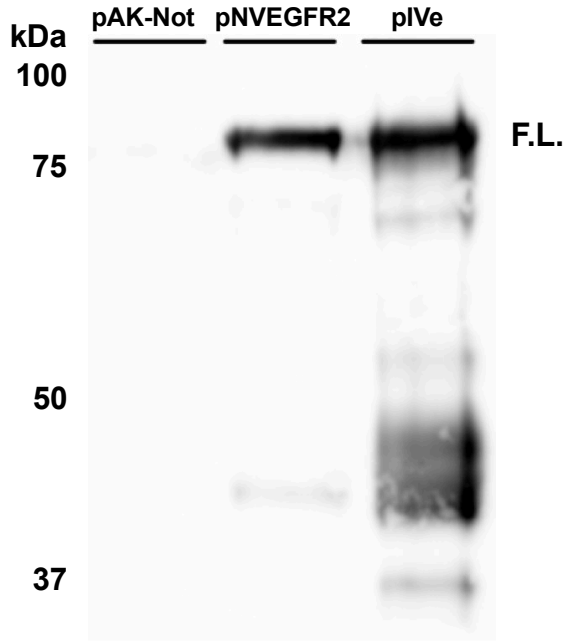

Figure 47. Western blot analysis of the expression for the invasin-nanobody construct. Samples analyzed contain whole-cell protein extracts from induced *E. coli* EcM1 cultures carrying the indicated plasmids. After electrophoresis, proteins were transferred to a membrane and incubated with anti-c-myc mouse mAb and secondary goat anti-mouse polyclonal serum conjugated with peroxidase (POD). The empty vector (pAK-Not) was used as a negative control. Molecular weight markers in kDa are indicated on the left. Bands corresponding to the full-length proteins are indicated as F.L.

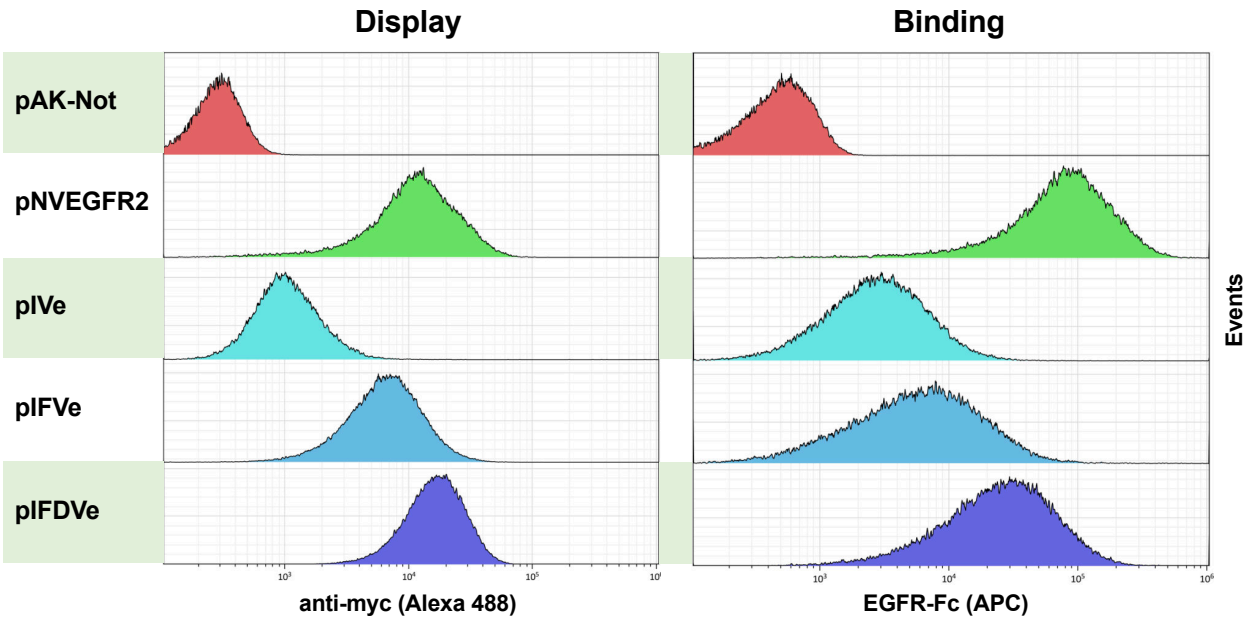

Figure 48. Display and antigen binding capabilities of the invasin-nanobody constructs with modifications for improving display. Flow cytometry analysis of *E. coli* EcM1 bacteria transformed with plasmids expressing either no construct (pAK-Not), the invasin-Nb construct (pIVe) with the L352F mutation (pIFVe) and lacking the D1 domain (pIFDVe) or the original intimin-Nb construct with LysM (pNVEGFR2) as positive control. Left, display of the constructs in the outer membrane. Histogram shows fluorescence intensity of bacteria stained with anti-myc tag mAb and secondary anti-mouse IgG-Alexa488. Right, binding of antigen by the displayed Nb. Histogram shows fluorescence intensity of bacteria incubated with 50 nM of biotinylated EGFR-Fc and secondary streptavidin-APC.

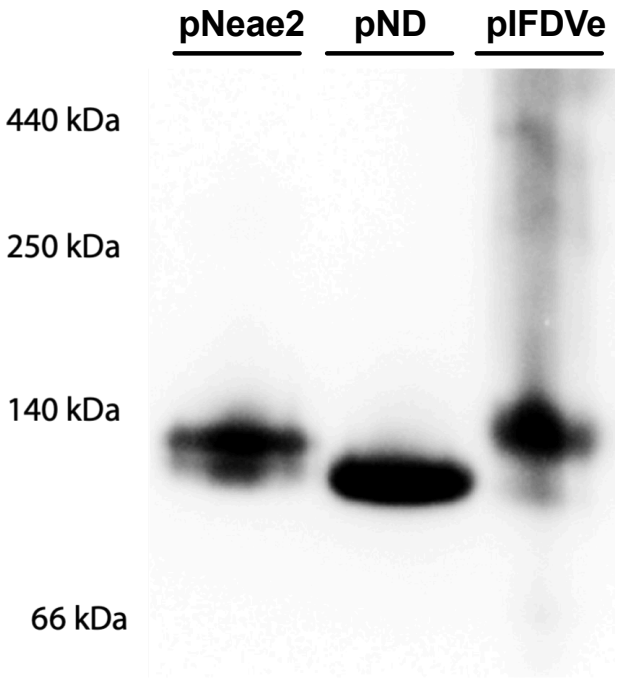

Figure 49. BN-PAGE analysis of the quaternary structure of the invasin construct with the L352F mutation and without the D1 domain. Protein samples were extracted from the OM of cultures of *E. coli* EcM1 carrying the intimin-6xHis constructs with (pND) and without (pNeae2) the LysM-deletion or the invasin construct with the L352F mutation and without the D1 domain. Native molecular weights in kDa are indicated on the left. Same process and staining as Figure 29.

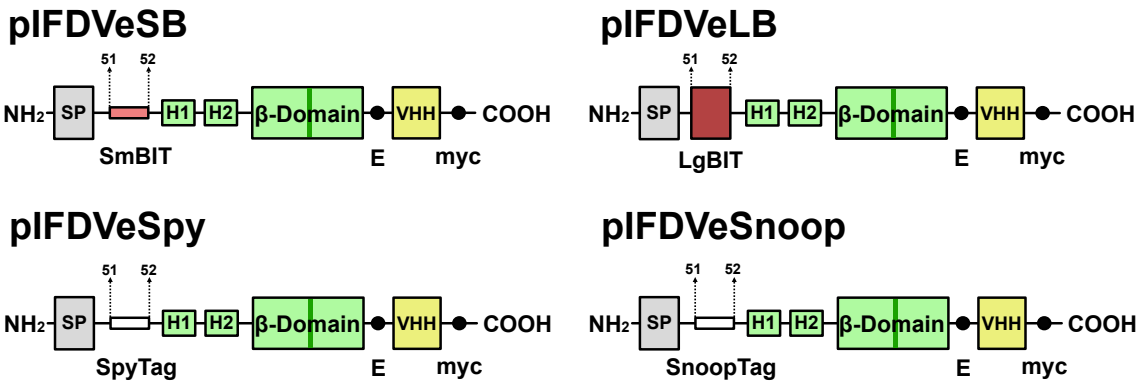

Figure 50. Schematic representation of the invasin-nanobody constructs with periplasmic fusions to NanoBiT fragments, SpyTag or SnoopTag. Each box represents a different feature. Numbers relate to the corresponding amino acid in the intimin WT protein based on its crystal (Fairman *et al.,* 2012). SP = Signal Peptide, H = helix, D = Ig-like domain, L352F = Leucine to phenylalanine mutation, E = E-tag, myc = c-myc-tag. Schemes are not to scale to maintain visual clarity.

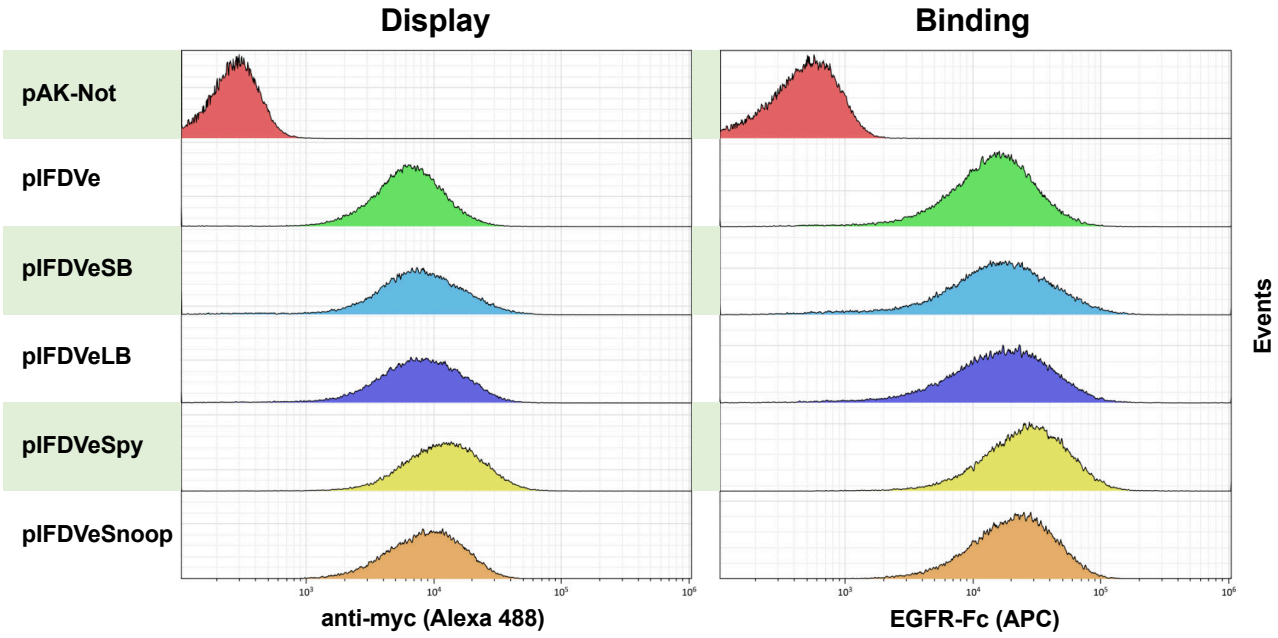

Figure 51. Display and antigen binding capabilities of the invasin-nanobody construct IFDVe with periplasmic fusions to NanoBiT fragments, SpyTag or SnoopTag. Flow cytometry analysis of *E. coli* EcM1 bacteria transformed with plasmids expressing either no construct (pAK-Not), the invasin-Nb IFDVe construct (pIFDVe) with periplasmic fusions to either the SmBiT fragment (pIFDVeSB), the LgBiT fragment (pIFDVeLB), Spytag (pIFDVeSpy) or SnoopTag (pIFDVeSnoop). Left, display of the constructs in the outer membrane. Histogram shows fluorescence intensity of bacteria stained with anti-myc tag mAb and secondary anti-mouse IgG-Alexa488. Right, binding of antigen by the displayed Nb. Histogram shows fluorescence intensity of bacteria incubated with 50 nM of biotinylated EGFR-Fc and secondary streptavidin-APC.

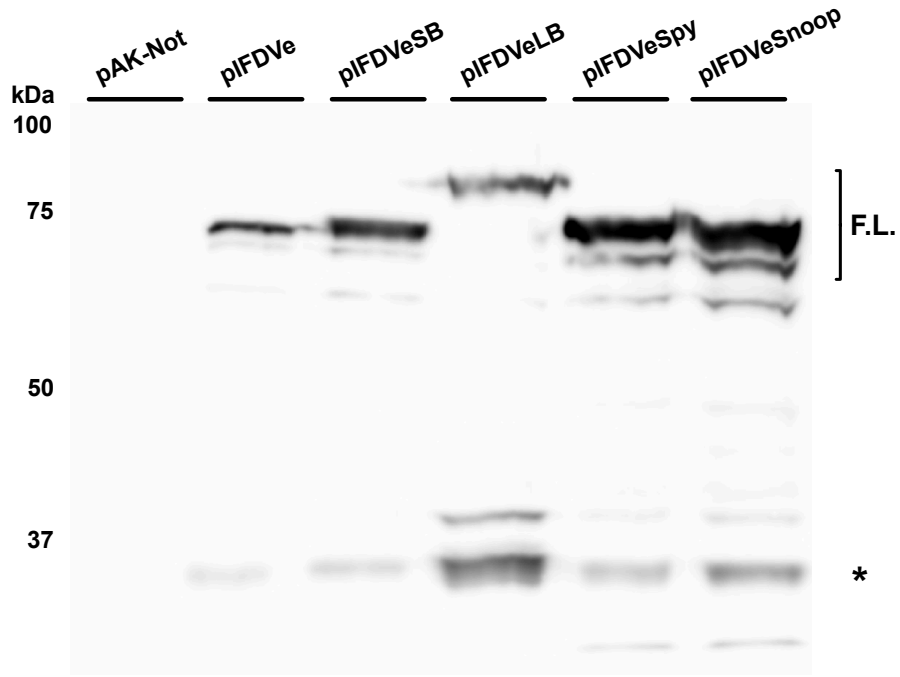

Figure 52. Western blot analysis of the expression for the invasin-nanobody construct IFDVe with periplasmic fusions to NanoBiT fragments, SpyTag or SnoopTag. Samples analyzed contain whole-cell protein extracts from induced *E. coli* EcM1 cultures carrying the indicated plasmids. After electrophoresis, proteins were transferred to a membrane and incubated with anti-c-myc mouse mAb and secondary goat anti-mouse polyclonal serum conjugated with peroxidase (POD). The empty vector (pAK-Not) was used as a negative control. Molecular weights in kDa are indicated on the left. Bands corresponding to the full-length proteins are indicated as F.L. Main proteolytic fragments are indicated with an asterisk.

Once again, we used AlphaFold to predict the structure of our invasin constructs. The algorithm predicted the correct folding of the invasin β-barrel and of the extracellular domains as well as the presence of flexible α-helices in the periplasm. In the case of pIFDVeLB, the LgBiT domain was predicted to be correctly folded (Figure 53). Interestingly, AlphaFold also predicted the presence of an Ig-like domain between the β-barrel and the D1 domain of invasin, in a similar case to the D00 domain of intimin (Figure 54). To our knowledge, the presence of this Ig-like domain has not been previously reported.

Taken together, our results demonstrate that invasin-based constructs have the capacity to display a functional Nb on the surface of *E. coli* while having a peptide and/or protein domain anchored in the periplasmic side.

A comparison of the predicted sequences of the β-barrel and displayed domains for the chimeras encoded by pNDVe and pIFDVe can be found in (Figure 55).

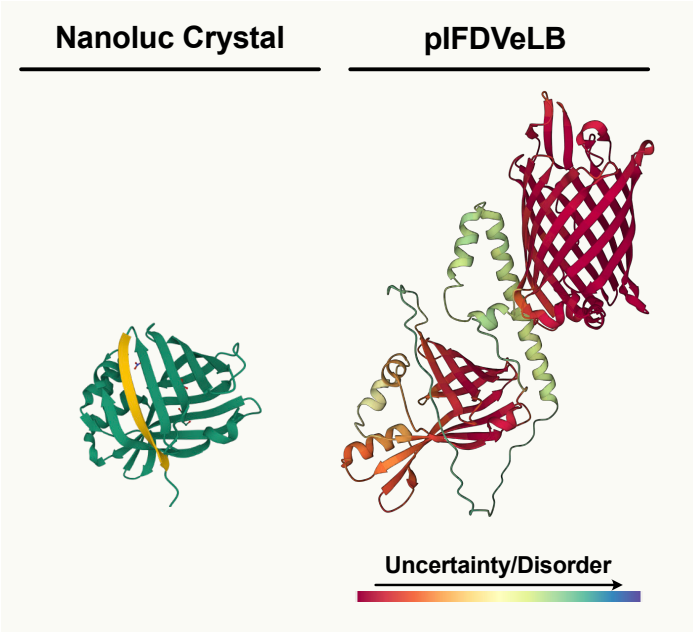

Figure 53. AlphaFold prediction of the structure of pIFDVeLB. Detail of the β-barrel and the periplasmic helices and LgBiT domain (right). The full NanoLuc crystal (PDB 7MJB) is shown in the left to compare the folding. The β-strand corresponding to the SmBiT is colored in yellow.

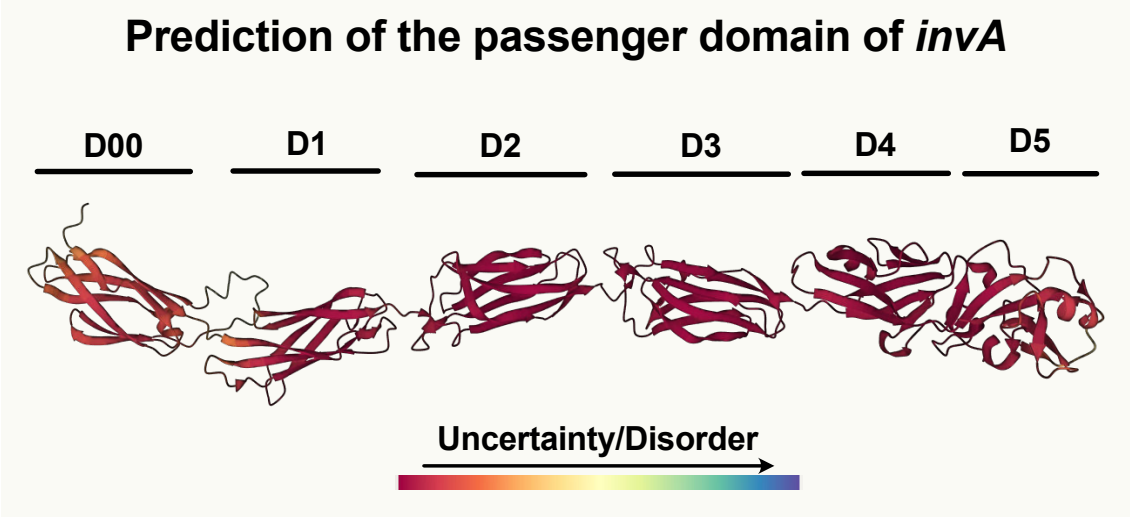

Figure 54. AlphaFold prediction of the passenger domain of the WT invasin. Each Ig-like domain is indicated. Notice the appearance of a previously undescribed D00 domain.

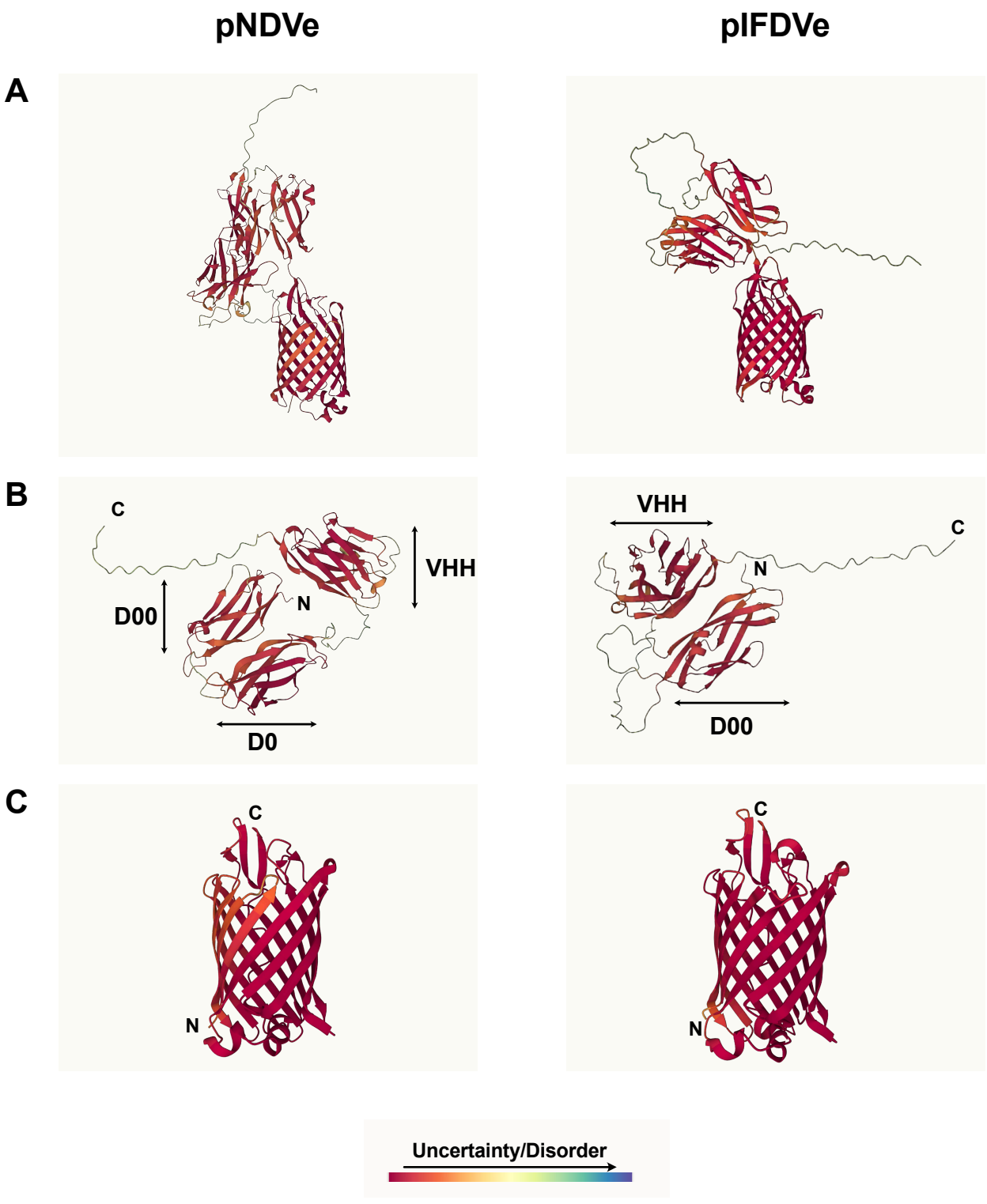

Figure 55. Comparison of the AlphaFold structure predictions for pNDVe and pIFDVeLB. Periplasmic helices have been omitted for visual clarity. **(A)** β-barrel and displayed Ig-like and Nb domains. **(B)** Detail of the Ig-like domains and the Nb. **(C)** Detail of the β-barrel.

2.4. Detection of extracellular antigen by bacteria co-expressing intimin and invasin protein sensors in the outer membrane.

We next investigated the capacity of our modified Nb surface display systems, based on intimin and invasin β-barrels and periplasmic split NanoLuc fragments, to detect an extracellular protein antigen (EGFR-Fc) and produce a change in the bioluminescence due to dimerization of the β-barrels and interaction of the split NanoLuc fragments. In order to co-express two of these constructs in the same cell, we first cloned the gene fusions from pNDVe, pNDVeSB, pIFDVe and pIFDVeLB into the backbone of a compatible pSEVA221 vector under control of a tetR-P_{tet} promoter region. The new plasmids (pSEVA221-Ptet-NDVe, pSEVA221-Ptet-NDVeSB, pSEVA221-Ptet-IFDVe and pSEVA221-Ptet-IFDVeLB), were co-transformed with either pNDVeLB or pIFDVeLB, into *E. coli* EcM1 strain. Additionally, we generated a positive control (called pAK-pelB-Nanoluc) for the production of bioluminescence by cloning into the pAK-Not vector the full-length NanoLuc gene fused in frame with to the N-terminal SP of PelB (Le Calvez et al., 1996; Thie et al., 2008) for its export into the bacterial periplasm. In our preliminary experiments we detected an impaired growth of bacteria carrying pNDVeLB (intimin and LgBiT) and a second plasmid, so we focused on combinations having pIFDVeLB (invasin and LgBiT) and a second compatible plasmid.

In an initial experiment, we compared the bioluminescence produced by the different combinations of IFDVeLB with either IFDVe, IFDVeSB or NDVeSB in the presence or not of their corresponding antigen, EGFR-Fc, or a control antigen PD-L1-Fc (Figure 56). As expected, the pair lacking the SmBiT, (IFDVeLB + IFDVe) produced low luminescence levels, comparable to the bacteria with the empty vector pAK-Not (negative control). On the other hand, both the IFDVeLB + IFDVeSB and IFDVeLB + NDVeSB pairs showed light emission, with values ~10-fold below the luminescence found for the full-length NanoLuc in the periplasm (positive control). From the two combinations, the homodimer of invasin β-barrels pair showed higher luminescence. Unexpectedly, both combinations of chimeric proteins produced higher bioluminescence in the absence of the specific antigen than when EGFR-Fc was added. While this behavior was opposed to our original hypothesis, we further investigated its potential for generating a biosensing platform.

As the IFDVeLB + NDVeSB combination showed the higher difference in luminescence between the presence and the absence of EGFR-Fc, we used this pair to test how different concentrations of the antigen affected the emission of light (Figure 57). The results showed that the reduction of the luminescence was dose-dependent, with an

inverted relationship between the antigen concentration and the emission of light. Luminescence showed no variation in the presence of the control antigen, nor in the presence of a low concentration of EGFR-Fc (0.5 nM) that is below the equilibrium dissociation constant of the displayed Nb (K_D = 1.92 nM) (Salema et al., 2016). These findings show that the system behaves as a bacterial biosensor that detect the presence of a soluble protein antigen in a dose-dependent manner and directly emits an easily quantifiable signal.

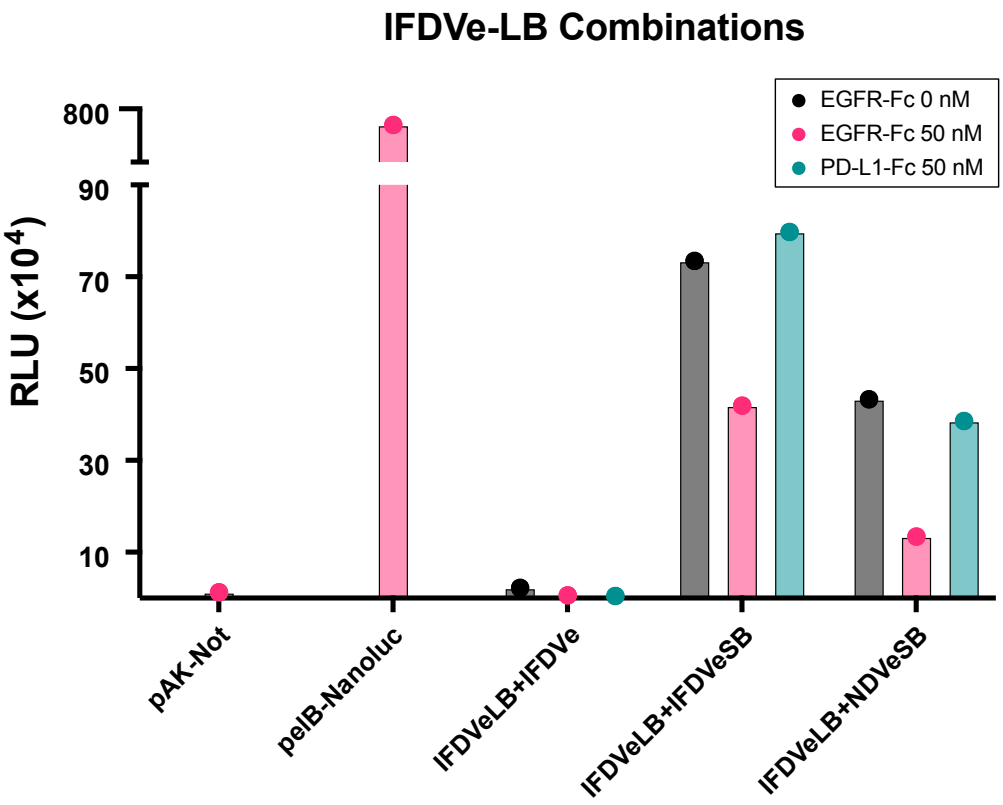

Figure 56. Detection of extracellular protein antigen by bacterial antigen receptors. Relative luminescence units (Lum/OD_{600}) of EcM1 bacteria transformed with the indicated combinations of bacterial antigen receptors of EGFR based on invasin LgBIT (IFDVeLB) and SmBIT fusions to invasin (IFDVeSB) or intimin (NDVeSB). Bacteria lacking SmBIT (IFDVe) and carrying the empty vector (pAK-Not) were used as negative controls. A culture of EcM1 bacteria expressing in the periplasm a fusion of the N-terminal SP of PelB to the full-length Nanoluc was used as positive control. When indicated, the protein antigens EGFR-Fc or PD-L1-Fc (negative control) were added at 50 nM to bacteria for 1 h prior to bioluminescence quantification.

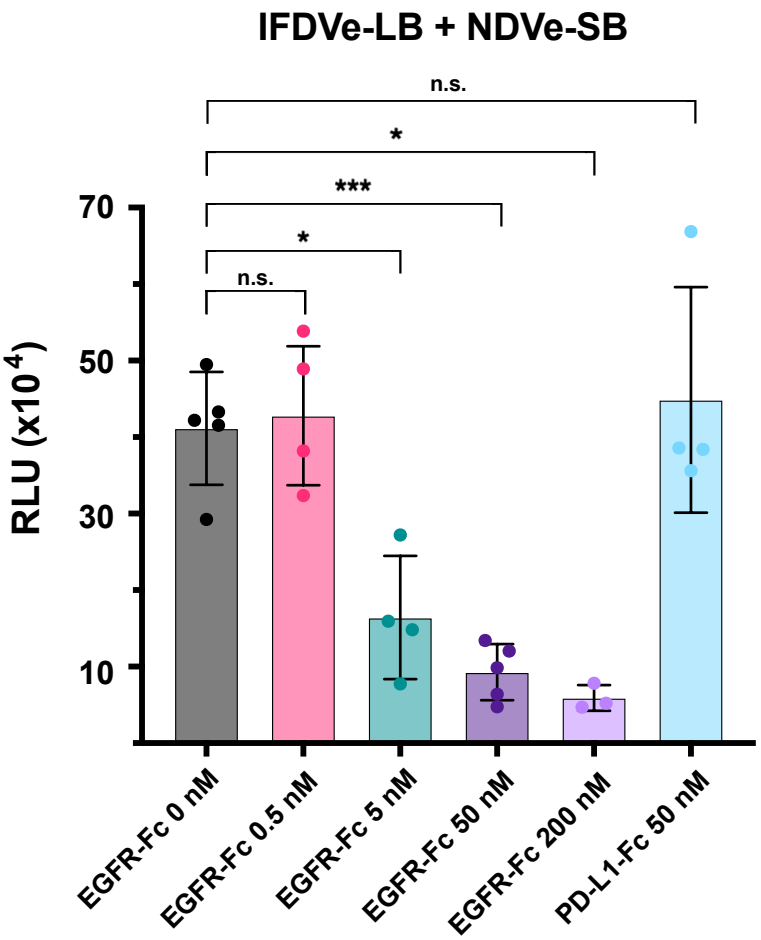

Figure 57. Dose-dependent detection of extracellular protein antigen by bacterial antigen receptors. Relative luminescence units (Lum/OD_{600}) of EcM1 bacteria expressing a combination of bacterial antigen receptors of EGFR based on invasin LgBIT (IFDVeLB) and intimin SmBIT (NDVeSB). Different concentrations of the protein antigen EGFR-Fc (from 0 to 200 nM, as indicated) or negative control antigen PD-L1-Fc (50 nM) were added to bacteria for 1 h prior to bioluminescence quantification. Error bars represent the standard deviation. Statistical significance inferred by paired t-test analysis. n.s. non-significant, (*) p-value < 0.05 (***) p-value < 0.001.

DISCUSSION

1. Toward safer therapeutic bacteria using synthetic biology.

Previous works from our group have aimed to engineer the non-pathogenic *E. coli* K-12 strain for tumor therapy by inserting genetic cassettes with different functionalities into its chromosome. By displaying in the OM of *E. coli* small antibody fragments, Nbs, against tumor cell surface antigens, our group managed to reduce 100-fold the necessary bacterial dose for colonizing the tumor (Piñero-Lambea et al., 2015). In a different work, the T3SS was implemented into our non-pathogenic *E. coli*, which could be used to deliver therapeutic proteins directly into the cytoplasm of cancer cells (Alejandro Asensio Calavia, 2021 (PhD thesis); Ruano-Gallego et al., 2015). Alternatively, we also used the protein invasin for the internalization of our bacteria into tumoral cells and subsequent release of protein cargo (Carmen Mañas Torres, 2019 (PhD thesis)). However, one possible drawback of the use of all these systems is the fact that the genes encoding them are under control of either constitutive promoters or promoters inducible by small chemical molecules such as IPTG, aTc or L-arabinose. Chemical inducers present some limitations, such as the toxicity associated to IPTG, and, when used *in vivo*, they must reach the tumor areas in sufficient concentration to stimulate transcription, which could be difficult for the poorly irrigated necrotic core of solid tumors. But perhaps the most important inconvenience of using this type of induction is that it is not tumor-specific. Bacteria outside the tumor could activate the expression of such therapeutic systems should a sufficient concentration of the inducer reached them, which could affect healthy tissue. Through this PhD thesis we have aimed to develop induction systems that respond to tumor-specific cues with the intention of using them to limit the activity of our therapeutic genes exclusively to the tumor microenvironment.

2. Characterization of tumor-sensing promoters integrated in the chromosome of *E. coli*.

We first characterized the activity of promoters that respond to soluble molecules present at higher concentrations inside tumors than in healthy tissue by using a GFP reporter. Promoters were tested while integrated in the chromosome of *E. coli*, as this allows for genetic stability without the need for antibiotics and also reduces the possibility of horizontal gene transfer (Lee et al., 2018).

L-lactate has been widely reported to accumulate inside tumors (Choi et al., 2013; Sonveaux et al., 2008). To use this molecule as an inducer, we selected the promoter $P_{lldP,}$ whose activity is repressed by the LldR regulator in the absence of L-lactate

(Aguilera et al., 2008; Dong et al., 1993). This promoter has been previously used to create *E. coli* biosensors for detecting L-lactate in cell cultures (Goers et al., 2017), 3D tumor spheroids (Zúñiga et al., 2021) and solid tumors (Chien et al., 2021); however, all of these examples relied on the use of plasmids. The promoter is also repressed by the ArcA regulator during anoxic conditions (Iuchi et al., 1994; Iuchi and Lin, 1988; Park et al., 2013). As this could reduce expression in hypoxic areas of the tumor, we also generated a mutated promoter, P_{lldP}*, where one of the binding sequences for ArcA was substituted by a randomized DNA sequence to reduce the repression by this regulator.

When bacteria carrying either version of the promoters were grown in a microplate reader at 30 ºC we found that GFP fluorescence decayed during exponential phase. When entering the lag phase the cultures showed an increase in fluorescence in a L-lactate dosage-dependent manner. Bacteria with the mutated promoter presented a higher baseline of expression as well as an increased response to the higher L-lactate concentrations. The differences between promoters disappeared when bacteria were cultured at 37 ºC in agitated flask cultures. In these conditions both promoters behaved almost identically, with a high leakage of expression when no L-lactate was added to the cultures and only ~2.5-fold increase in fluorescence with the maximum concentration of L-lactate. In this experiment, the fluorescence peak was reached during the first hours of induction, in contrast to the microplate assay. A possible explanation for this different behavior could be attributed to the carbon catabolite repression that has been shown to affect this operon (Aguilera et al., 2008). LB is a complex medium, and carbon sources other than L-lactate could be preferentially used during the exponential phase, as has been shown for glucose (Goers et al., 2017; Zúñiga et al., 2021). When the culture reaches the lag phase these initial carbon sources could be mostly depleted and the CCR would stop repressing the expression of the promoters.

This hypothesis is also supported by 37 ºC experiments, where the increased growth rate may consume these other carbon sources faster. The mutated P_{lldP}* promoter showed a higher expression than the WT P_{lldP} during microplate experiments, where oxygen availability is probably limited (Somerville and Proctor, 2013), but almost no difference was observed in the agitated flask, which has strong aeration. These results suggest that the repression by ArcA is indeed reduced in the mutated promoter, as this repressor is especially active during microaerobic conditions but almost inactive during complete anoxia or high oxygenation (Alexeeva et al., 2003; Georgellis et al., 1997; Jeon et al., 2001; Kwon et al., 2000). Increased expression in hypoxic conditions makes P_{lldP}* a better candidate for *in vivo* tumor induction than its WT counterpart. However, it still

presents high leakage, especially in aerobic conditions. This basal expression, which in consequence reduces the dynamic range of the promoter, had been previously observed in the aforementioned works where P_{lldP} was used to create whole-cell biosensors. To reduce the leakage, authors increased the expression of LldR through the use of synthetic promoters and plasmids with different copy numbers, successfully reducing the basal expression and increasing the dynamic range (Chien et al., 2021; Goers et al., 2017; Zúñiga et al., 2021). Since in our own biosensor the LldR protein is endogenously generated by the *lldPRD* operon, we believe that artificially increasing the expression of the repressor through a stronger constitutive promoter could reduce the leakage of our biosensor. Thus, by combining an increased LldR concentration to reduce expression in the absence of L-lactate with the microaerobic functionality of P_{lldP}* we could generate an ideal expression system for tumor targeting bacterial therapies.

Tumors present a higher concentration of ROS than healthy tissue (Liou and Storz, 2010) and an increased production of H_2O_2 has been shown for cancer cell lines (Szatrowski and Nathan, 1991). The promoter controlling the expression of the genes *uof* and *fur*, P_{uof}, is activated by two transcriptional regulators that participate in the response to ROS stress, SoxS and OxyR, with the latter being fundamental for its activation. Experiments using H_2O_2 showed that this molecule increased the expression of *fur* (Varghese et al., 2007; Zheng et al., 1999). Thus, we decided to test if the P_{uof} promoter could be used for inducing therapeutic bacteria inside tumors. Our results using the microplate reader showed a significant fluorescence increase only when the concentration of H_2O_2 was as high as 5 mM, but no fluorescence was detected for lower concentrations. The need for such a high amount of H_2O_2 was unexpected, as the response by OxyR has been reported to be activated with concentrations as low as 100 nM H_2O_2 (Hou et al., 2019). After adding 5 mM H_2O_2 to the culture, fluorescence exponentially increased, peaking at 1 h with a ~2-fold of induction, and decreased at the same rate afterwards. These results are similar to the ones reported in the recently published work of Roth et al., 2022, where they analyzed the expression of *fur* in the presence of 2.5 mM H_2O_2. They observed a 2-fold of induction for *fur* after 10 min, which decreased to 1-fold after 60 min. This rapid decrease of the expression was attributed to the quick degradation of H_2O_2, which they reported to be completely absent from the culture after 25 min. Differences in the induction between our experiments and theirs may relate to the fact that we used a double concentration of H_2O_2 and possibly a slower degradation of this molecule at 30 ºC. Besides the fact that such high concentrations of H_2O_2 are probably not reached inside a tumor, they also reported that concentrations of 2.5 mM and above generated DNA damage and slowed protein synthesis, which severely difficult the use of the P_{uof}

promoter even for other whole-cell non-therapeutic applications. When we evaluated the promoter using shaking flasks at 37 ºC, we found that it behaved as constitutive, with no response to H_2O_2. Although OxyR has been shown not to be induced by high oxygenation (Baez and Shiloach, 2013; Somerville and Proctor, 2013) we repeated the same experiment in static flasks. Once again, the cultures showed no differences in GFP fluorescence no matter the concentration of H_2O_2. Since OxyR has been reported to be unresponsive in anaerobic conditions (Hou et al., 2019), we theorize that the lack of induction by H_2O_2 in this experiment may be due to a low oxygen concentration in the static culture. This result, together with the fact that the microplate assays did show induction, also support the hypothesis that microplate cultures were subjected to hypoxic, but not anaerobic conditions.

The high leakage exhibited by P_{uof} may be reduced in its original operon by the regulators Fur (Z. Chen et al., 2007; De Lorenzo et al., 1988) and Crp (De Reuse and Danchin, 1988), whose binding sequences are present in the downstream region of the transcriptional starting site, which our construct did not include. A non-coding small RNA, RhyB, has also been demonstrated to hinder translation by binding the start of the *uof* sequence (Vecerek et al., 2007). All things considered, the low sensitivity and high leakage of the P_{uof} promoter make it a non-adequate candidate for controlling therapeutic bacteria expression. Further attempts at using ROS as an induction signal should focus in other promoters such as the promoter of the catalase/hydroperoxidase HPI (*katG*) or the promoter controlling the regulatory RNA OxyS, which had been previously used to detect H_2O_2 with great sensitivity (Rubens et al., 2016).

The final tumor-specific signal that we considered was the increased concentration of NO, which accumulates in tumor areas due to overexpression of NO synthases and poor vascularization (Chen et al., 2007; Cheng et al., 2014). We selected promoters that had been previously used in plasmid-based whole-cell *E. coli* biosensors for NO: the promoter of the nitric oxide dioxygenase (*hmp*), P_{hmp}, (McKay et al., 2018) and P_{norV}, the promoter controlling flavorubredoxin (*norV*) and its corresponding reductase (*norW*) (Archer et al., 2012; Chen et al., 2021). Microplate reader experiments showed strong induction of bacteria carrying both promoters, in a dose-dependent manner and reaching maximum fluorescence at the 1-hour time point. Fluorescence levels quickly fell after that point, although for P_{hmp}, a detectable signal was still present after 6 h post induction. Both promoters showed low leakage without any NO donor in the media. However, P_{hmp} showed remarkably low levels of expression, with a fluorescence signal close to the parental strain with no GFP. We then proceeded to evaluate these promoters while

bacteria were grown in agitated flasks at 37 ºC. P_{norV} cultures showed limited sensitivity, with fluorescence detectable only for the highest Spermine NONOate concentrations. This could be attributed to high oxygenation, as the NO-sensing activator of this promoter, NorR (Tucker et al., 2006, 2004), is less active in the presence of oxygen (da Costa et al., 2003). A possible solution for this could be the reduction of NorR concentration, which has been shown to increase the promoter sensitivity (Chen et al., 2021). On the other hand, P_{hmp} cultures displayed good induction even for the lowest inducer concentrations, with a subtle increase of fluorescence in higher concentrations. In both cases, no detectable leakage was observed, showing a tight control of the expression when no NO is present. The increased sensitivity of P_{hmp} may be explained by the fact that its main NO-sensing repressor, NsrR (Bodenmiller and Spiro, 2006), is only present in a low concentration in the cell due to a GUG start codon that hinders the translation of its encoding mRNA (Chhabra and Spiro, 2015). The regulatory sequence of this promoter also includes binding sites for the anaerobic repressor FNR, which has been shown to bind NO in anoxia (Cruz-Ramos et al., 2002), and the regulator of methionine synthesis MetR, which upregulates the expression of the promoter in the presence of nitrosated homocysteine (Membrillo-Hernández et al., 1998). The simultaneous presence of these three NO-sensing regulatory mechanisms could explain the promoter's low leakage coupled with a fast and sensitive expression once NO is present. Both promoters showed promising results for inducing therapeutic systems inside the NO-rich tumor microenvironment. As tumors present hypoxic areas, the reduced sensitivity of P_{norV} in aerobic conditions may be an advantage for its *in vivo* use, as it would hinder any kind of expression outside the TME. While the P_{hmp} promoter did present a more lasting expression, this may not be relevant in the context of a sustained tumoral production of NO and it could also be undesirable in the event of bacteria escaping the TME after being induced.

Summarizing, in our search for promoters that could be used to induce therapeutic bacteria inside tumors we have found two NO-sensing promoters and a promising L-lactate-detecting promoter that could be further improved. However, these promoters still need to be tested using *in vitro* and *in vivo* tumor models to demonstrate their usefulness for their intended applications. Other TME characteristics could be also explored, including promoters responding to hypoxic conditions such as the derivatives of the *pepT* promoter from *Salmonella* (Mengesha et al., 2006) or the promoter of the *fnrS* RNA (Durand and Storz, 2010; Leventhal et al., 2020). Another option could be the promoter of the *cadBA* operon, which senses low pH (Chien et al., 2021; Lee et al., 2008).

3. Chromosome-integrated serine integrases for genetic logic circuits and memory.

Combining different inputs for controlling a programmed response increases the safety and specificity of therapeutic and diagnostic bacteria, as they can be designed to initiate their intended activity only when several conditions are encountered or block the response if a different, undesired input was found. Serine integrases have been used to generate genetic logic circuits that compute multiple inputs and maintain the result in form of permanent modifications of DNA that are conserved through the next cell generations. However, most applications of these proteins have placed the targets in plasmids, with only a few exceptions (Bonnet et al., 2012; Hsiao et al., 2016). In order to avoid the use of plasmids, we integrated into the chromosome of *E. coli* and tested several excision and inversion targets for the serine integrases Bxb1, Tp901 and Int7. By using constitutive plasmid expression of these integrases, we showed that both excision and inversion of integrated targets is possible for the three of them. Excision; however, was clearly more efficient than inversion in all cases, which may indicate that the inversion process may be hindered by the chromosomal context. Despite a similar architecture of the targets, we found some differences in expression between them, which could be attributed to the cryptic promoter and terminator activities that have been reported for attP and attB sites (Bonnet et al., 2013; Guiziou et al., 2019). We also found that, out of the three integrases, Bxb1 was the most efficient one, allowing for an almost digital behavior. Populations carrying the Tp901 and Int7 excision targets showed intermediate fluorescence values between the OFF states and the maximum fluorescence values that we considered the ON states. A similar effect was previously reported and attributed to the stability of the mRNA due to the different RNA secondary structures arising from the presence of the recombination sites (Bonnet et al., 2013). To avoid such a problem, we used mRNA processing in designing the excision and inversion AND gates using Tp901 and Bxb1 targets. As expected based on previous results, the excision AND gate demonstrated higher efficiency, although both gate configurations exhibited no fluorescence unless both integrases were present. These findings prove that genetic logic and memory can be established in the chromosome of our *E. coli* bacteria. It is reasonable to assume that other logic gates, such as NOR and OR gates, may also be functional and could be explored in future studies.

We have also demonstrated that integrases can be expressed using an inducible promoter (P_{tet}) from chromosome-integrated genetic circuits and act upon integrated targets. Inducible expression of integrases was shown to be leaky, something that could

be solved by using a weaker RBS or fusing these proteins to ssrA proteolysis tags (Andersen et al., 1998; Bonnet et al., 2012). We also showed that a NO-sensing promoter (P_{hmp}) can be used to express Bxb1 and activate an excision target when the bacteria are exposed to SPER/NO concentrations that mimic tumor levels of NO. This system makes our bacteria whole-cell biosensors of NO with genetic memory that is conserved through the following generations. Such sensor could be employed as a diagnostic tool, as bacteria could colonize a tumor and produce a reporter gene exclusively inside of it, allowing its detection. Furthermore, by placing a therapeutic gene under control of the target, the therapeutic activity would be constrained to bacteria that have reached the tumor. After the terminator is eliminated through excision, the expression of this gene could be constitutive or use an inducible promoter for further control. Other possibilities include using several targets that both activate therapeutic or diagnostic genes while simultaneously reducing the capacity of these activated bacteria to abandon the tumor and proliferate outside of it. This could be achieved by excision of specific genes involved in metabolic processes, thereby creating auxotrophies. Obtaining other tumor-sensing promoters with a tight control of the expression and high sensitivity could also allow us to combine signals through AND gates, to further restrict any response to the TME. This kind of biosensor could also be useful for bacterial therapy of inflammatory bowel diseases, which also present increased concentrations of NO (Avdagić et al., 2013).

4. Generation of a whole-cell antigen biosensor with chimeric outer membrane protein receptors.

Detection of tumor-associated protein antigens is also a potential way to specifically trigger diagnostic and therapeutic responses in engineered bacteria. As a proof-of-concept, in this thesis we have developed a whole-cell biosensor *E. coli* that is able to detect the presence of a tumor-associated protein, EGFR, through the display in the OM of chimeric proteins pairs consisting of an exposed Nb fused to a membrane anchored T5SS β-barrel that carries a split enzyme fragment (NanoBiT).

In our original hypothesis, the protein pairs would not interact unless a dimeric antigen bound both Nbs, forcing their dimerization. Therefore, we aimed to obtain Nb-barrel fusions that behaved as monomers. We first tried to modify the intimin periplasmic region, as it had been reported that the LysM domain and its spacer were mainly responsible for its dimeric nature (Leo et al., 2015). However, constructs where that region was deleted still behaved as dimers, shown by cross-linking and BN-PAGE, which

indicated that other protein features of intimin must be responsible for its dimerization. In Leo et al., 2015a authors also suggested that the second α-helix of intimin may contribute to dimerization. We expressed intimin constructs with a deletion of both LysM and the helices, but these proteins failed to correctly insert into the OM and display the passenger domain on the bacterial surface. Hence, we decided to test a homologous protein of intimin, invasin from *Y. pseudotuberculosis*. Although the different invasin fragments used in the fusions excluded the D2 Ig-like domain, which had been reported as responsible for its self-association (Dersch and Isberg, 2000), BN-PAGE still showed invasin constructs as dimers. Taken together, these results suggest that the dimeric nature of intimin and invasin could be an uncharacterized intrinsic feature of their β-barrels.

Importantly, we successfully fused the split enzyme fragments of the NanoLuc luciferase to the periplasmic regions of intimin and invasin constructs. The small peptide SmBiT was well tolerated, as were the SpyTag and SnoopTag peptides. However, the bulkier LgBiT fragment clearly reduced the display and binding of the intimin construct, although it did not affect the invasin construct. We also investigated the use of monomeric barrels from classic ATs to test periplasmic fusions of split NanoLuc fragments. In the case of the EhaA barrel, which had already been proven to be able to display Nbs (Salema et al., 2013,) the periplasmic fusion to LgBiT severely hindered surface display. We reduced this effect by using the full-length periplasmic linker of OmpA (Ortiz-Suarez et al., 2016). By increasing the distance between the β-barrel and LgBiT we succeeded in recovering surface display levels similar to the original Nb-EhaA construct without periplasmic fusion. Structure predictions using AlphaFold suggest that the LgBiT domain would be better folded in the fusion using the longer linker. Considering all the evidence, these results indicate that the proximity between β-barrel and periplasmic domain may interfere in the correct folding of the chimeric protein.

Additionally, we attempted similar fusions to the β-barrel of different ATs of *E. coli* that had been previously used by other groups for the surface display of proteins, such as AIDA-I (Gustavsson et al., 2011), EspP (Binder et al., 2010) and Ag43 (Dvořák et al., 2020; Jong et al., 2018; Muñoz-Gutiérrez et al., 2014). Neither the AIDA-I nor the EspP constructs were successfully displayed on the bacterial surface, even when utilizing the full-length OmpA linker. Although the two Ag43 constructs with different passenger lengths were displayed on the bacterial surface, no binding to the antigen was detected.

Therefore, Ag43 constructs appear to affect the folding and/or functionality of the Nb, and we did not proceed with these fusions despite their higher surface display levels.

The engineered chimeric proteins of intimin and invasin allowed us to generate a whole-cell biosensor for detecting the presence of soluble EGFR-Fc in a specific and dose-dependent manner. However, to our surprise, the biosensor behaved contrary to that of our original hypothesis. Contrary to our initial hypothesis, we observed luminescence in the absence of antigen for both intimin and invasin constructs, indicating that their interaction was not solely dependent on the presence of a dimeric antigen. Surprisingly, the addition of the antigen resulted in a reduction of luminescence rather than an increase.

The mechanism behind our sensor is clearly different from what we had expected and therefore we need to evaluate our results to understand its behavior. BN-PAGE results showed that both our intimin and invasin constructs behave as homodimers. This premise was further supported by our *in vivo* luminescence measuring assays, where we detected light emission when invasin constructs carrying both NanoBiT fragments were co-expressed, indicating that they were interacting in a close-enough manner to reconstitute the split NanoLuc luciferase. This was also true for co-expression of the invasin construct carrying LgBiT and the intimin construct carrying SmBiT, which implies the spontaneous formation of heterodimers. Recent studies of OMP dynamics have shown that constant homologous and heterologous interactions occur between the β-barrels of these proteins in the OM, limiting their diffusion to patches around their BAM insertion point (Kleanthous et al., 2015; Mamou et al., 2022; Rassam et al., 2015; Ursell et al., 2012). These findings support the idea that heterodimers may be formed, at least transiently, and lead us to believe that our chimeric proteins may also be an interesting tool for studying OMP interactions. We also found that luminescence production was higher for a homologous pair than for a heterologous one, suggesting that homologous interactions may be more frequent. The addition of the dimeric antigen reduced luminescence, which must correlate with a reduction in the formation of heterologous pairs. This reduction of luminescence was proportional to the concentration of the antigen.

Taking into account the above findings, we propose a model for our biosensor (Figure 58). In the absence of antigen, the Nb-displaying constructs of intimin and invasin interact mainly as homodimers in the OM. However, they can also transiently form heterodimers, likely because homodimers are in equilibrium with free monomers of each β-barrel. The

formation of these heterodimers forces the interaction of NanoBiT fragments, generating luminescence in the presence of the luciferase substrate. When the dimeric antigen is added to the media, it may simultaneously bind to both Nbs in a dimer, stabilizing them. Antigen binding may not stabilize heterodimers in the same manner. Although the reason for this is unclear, it might be related to the different symmetry of the displayed Nbs in the homodimers versus the heterodimers. In this scenario, increasing the concentration of antigen reduces the number of free monomers since they do not dissociate from the homodimers, which in turn reduces the pool of functional heterodimers. Thus, by increasing the antigen concentration, the production of luminescence is reduced, resulting in a measurable output.

We believe that the modular architecture of this biosensor offers a great potential to the system. We can distinguish three main components that, in principle, can be modified as independent modules to alter the sensor characteristics: the Nb, the OMP barrel and the split reporter.

Nbs confer to our system the specificity for the detected protein. Here, we chose a VHH against EGFR for this proof of concept; however, in previous works our laboratory has generated intimin-Nb constructs against other tumor-associated proteins such as HER2 or PD-L1 (Eva Pico Sánchez, 2020 (PhD thesis)). Thus, we could aim to detect such proteins with our biosensor by using the same Nbs. In this first approach, we used the same Nb in both components of the sensor, which limited detection to dimeric antigens; however, we could seek to target monomeric proteins by using two different Nbs that bind different epitopes in the same protein. Moreover, the system may not be limited to tumor-associated proteins, as multiple Nbs have been already described against all kind of proteins (Deszyński et al., 2022). For instance, some Nbs selected in our laboratory could enable us to detect pathogenic EHEC (Ruano-Gallego et al., 2019) or different variants of the SARS-CoV-2 virus (Casasnovas et al., 2022).

Our second modular part is the β-barrel, which acts as a scaffold and OM anchor for the Nb and the reporter system. We engineered three different barrels for their use in our biosensor based on invasin, intimin and the EhaA ATs. In this work we demonstrated the functionality of the system using the invasin-Nb-LgBiT construct as the main component. However, using intimin or EhaA barrels for the LgBiT component may generate different results in sensitivity. Being previously described as a monomeric protein (Marin et al., 2010), the use of EhaA barrel could even result in a biosensor more akin to our original hypothesis, where luminescence is only generated when the antigen is present.

The bacterial antigen receptors (BAR) described in this thesis may be useful for detecting not only soluble antigen, but antigen present in both abiotic and cellular surfaces. Previous works from our laboratory have shown how Nb displaying through intimin allow bacteria to attach to antigen-covered surfaces and tumor cells (Piñero-Lambea et al., 2015). Hence, the use of BAR might also signal bacterial adhesion to a tumor cell.

The final module, the reporter system, is based on the interaction of a split enzyme. Here, we chose the split version of the NanoLuc luciferase, NanoBiT, due to its fast, simple and sensitive detection method (England et al., 2016). However, other split proteins have been developed for protein complementation assays (PCA) that measure protein-protein interactions. Examples of split proteins used in PCAs include fluorescent reporters of multiple colors (Cabantous et al., 2013; Hu and Kerppola, 2003), enzymes such as β-lactamase (Galarneau et al., 2002; Porter et al., 2007) and β-galactosidase (Broome et al., 2010) for colorimetric assays, thymidine kinase for positron emission tomography (Massoud et al., 2010) and proteases such as the tobacco etch virus (TEV) split protease, which allows cleavage of proteins and creates complex reporter approaches such as reducing the levels of a marked protein or releasing anchored TFs (Wintgens et al., 2017). Since all these systems are based on the same principle of interaction between their fused partners, we could evaluate how to implement them as reporter systems for our biosensor, broadening its potential for diagnostic applications both *in vivo* and *in vitro*. Moreover, the interaction signal could be further engineered to reach the cytoplasm and activate a genetically encoded response, which would open our system to therapeutic applications of high specificity. Such signal could even be integrated together with the specific promoters and integrase-derived genetic logic in order to compute both metabolic and antigenic stimuli into the triggering of a response.

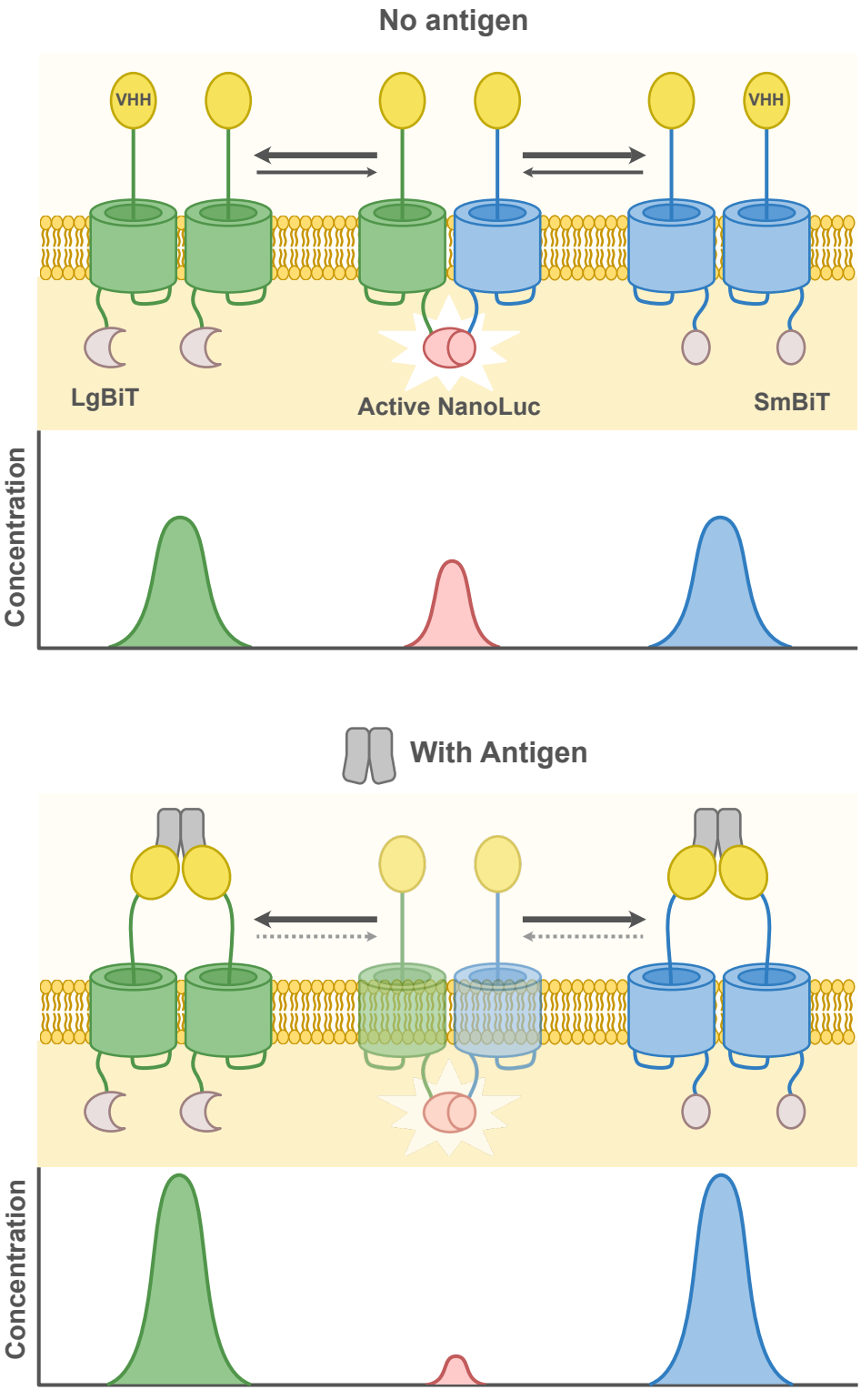

Figure 58. Proposed model for the functioning of our antigen biosensor. In the absence of antigen, the chimeric intimin and invasin proteins form homodimers with a higher frequency than heterodimers. When the dimeric antigen is present, it binds simultaneously to both Nbs in the pair, stabilizing the homodimers and reducing their capacity to dissociate and form heterodimers. This reduces the luminescence signal produced by the heterodimers. The barrels of invasin are colored green and those of intimin in blue. Nbs are colored in yellow. SmBiT (ovals) and LgBiT (half-moons) are colored in grey when inactive and in red when they complement each other to produce luminescence.

CONCLUSIONS

Conclusions

1. The inducible P_{lldP} promoter of *E. coli*, integrated in the chromosome, strongly responds to L-lactate concentrations similar to those found in tumors but show leakage in the absence of inducer, especially when bacteria were grown at 37 ºC with strong agitation. A mutated version of this promoter increased its response under low-oxygen conditions but also presented leakage in the absence of inducer.

2. The inducible P_{uof} promoter of *E. coli,* integrated in the chromosome, showed a low response to the presence of H_2O_2 and a high leakage during growth at 37 ºC.

3. The NO-activated promoters P_{norV} and P_{hmp} integrated in the chromosome of *E. coli* show induction with NO generators that mimic tumor conditions, with low leakage in the absence of NO. P_{hmp} has a higher sensitivity and induction levels when bacteria are grown at 37 ºC.

4. Using three serine integrases, BxB1, Tp901 and Int7, we have demonstrated that genetic logic circuits and genetic memory can be generated employing targets integrated in the chromosome of *E. coli*, with excision being more efficient than inversion.

5. The serine integrases Bxb1 and Tp901 can be induced from genes integrated in the chromosome at sufficient levels for the excision of targets also integrated in the chromosome of *E. coli*.

6. We have engineered a NO biosensor in *E. coli* that generates genetic memory by using the P_{hmp} promoter controlling the Bxb1 serine integrase, with all the component integrated in the chromosome. The activation of the promoter by NO produces Bxb1 and the subsequent excision of a transcriptional terminator, eliciting expression of a GFP reporter that is stably maintained in the following generations.

7. We have generated chimeric outer membrane proteins that display a nanobody on the bacterial surface and a protein fusion in the periplasm. These chimeric proteins are based on the β-barrels of T5SS members intimin, invasin and EhaA.

The periplasmic fusions tolerate short peptides (SmBiT, SpyTag, SnoopTag) as well as large fragments of enzymes (LgBiT).

8. We have shown that intimin and invasin β-barrels form homodimers even in the absence of protein domains reported to participate in dimerization, such as the periplasmic LysM and its spacer on intimin and the surface-exposed D2 domain of invasin from *Y. pseudotuberculosis*.

9. We have demonstrated that the engineered chimeric outer membrane proteins can generate *E. coli* bacteria able to detect the presence of an extracellular tumor associated antigen (i.e., human EGFR). This bacterial biosensor is based on the coexpression of two chimeric proteins consisting of a nanobody binding the protein antigen, a β-barrel domain of intimin or invasin and periplasmic fusions to the SmBiT and LgBiT fragments of NanoLuc luciferase. Bacteria produce a bioluminescent signal that is specifically reduced in the presence of the extracellular tumor antigen in a dose-dependent manner.

Conclusiones

1. El promotor inducible P_{lldP} de *E. coli*, integrado en el cromosoma, responde fuertemente a concentraciones de L-lactato similares a aquellas encontradas en tumores, pero presenta inducción en ausencia del inductor, especialmente cuando las bacterias son cultivadas a 37 ºC con una fuerte agitación. Una versión mutada de este promotor presentó un aumento de su respuesta en condiciones de poco oxígeno, pero también mostraba inducción en ausencia del inductor.

2. El promotor inducible P_{uof} de *E. coli*, integrado en el cromosoma, presentó una baja respuesta a la presencia de H_2O_2 y un alto escape durante el crecimiento a 37 ºC.

3. Los promotores activables por NO P_{norV} and P_{hmp}, integrados en el cromosoma de *E. coli*, presentan inducción en la presencia de generadores de NO que imitan las condiciones tumorales, con un bajo escape en ausencia de NO. P_{hmp} tiene una mayor sensibilidad y mayores niveles de inducción cuando las bacterias son cultivadas a 37 ºC.

4. Empleando tres serin-integrasas, Bxb1, Tp901 y Int7, hemos demostrado que se pueden generar circuitos genéticos lógicos y de memoria utilizando dianas integradas en el cromosoma de *E. coli*, siendo la excisión más eficiente que la inversión.

5. Las serin-integrasas Bxb1 y Tp901 pueden ser inducidas desde genes integrados en el cromosoma hasta niveles suficientes para la excisión de dianas integradas en el cromosoma de *E. coli*.

6. Hemos generado un biosensor de NO en *E. coli* que produce memoria genética usando el promotor P_{hmp} para controlar la serin-integrasa Bxb1, con todos los componentes integrados en el cromosoma. La activación del promotor por NO produce Bxb1 y la consiguiente excisión de un terminador transcripcional, provocando la expresión de un gen reportero, GFP, que se expresa de manera estable en las siguientes generaciones.

7. Hemos generado proteínas quiméricas de membrana externa que presentan un nanoanticuerpo en la superficie bacteriana y una fusión proteica en el

periplasma. Estas proteínas quiméricas están basadas en los barriles β de las proteínas pertenecientes al T5SS intimina, invasina y EhaA. Las fusiones periplásmicas toleran tanto péptidos cortos (SmBiT, SpyTag, SnoopTag) como fragmentos grandes de enzimas (LgBiT).

8. Hemos demostrado que los barriles β de intimina e invasina forman homodímeros incluso en ausencia de aquellos dominios proteicos que habían sido previamente relacionados con el proceso de dimerización, como el dominio periplásmico LysM y su secuencia espaciadora en intimina y el dominio D2 expuesto en la superficie bacteriana por la invasina de *Y. pseudotuberculosis*.

9. Hemos demostrado que las proteínas quiméricas de membrana externa generadas pueden emplearse para generar una *E. coli* capaz de detectar la presencia de un antígeno asociado a tumores extracelular (p. ej. EGFR humano). Este biosensor bacteriano está basado en la coexpresión de dos proteínas quiméricas consistentes en un nanoanticuerpo capaz de unirse el antígeno proteico, el dominio barril β de intimina o invasina y fusiones periplásmicas a los fragmentos SmBiT y LgBiT de la luciferasa NanoLuc. Las bacterias producen una señal bioluminiscente que se reduce específicamente por la presencia extracelular del antígeno asociado a tumores, con dependencia de la dosis.

REFERENCES

Abedi, M.H. *et al.* (2022) 'Ultrasound-controllable engineered bacteria for cancer immunotherapy', *Nature Communications*, 13(1), p. 1585. Available at: https://doi.org/10.1038/s41467-022-29065-2.

Aguilera, L. *et al.* (2008) 'Dual Role of LldR in Regulation of the lldPRD Operon, Involved in L-Lactate Metabolism in *Escherichia coli*', *Journal of Bacteriology*, 190(8), pp. 2997–3005. Available at: https://doi.org/10.1128/JB.02013-07.

Alejandro Asensio Calavia (2021) *Engineering of E. coli for protein translocation into target mammalian cells and its in vivo application in tumor therapy*. Universidad Autónoma de Madrid. Available at: http://hdl.handle.net/10486/695770.

Alexeeva, S., Hellingwerf, K.J. and Teixeira de Mattos, M.J. (2003) 'Requirement of ArcA for redox regulation in *Escherichia coli* under microaerobic but not anaerobic or aerobic conditions', *Journal of Bacteriology*, 185(1), pp. 204–209. Available at: https://doi.org/10.1128/JB.185.1.204-209.2003.

Alhunaidi, O. and Zlotta, A.R. (2019) 'The use of intravesical BCG in urothelial carcinoma of the bladder', *Ecancermedicalscience*, 13, p. 905. Available at: https://doi.org/10.3332/ecancer.2019.905.

Andersen, J.B. *et al.* (1998) 'New unstable variants of green fluorescent protein for studies of transient gene expression in bacteria', *Applied and Environmental Microbiology*, 64(6), pp. 2240–2246. Available at: https://doi.org/10.1128/AEM.64.6.2240-2246.1998.

Anderson, J.C. *et al.* (2006) 'Environmentally controlled invasion of cancer cells by engineered bacteria', *Journal of Molecular Biology*, 355(4), pp. 619–627. Available at: https://doi.org/10.1016/j.jmb.2005.10.076.

Andreas, S. *et al.* (2002) 'Enhanced efficiency through nuclear localization signal fusion on phage PhiC31-integrase: activity comparison with Cre and FLPe recombinase in mammalian cells', *Nucleic Acids Research*, 30(11), pp. 2299–2306. Available at: https://doi.org/10.1093/nar/30.11.2299.

Archer, E.J., Robinson, A.B. and Süel, G.M. (2012) 'Engineered *E. coli* That Detect and Respond to Gut Inflammation through Nitric Oxide Sensing', *ACS Synthetic Biology*, 1(10), pp. 451–457. Available at: https://doi.org/10.1021/sb3000595.

Arezumand, R. *et al.* (2017) 'Nanobodies As Novel Agents for Targeting Angiogenesis in Solid Cancers', *Frontiers in Immunology*, 8, p. 1746. Available at: https://doi.org/10.3389/fimmu.2017.01746.

Ashok Kumar, T. (2013) 'CFSSP: Chou and Fasman Secondary Structure Prediction server'. Zenodo. Available at: https://doi.org/10.5281/zenodo.50733.

Ausubel, F.M. *et al.* (2002) *Short protocols in molecular biology*. 5th edn. John Wiley & Sons, New York.

Avdagić, N. *et al.* (2013) 'Nitric oxide as a potential biomarker in inflammatory bowel disease', *Bosnian Journal of Basic Medical Sciences*, 13(1), pp. 5–9. Available at: https://doi.org/10.17305/bjbms.2013.2402.

Babu, M. *et al.* (2018) 'Global landscape of cell envelope protein complexes in *Escherichia coli*', *Nature Biotechnology*, 36(1), pp. 103–112. Available at: https://doi.org/10.1038/nbt.4024.

Bader, J.E., Voss, K. and Rathmell, J.C. (2020) 'Targeting Metabolism to Improve the Tumor Microenvironment for Cancer Immunotherapy', *Molecular Cell*, 78(6), pp. 1019–1033. Available at: https://doi.org/10.1016/j.molcel.2020.05.034.

Baez, A. and Shiloach, J. (2013) '*Escherichia coli* avoids high dissolved oxygen stress by activation of SoxRS and manganese-superoxide dismutase', *Microbial Cell Factories*, 12(1), p. 23. Available at: https://doi.org/10.1186/1475-2859-12-23.

Bamert, R.S. *et al.* (2017) 'Structural basis for substrate selection by the translocation and assembly module of the β-barrel assembly machinery', *Molecular Microbiology*, 106(1), pp. 142–156. Available at: https://doi.org/10.1111/mmi.13757.

Barnard, T.J. *et al.* (2007) 'Autotransporter structure reveals intra-barrel cleavage followed by conformational changes', *Nature Structural & Molecular Biology*, 14(12), pp. 1214–1220. Available at: https://doi.org/10.1038/nsmb1322.

Beimfohr, C. (2016) 'A Review of Research Conducted with Probiotic *E. coli* Marketed as Symbioflor', *International Journal of Bacteriology*, 2016, p. 3535621. Available at: https://doi.org/10.1155/2016/3535621.

van den Berg, B. (2010) 'Crystal structure of a full-length autotransporter', *Journal of Molecular Biology*, 396(3), pp. 627–633. Available at: https://doi.org/10.1016/j.jmb.2009.12.061.

Bernstein, H.D. (2007) 'Are bacterial "autotransporters" really transporters?', *Trends in Microbiology*, 15(10), pp. 441–447. Available at: https://doi.org/10.1016/j.tim.2007.09.007.

Bertram, R. and Hillen, W. (2008) 'The application of Tet repressor in prokaryotic gene regulation and expression', *Microbial Biotechnology*, 1(1), pp. 2–16. Available at: https://doi.org/10.1111/j.1751-7915.2007.00001.x.

Binder, U. *et al.* (2010) 'High-throughput Sorting of an Anticalin Library via EspP-mediated Functional Display on the *Escherichia coli* Cell Surface', *Journal of Molecular Biology*, 400(4), pp. 783–802. Available at: https://doi.org/10.1016/j.jmb.2010.05.049.

Blattner, F.R. *et al.* (1997) 'The Complete Genome Sequence of *Escherichia coli* K-12', *Science*, 277(5331), pp. 1453–1462. Available at: https://doi.org/10.1126/science.277.5331.1453.

Bodelon, G., Marin, E. and Fernandez, L.A. (2009) 'Role of periplasmic chaperones and BamA (YaeT/Omp85) in folding and secretion of intimin from enteropathogenic *Escherichia coli* strains', *J Bacteriol*, 191(16), pp. 5169–79. Available at: https://doi.org/10.1128/JB.00458-09.

Bodenmiller, D.M. and Spiro, S. (2006) 'The yjeB (nsrR) gene of *Escherichia coli* encodes a nitric oxide-sensitive transcriptional regulator', *Journal of Bacteriology*, 188(3), pp. 874–881. Available at: https://doi.org/10.1128/JB.188.3.874-881.2006.

Böldicke, T. (2017) 'Single domain antibodies for the knockdown of cytosolic and nuclear proteins', *Protein Science: A Publication of the Protein Society*, 26(5), pp. 925–945. Available at: https://doi.org/10.1002/pro.3154.

Bonnet, J. *et al.* (2013) 'Amplifying genetic logic gates', *Science*, 340(6132), pp. 599–603. Available at: https://doi.org/10.1126/science.1232758.

Bonnet, J., Subsoontorn, P. and Endy, D. (2012) 'Rewritable digital data storage in live cells via engineered control of recombination directionality', *Proceedings of the National Academy of Sciences of the United States of America*, 109(23), pp. 8884–8889. Available at: https://doi.org/10.1073/pnas.1202344109.

Boute, N. *et al.* (2016) 'NanoLuc Luciferase - A Multifunctional Tool for High Throughput Antibody Screening', *Frontiers in Pharmacology*, 7, p. 27. Available at: https://doi.org/10.3389/fphar.2016.00027.

Brizel, D.M., Walenta, S. and Mueller-Klieser, W. (2001) 'Elevated Tumor Lactate Concentrations Predict For An Increased Risk Of Metastases In Head-And-Neck Cancer', 51(2), p. 5.

Brockstedt, D.G. *et al.* (2004) 'Listeria-based cancer vaccines that segregate immunogenicity from toxicity', *Proceedings of the National Academy of Sciences*, 101(38), pp. 13832–13837. Available at: https://doi.org/10.1073/pnas.0406035101.

Broome, A.-M. *et al.* (2010) 'Expanding the utility of β-galactosidase complementation: piece by piece', *Molecular pharmaceutics*, 7(1), pp. 60–74. Available at: https://doi.org/10.1021/mp900188e.

Cabantous, S. *et al.* (2013) 'A New Protein-Protein Interaction Sensor Based on Tripartite Split-GFP Association', *Scientific Reports*, 3(1), p. 2854. Available at: https://doi.org/10.1038/srep02854.

Carmeliet, P. and Jain, R.K. (2011) 'Molecular mechanisms and clinical applications of angiogenesis', *Nature*, 473(7347), pp. 298–307. Available at: https://doi.org/10.1038/nature10144.

Carmen Mañas Torres (2019) *Engineering E. coli to target bladder and colon tumor cells and characterization of the adhesion process.* Universidad Autónoma de Madrid. Available at: http://hdl.handle.net/10486/690418.

Casasnovas, J.M. *et al.* (2022) 'Nanobodies Protecting From Lethal SARS-CoV-2 Infection Target Receptor Binding Epitopes Preserved in Virus Variants Other Than Omicron', *Frontiers in Immunology*, 13, p. 863831. Available at: https://doi.org/10.3389/fimmu.2022.863831.

Castagliuolo, I. *et al.* (2005) 'Engineered *E. col*i delivers therapeutic genes to the colonic mucosa', *Gene Therapy*, 12(13), pp. 1070–1078. Available at: https://doi.org/10.1038/sj.gt.3302493.

Chabloz, A. *et al.* (2020) '*Salmonella*-based platform for efficient delivery of functional binding proteins to the cytosol', *Communications Biology*, 3(1), pp. 1–11. Available at: https://doi.org/10.1038/s42003-020-1072-4.

Chang, H.-J. *et al.* (2018) 'A Modular Receptor Platform To Expand the Sensing Repertoire of Bacteria', *ACS Synthetic Biology*, 7(1), pp. 166–175. Available at: https://doi.org/10.1021/acssynbio.7b00266.

Chang, Z.L. *et al.* (2018) 'Rewiring T-cell responses to soluble factors with chimeric antigen receptors', *Nature Chemical Biology*, 14(3), pp. 317–324. Available at: https://doi.org/10.1038/nchembio.2565.

Chaplain, M.A.J. (1993) 'The Development of a Spatial Pattern in a Model for Cancer Growth', in H.G. Othmer, P.K. Maini, and J.D. Murray (eds) *Experimental and Theoretical Advances in Biological Pattern Formation*. Boston, MA: Springer US, pp. 45–59. Available at: https://doi.org/10.1007/978-1-4615-2433-5_7.

Chauhan, N. *et al.* (2016) '*Yersinia* adhesins: An arsenal for infection', *PROTEOMICS - Clinical Applications*, 10(9–10), pp. 949–963. Available at: https://doi.org/10.1002/prca.201600012.

Chen, X. *et al.* (2007) 'A model of NO/O2 transport in capillary-perfused tissue containing an arteriole and venule pair', *Annals of Biomedical Engineering*, 35(4), pp. 517–529. Available at: https://doi.org/10.1007/s10439-006-9236-z.

Chen, X.J. *et al.* (2021) 'Rational Design and Characterization of Nitric Oxide Biosensors in *E. coli* Nissle 1917 and Mini SimCells', *ACS Synthetic Biology*, p. acssynbio.1c00223. Available at: https://doi.org/10.1021/acssynbio.1c00223.

Chen, Z. *et al.* (2007) 'Discovery of Fur binding site clusters in *Escherichia coli* by information theory models', *Nucleic Acids Research*, 35(20), pp. 6762–6777. Available at: https://doi.org/10.1093/nar/gkm631.

Cheng, R.Y. *et al.* (2014) 'Gene Expression Profiles of NO- and HNO-donor Treated Breast Cancer Cells: Insights into Tumor Response and Resistance Pathways', *Nitric oxide : biology and chemistry / official journal of the Nitric Oxide Society*, 43, pp. 17–28. Available at: https://doi.org/10.1016/j.niox.2014.08.003.

Chhabra, S. and Spiro, S. (2015) 'Inefficient translation of nsrR constrains behaviour of the NsrR regulon in *Escherichia coli*', *Microbiology (Reading, England)*, 161(10), pp. 2029–2038. Available at: https://doi.org/10.1099/mic.0.000151.

Chien, T. *et al.* (2021) 'Enhancing the tropism of bacteria via genetically programmed biosensors', *Nature Biomedical Engineering* [Preprint]. Available at: https://doi.org/10.1038/s41551-021-00772-3.

Chien, T., Doshi, A. and Danino, T. (2017) 'Advances in bacterial cancer therapies using synthetic biology', *Current Opinion in Systems Biology*, 5, pp. 1–8. Available at: https://doi.org/10.1016/j.coisb.2017.05.009.

Choi, S.Y.C. *et al.* (2013) 'Cancer-generated lactic acid: a regulatory, immunosuppressive metabolite?', *The Journal of Pathology*, 230(4), pp. 350–355. Available at: https://doi.org/10.1002/path.4218.

Chung, C.T., Niemela, S.L. and Miller, R.H. (1989) 'One-step preparation of competent *Escherichia coli*: transformation and storage of bacterial cells in the same solution', *Proceedings of the National Academy of Sciences of the United States of America*, 86(7), pp. 2172–2175. Available at: https://doi.org/10.1073/pnas.86.7.2172.

Coley, W.B. (1891) 'II. Contribution to the Knowledge of Sarcoma', *Annals of Surgery*, 14(3), pp. 199–220.

Coley, W.B. (1910) 'The Treatment of Inoperable Sarcoma by Bacterial Toxins (the Mixed Toxins of the Streptococcus erysipelas and the Bacillus prodigiosus)', *Proceedings of the Royal Society of Medicine*, 3(Surg Sect), pp. 1–48.

Colloms, S.D. *et al.* (2014) 'Rapid metabolic pathway assembly and modification using serine integrase site-specific recombination', *Nucleic Acids Research*, 42(4), p. e23. Available at: https://doi.org/10.1093/nar/gkt1101.

Corcoran, C.P., Cameron, A.D.S. and Dorman, C.J. (2010) 'H-NS Silences gfp, the Green Fluorescent Protein Gene: gfpTCD Is a Genetically Remastered gfp Gene with Reduced Susceptibility to H-NS-Mediated Transcription Silencing and with Enhanced Translation', *Journal of Bacteriology*, 192(18), pp. 4790–4793. Available at: https://doi.org/10.1128/JB.00531-10.

da Costa, P.N., Teixeira, M. and Saraiva, L.M. (2003) 'Regulation of the flavorubredoxin nitric oxide reductase gene in *Escherichia coli*: nitrate repression, nitrite induction, and possible post-transcription control', *FEMS microbiology letters*, 218(2), pp. 385–393. Available at: https://doi.org/10.1016/S0378-1097(02)01186-2.

Courbet, A. *et al.* (2015) 'Detection of pathological biomarkers in human clinical samples via amplifying genetic switches and logic gates', *Science Translational Medicine*, 7(289). Available at: https://doi.org/10.1126/scitranslmed.aaa3601.

Craig NL *et al.* (2002) *Mobile DNA II*. 2nd Edition. Washington, DC: ASM Press. Available at: https://www.wiley.com/en-uz/Mobile+DNA+II%2C+2nd+Edition-p-9781555812096 (Accessed: 2 October 2022).

Critchley, R.J. *et al.* (2004) 'Potential therapeutic applications of recombinant, invasive *E. coli*', *Gene Therapy*, 11(15), pp. 1224–1233. Available at: https://doi.org/10.1038/sj.gt.3302281.

Cruz-Ramos, H. *et al.* (2002) 'NO sensing by FNR: regulation of the *Escherichia coli* NO-detoxifying flavohaemoglobin, Hmp', *The EMBO journal*, 21(13), pp. 3235–3244. Available at: https://doi.org/10.1093/emboj/cdf339.

Curtiss, R. and Kelly, S.M. (1987) '*Salmonella typhimurium* deletion mutants lacking adenylate cyclase and cyclic AMP receptor protein are avirulent and immunogenic', *Infection and Immunity*, 55(12), pp. 3035–3043. Available at: https://doi.org/10.1128/iai.55.12.3035-3043.1987.

Danino, T. *et al.* (2015) 'Programmable probiotics for detection of cancer in urine', *Science Translational Medicine*, 7(289), pp. 289ra84-289ra84. Available at: https://doi.org/10.1126/scitranslmed.aaa3519.

Daringer, N.M. *et al.* (2014) 'Modular extracellular sensor architecture for engineering mammalian cell-based devices', *ACS synthetic biology*, 3(12), pp. 892–902. Available at: https://doi.org/10.1021/sb400128g.

Datsenko, K.A. and Wanner, B.L. (2000) 'One-step inactivation of chromosomal genes in *Escherichia coli* K-12 using PCR products', *Proceedings of the National Academy of Sciences*, 97(12), pp. 6640–6645. Available at: https://doi.org/10.1073/pnas.120163297.

De Lorenzo, V. *et al.* (1988) 'Fur (ferric uptake regulation) protein and CAP (catabolite-activator protein) modulate transcription of fur gene in *Escherichia coli*', *European Journal of Biochemistry*, 173(3), pp. 537–546. Available at: https://doi.org/10.1111/j.1432-1033.1988.tb14032.x.

De Reuse, H. and Danchin, A. (1988) 'The *ptsH*, *ptsI*, and *crr* genes of the *Escherichia coli* phosphoenolpyruvate-dependent phosphotransferase system: a complex operon with several modes of transcription', *Journal of Bacteriology*, 170(9), pp. 3827–3837. Available at: https://doi.org/10.1128/jb.170.9.3827-3837.1988.

Del Monte, U. (2009) 'Does the cell number 109 still really fit one gram of tumor tissue?', *Cell Cycle*, 8(3), pp. 505–506. Available at: https://doi.org/10.4161/cc.8.3.7608.

Dersch, P. and Isberg, R.R. (2000) 'An Immunoglobulin Superfamily-Like Domain Unique to the *Yersinia pseudotuberculosis* Invasin Protein Is Required for Stimulation of Bacterial Uptake via Integrin Receptors', *Infection and Immunity*. Edited by J.D. Clements, 68(5), pp. 2930–2938. Available at: https://doi.org/10.1128/IAI.68.5.2930-2938.2000.

Deszyński, P. *et al.* (2022) 'INDI-integrated nanobody database for immunoinformatics', *Nucleic Acids Research*, 50(D1), pp. D1273–D1281. Available at: https://doi.org/10.1093/nar/gkab1021.

Deyneko, I.V. *et al.* (2016) 'Composing a Tumor Specific Bacterial Promoter', *PLOS ONE*. Edited by I.C. Allen, 11(5), p. e0155338. Available at: https://doi.org/10.1371/journal.pone.0155338.

Din, M.O. *et al.* (2016) 'Synchronized cycles of bacterial lysis for in vivo delivery', *Nature*, 536(7614), pp. 81–85. Available at: https://doi.org/10.1038/nature18930.

Dixon, A.S. *et al.* (2016) 'NanoLuc Complementation Reporter Optimized for Accurate Measurement of Protein Interactions in Cells', *ACS Chemical Biology*, 11(2), pp. 400–408. Available at: https://doi.org/10.1021/acschembio.5b00753.

Dong, J.M. *et al.* (1993) 'Three overlapping *lct* genes involved in L-lactate utilization by *Escherichia coli*', *Journal of Bacteriology*, 175(20), pp. 6671–6678. Available at: https://doi.org/10.1128/jb.175.20.6671-6678.1993.

Doyle, M.T. and Bernstein, H.D. (2021) 'BamA forms a translocation channel for polypeptide export across the bacterial outer membrane', *Molecular Cell*, 81(9), pp. 2000-2012.e3. Available at: https://doi.org/10.1016/j.molcel.2021.02.023.

Drobnak, I. *et al.* (2015) 'Of linkers and autochaperones: An unambiguous nomenclature to identify common and uncommon themes for autotransporter secretion*', *Molecular microbiology*, 95(1), pp. 1–16. Available at: https://doi.org/10.1111/mmi.12838.

Durand, S. and Storz, G. (2010) 'Reprogramming of anaerobic metabolism by the FnrS small RNA', *Molecular Microbiology*, 75(5), pp. 1215–1231. Available at: https://doi.org/10.1111/j.1365-2958.2010.07044.x.

Durfee, T. *et al.* (2008) 'The Complete Genome Sequence of *Escherichia coli* DH10B: Insights into the Biology of a Laboratory Workhorse', *Journal of Bacteriology*, 190(7), pp. 2597–2606. Available at: https://doi.org/10.1128/JB.01695-07.

Dvorak, P. *et al.* (2015) 'Exacerbation of substrate toxicity by IPTG in *Escherichia coli* BL21(DE3) carrying a synthetic metabolic pathway', *Microbial Cell Factories*, 14, p. 201. Available at: https://doi.org/10.1186/s12934-015-0393-3.

Dvořák, P., Bayer, E.A. and de Lorenzo, V. (2020) 'Surface Display of Designer Protein Scaffolds on Genome-Reduced Strains of *Pseudomonas putida*', *ACS Synthetic Biology*, 9(10), pp. 2749–2764. Available at: https://doi.org/10.1021/acssynbio.0c00276.

Elowitz, M.B. and Leibler, S. (2000) 'A synthetic oscillatory network of transcriptional regulators', *Nature*, 403(6767), pp. 335–338. Available at: https://doi.org/10.1038/35002125.

England, C.G., Ehlerding, E.B. and Cai, W. (2016) 'NanoLuc: A Small Luciferase Is Brightening Up the Field of Bioluminescence', *Bioconjugate Chemistry*, 27(5), pp. 1175–1187. Available at: https://doi.org/10.1021/acs.bioconjchem.6b00112.

Eva Pico Sánchez (2020) *Engineering of E. coli bacteria for targeting human and murine epithelial tumor cells expressing HER2 and PD-L1 markers and their application in the colonization of mouse bladder tumors in vivo*. Universidad Autónoma de Madrid. Available at: http://hdl.handle.net/10486/694084.

Fábrega, M.-J. *et al.* (2017) 'Intestinal Anti-inflammatory Effects of Outer Membrane Vesicles from *Escherichia coli* Nissle 1917 in DSS-Experimental Colitis in Mice', *Frontiers in Microbiology*, 8, p. 1274. Available at: https://doi.org/10.3389/fmicb.2017.01274.

Fairman, J.W. *et al.* (2012) 'Crystal structures of the outer membrane domain of intimin and invasin from enterohemorrhagic *E. coli* and enteropathogenic *Y. pseudotuberculosis*', *Structure*, 20(7), pp. 1233–43. Available at: https://doi.org/10.1016/j.str.2012.04.011.

Ferrières, L. *et al.* (2010) 'Silent Mischief: Bacteriophage Mu Insertions Contaminate Products of *Escherichia coli* Random Mutagenesis Performed Using Suicidal Transposon Delivery Plasmids Mobilized by Broad-Host-Range RP4 Conjugative Machinery', *Journal of Bacteriology*, 192(24), pp. 6418–6427. Available at: https://doi.org/10.1128/JB.00621-10.

Flickinger, J.C., Rodeck, U. and Snook, A.E. (2018) '*Listeria monocytogenes* as a Vector for Cancer Immunotherapy: Current Understanding and Progress', *Vaccines*, 6(3), p. 48. Available at: https://doi.org/10.3390/vaccines6030048.

Food and Agriculture Organization of the United Nations and World Health Organization (2002) *Guidelines for the evaluation of probiotics in food: report of a Joint FAO/WHO Working Group.* London, Ontario, Canada.

Forbes, N.S. *et al.* (2003) 'Sparse initial entrapment of systemically injected *Salmonella typhimurium* leads to heterogeneous accumulation within tumors', *Cancer Research*, 63(17), pp. 5188–5193.

Forbes, N.S. (2010) 'Engineering the perfect (bacterial) cancer therapy', *Nature Reviews Cancer*, 10(11), pp. 785–794. Available at: https://doi.org/10.1038/nrc2934.

Forbes, N.S. *et al.* (2018) 'White paper on microbial anti-cancer therapy and prevention', *Journal for ImmunoTherapy of Cancer*, 6(1), p. 78. Available at: https://doi.org/10.1186/s40425-018-0381-3.

Fu, A. *et al.* (2022) 'Tumor-resident intracellular microbiota promotes metastatic colonization in breast cancer', *Cell*, 185(8), pp. 1356-1372.e26. Available at: https://doi.org/10.1016/j.cell.2022.02.027.

Galarneau, A. *et al.* (2002) 'β-Lactamase protein fragment complementation assays as in vivo and in vitro sensors of protein–protein interactions', *Nature Biotechnology*, 20, p. 619. Available at: https://doi.org/10.1038/nbt0602-619.

Galdzicki, M. *et al.* (2014) 'The Synthetic Biology Open Language (SBOL) provides a community standard for communicating designs in synthetic biology', *Nature Biotechnology*, 32(6), pp. 545–550. Available at: https://doi.org/10.1038/nbt.2891.

Gandhi, N.M., Morales, A. and Lamm, D.L. (2013) 'Bacillus Calmette-Guérin immunotherapy for genitourinary cancer', *BJU international*, 112(3), pp. 288–297. Available at: https://doi.org/10.1111/j.1464-410X.2012.11754.x.

Gardner, T.S., Cantor, C.R. and Collins, J.J. (2000) 'Construction of a genetic toggle switch in *Escherichia coli*', *Nature*, 403(6767), pp. 339–342. Available at: https://doi.org/10.1038/35002131.

Garnier, J., Osguthorpe, D.J. and Robson, B. (1978) 'Analysis of the accuracy and implications of simple methods for predicting the secondary structure of globular proteins', *Journal of Molecular Biology*, 120(1), pp. 97–120. Available at: https://doi.org/10.1016/0022-2836(78)90297-8.

Gawarzewski, I. *et al.* (2013) 'Structural comparison of the transport units of type V secretion systems', *Biological Chemistry*, 394(11), pp. 1385–1398. Available at: https://doi.org/10.1515/hsz-2013-0162.

Geller, L.T. *et al.* (2017) 'Potential role of intratumor bacteria in mediating tumor resistance to the chemotherapeutic drug gemcitabine', *Science (New York, N.Y.)*, 357(6356), pp. 1156–1160. Available at: https://doi.org/10.1126/science.aah5043.

Georgellis, D., Lynch, A.S. and Lin, E.C. (1997) 'In vitro phosphorylation study of the arc two-component signal transduction system of *Escherichia coli*', *Journal of Bacteriology*, 179(17), pp. 5429–5435. Available at: https://doi.org/10.1128/jb.179.17.5429-5435.1997.

Gibbs, K.A. *et al.* (2004) 'Complex spatial distribution and dynamics of an abundant *Escherichia coli* outer membrane protein, LamB', *Molecular Microbiology*, 53(6), pp. 1771–1783. Available at: https://doi.org/10.1111/j.1365-2958.2004.04242.x.

Gibson, D.G. *et al.* (2009) 'Enzymatic assembly of DNA molecules up to several hundred kilobases.', *Nature methods*, 6(5), pp. 343–345. Available at: https://doi.org/10.1038/nmeth.1318.

Goers, L. *et al.* (2017) 'Whole-cell *Escherichia coli* lactate biosensor for monitoring mammalian cell cultures during biopharmaceutical production', *Biotechnology and Bioengineering*, 114(6), pp. 1290–1300. Available at: https://doi.org/10.1002/bit.26254.

Goh, K.G.K. *et al.* (2019) 'Bioinformatic and Molecular Analysis of Inverse Autotransporters from *Escherichia col*i', *mSphere*, 4(4), pp. e00572-19. Available at: https://doi.org/10.1128/mSphere.00572-19.

Green, E.R. and Mecsas, J. (2016) 'Bacterial Secretion Systems: An Overview', *Microbiology Spectrum*, 4(1). Available at: https://doi.org/10.1128/microbiolspec.VMBF-0012-2015.

Grijpstra, J. *et al.* (2013) 'Autotransporter secretion: varying on a theme', *Research in Microbiology*, 164(6), pp. 562–582. Available at: https://doi.org/10.1016/j.resmic.2013.03.010.

Grindley, N.D.F., Whiteson, K.L. and Rice, P.A. (2006) 'Mechanisms of site-specific recombination', *Annual Review of Biochemistry*, 75, pp. 567–605. Available at: https: //doi.org/10.1146/annurev.biochem.73.011303.073908.

Gruss, F. *et al.* (2013) 'The structural basis of autotransporter translocation by TamA', *Nature Structural & Molecular Biology*, 20(11), pp. 1318–1320. Available at: https://doi.org/10.1038/nsmb.2689.

Guérin, J. *et al.* (2017) 'Two-Partner Secretion: Combining Efficiency and Simplicity in the Secretion of Large Proteins for Bacteria-Host and Bacteria-Bacteria Interactions', *Frontiers in Cellular and Infection Microbiology*, 7, p. 148. Available at: https://doi.org/10.3389/fcimb.2017.00148.

Guiziou, S., Mayonove, P. and Bonnet, J. (2019) 'Hierarchical composition of reliable recombinase logic devices', *Nature Communications*, 10(1), p. 456. Available at: https://doi.org/10.1038/s41467-019-08391-y.

Gustavsson, M., Bäcklund, E. and Larsson, G. (2011) 'Optimisation of surface expression using the AIDA autotransporter', *Microbial Cell Factories*, 10(1), p. 72. Available at: https://doi.org/10.1186/1475-2859-10-72.

Hagan, C.L., Silhavy, T.J. and Kahne, D. (2011) 'β-Barrel membrane protein assembly by the Bam complex', *Annual Review of Biochemistry*, 80, pp. 189–210. Available at: https://doi.org/10.1146/annurev-biochem-061408-144611.

Hall, B.A., Armitage, J.P. and Sansom, M.S.P. (2012) 'Mechanism of Bacterial Signal Transduction Revealed by Molecular Dynamics of Tsr Dimers and Trimers of Dimers in Lipid Vesicles', *PLOS Computational Biology*, 8(9), p. e1002685. Available at: https://doi.org/10.1371/journal.pcbi.1002685.

Ham, T.S. *et al.* (2008) 'Design and construction of a double inversion recombination switch for heritable sequential genetic memory', *PloS One*, 3(7), p. e2815. Available at: https://doi.org/10.1371/journal.pone.0002815.

Hamburger, Z.A. *et al.* (1999) 'Crystal structure of invasin: a bacterial integrin-binding protein', *Science (New York, N.Y.)*, 286(5438), pp. 291–295. Available at: https://doi.org/10.1126/science.286.5438.291.

Harmsen, M.M. and De Haard, H.J. (2007) 'Properties, production, and applications of camelid single-domain antibody fragments', *Applied Microbiology and Biotechnology*, 77(1), pp. 13–22. Available at: https://doi.org/10.1007/s00253-007-1142-2.

Hatlem, D. *et al.* (2019) 'Catching a SPY: Using the SpyCatcher-SpyTag and Related Systems for Labeling and Localizing Bacterial Proteins', *International Journal of Molecular Sciences*, 20(9), p. 2129. Available at: https://doi.org/10.3390/ijms20092129.

Hegde, R.S. and Bernstein, H.D. (2006) 'The surprising complexity of signal sequences', *Trends in Biochemical Sciences*, 31(10), pp. 563–571. Available at: https://doi.org/10.1016/j.tibs.2006.08.004.

Heinz, E. *et al.* (2016) 'Conserved Features in the Structure, Mechanism, and Biogenesis of the Inverse Autotransporter Protein Family', *Genome Biol Evol*, 8(6), pp. 1690–705. Available at: https://doi.org/10.1093/gbe/evw112.

Henderson, I.R. *et al.* (2004) 'Type V protein secretion pathway: the autotransporter story', *Microbiology and molecular biology reviews: MMBR*, 68(4), pp. 692–744. Available at: https://doi.org/10.1128/MMBR.68.4.692-744.2004.

Hernández-Luna, M.A. and Luria-Pérez, R. (2018) 'Cancer Immunotherapy: Priming the Host Immune Response with Live Attenuated *Salmonella enterica*', *Journal of Immunology Research*, 2018, p. 2984247. Available at: https://doi.org/10.1155/2018/2984247.

Herring, C.D., Glasner, J.D. and Blattner, F.R. (2003) 'Gene replacement without selection: regulated suppression of amber mutations in *Escherichia coli*', *Gene*, 311, pp. 153–163. Available at: https://doi.org/10.1016/S0378-1119(03) 00585-7.

Hoption Cann, S.A., van Netten, J.P. and van Netten, C. (2003) 'Dr William Coley and tumour regression: a place in history or in the future', *Postgraduate Medical Journal*, 79(938), pp. 672–680.

Hou, N. *et al.* (2019) 'OxyR senses sulfane sulfur and activates the genes for its removal in *Escherichia coli*', *Redox Biology*, 26, p. 101293. Available at: https://doi.org/10.1016/j.redox.2019.101293.

Hsiao, V. *et al.* (2016) 'A population-based temporal logic gate for timing and recording chemical events', *Molecular Systems Biology*, 12(5), p. 869. Available at: https://doi.org/10.15252/msb.20156663.

Hu, C.-D. and Kerppola, T.K. (2003) 'Simultaneous visualization of multiple protein interactions in living cells using multicolor fluorescence complementation analysis', *Nature Biotechnology*, 21(5), pp. 539–545. Available at: https://doi.org/10.1038/nbt816.

Ieva, R. and Bernstein, H.D. (2009) 'Interaction of an autotransporter passenger domain with BamA during its translocation across the bacterial outer membrane', *Proceedings of the National Academy of Sciences of the United States of America*, 106(45), pp. 19120–19125. Available at: https://doi.org/10.1073/pnas.0907912106.

Isabella, V.M. *et al.* (2018) 'Development of a synthetic live bacterial therapeutic for the human metabolic disease phenylketonuria', *Nature Biotechnology*, 36(9), pp. 857–864. Available at: https://doi.org/10.1038/nbt.4222.

Isberg, R.R. and Leong, J.M. (1990) 'Multiple beta 1 chain integrins are receptors for invasin, a protein that promotes bacterial penetration into mammalian cells', *Cell*, 60(5), pp. 861–871. Available at: https://doi.org/10.1016/0092-8674(90)90099-z.

Isberg, R.R., Voorhis, D.L. and Falkow, S. (1987) 'Identification of invasin: a protein that allows enteric bacteria to penetrate cultured mammalian cells', *Cell*, 50(5), pp. 769–778. Available at: https://doi.org/10.1016/0092-8674(87)90335-7.

Iuchi, S. *et al.* (1994) 'Effects of nitrate respiration on expression of the Arc-controlled operons encoding succinate dehydrogenase and flavin-linked L-lactate dehydrogenase', *Journal of Bacteriology*, 176(6), pp. 1695–1701. Available at: https://doi.org/10.1128/jb.176.6.1695-1701.1994.

Iuchi, S. and Lin, E.C.C. (1988) 'arcA (dye), a global regulatory gene in *Escherichia coli* mediating repression of enzymes in aerobic pathways', *Proceedings of the National Academy of Sciences*, 85, pp. 1888–1892.

Jeon, Y. *et al.* (2001) 'Multimerization of phosphorylated and non-phosphorylated ArcA is necessary for the response regulator function of the Arc two-component signal transduction system', *The Journal of Biological Chemistry*, 276(44), pp. 40873–40879. Available at: https://doi.org/10.1074/jbc.M104855200.

Jiang, S.-N. *et al.* (2010) 'Inhibition of Tumor Growth and Metastasis by a Combination of *Escherichia coli*–mediated Cytolytic Therapy and Radiotherapy', *Molecular Therapy*, 18(3), pp. 635–642. Available at: https://doi.org/10.1038/mt.2009.295.

Jong, W.S.P. *et al.* (2018) 'Comparing autotransporter β-domain configurations for their capacity to secrete heterologous proteins to the cell surface', *PLOS ONE*. Edited by E. Cascales, 13(2), p. e0191622. Available at: https://doi.org/10.1371/journal.pone.0191622.

Jumper, J. *et al.* (2021) 'Highly accurate protein structure prediction with AlphaFold', *Nature*, 596(7873), pp. 583–589. Available at: https://doi.org/10.1038/s41586-021-03819-2.

Junker, M. *et al.* (2006) 'Pertactin β-helix folding mechanism suggests common themes for the secretion and folding of autotransporter proteins', *Proceedings of the National Academy of Sciences*, 103(13), pp. 4918–4923. Available at: https://doi.org/10.1073/pnas.0507923103.

Kalos, M. *et al.* (2011) 'T cells with chimeric antigen receptors have potent antitumor effects and can establish memory in patients with advanced leukemia', *Science Translational Medicine*, 3(95), p. 95ra73. Available at: https://doi.org/10.1126/scitranslmed.3002842.

Karow, M. *et al.* (2011) 'Site-specific recombinase strategy to create induced pluripotent stem cells efficiently with plasmid DNA', *Stem cells (Dayton, Ohio)*, 29(11), pp. 1696–1704. Available at: https://doi.org/10.1002/stem.730.

Kasinskas, R.W. and Forbes, N.S. (2006) '*Salmonella typhimurium* specifically chemotax and proliferate in heterogeneous tumor tissue in vitro', *Biotechnology and Bioengineering*, 94(4), pp. 710–721. Available at: https://doi.org/10.1002/bit.20883.

Kaur, Sumanpreet and Kaur, Sukhraj (2015) 'Bacteriocins as Potential Anticancer Agents', *Frontiers in Pharmacology*, 6, p. 272. Available at: https://doi.org/10.3389/fphar.2015.00272.

Kelly, V.W., Liang, B.K. and Sirk, S.J. (2020) 'Living Therapeutics: The Next Frontier of Precision Medicine', *ACS synthetic biology*, 9(12), pp. 3184–3201. Available at: https://doi.org/10.1021/acssynbio.0c00444.

Khan, S. *et al.* (2011) 'Crystal Structure of the Passenger Domain of the *Escherichia coli* Autotransporter EspP', *Journal of Molecular Biology*, 413(5), pp. 985–1000. Available at: https://doi.org/10.1016/j.jmb.2011.09.028.

Kimkes, T.E.P. and Heinemann, M. (2020) 'How bacteria recognise and respond to surface contact', *FEMS microbiology reviews*, 44(1), pp. 106–122. Available at: https://doi.org/10.1093/femsre/fuz029.

Kimura, N.T. *et al.* (1980) 'Selective localization and growth of *Bifidobacterium bifidum* in mouse tumors following intravenous administration', *Cancer Research*, 40(6), pp. 2061–2068.

Klauser, T., Pohlner, J. and Meyer, T.F. (1993) 'The secretion pathway of IgA protease-type proteins in gram-negative bacteria', *BioEssays: News and Reviews in Molecular, Cellular and Developmental Biology*, 15(12), pp. 799–805. Available at: https://doi.org/10.1002/bies.950151205.

Kleanthous, C., Rassam, P. and Baumann, C.G. (2015) 'Protein–protein interactions and the spatiotemporal dynamics of bacterial outer membrane proteins', *Current Opinion in Structural Biology*, 35, pp. 109–115. Available at: https://doi.org/10.1016/j.sbi.2015.10.007.

Klemm, P. (1986) 'Two regulatory *fim* genes, *fimB* and *fimE*, control the phase variation of type 1 fimbriae in *Escherichia coli*', *The EMBO journal*, 5(6), pp. 1389–1393. Available at: https://doi.org/10.1002/j.1460-2075.1986.tb04372.x.

Koebnik, R. (1999) 'Membrane assembly of the *Escherichia coli* outer membrane protein OmpA: exploring sequence constraints on transmembrane beta-strands', *Journal of Molecular Biology*, 285(4), pp. 1801–1810. Available at: https://doi.org/10.1006/jmbi.1998.2405.

Koebnik, R., Locher, K.P. and Van Gelder, P. (2000) 'Structure and function of bacterial outer membrane proteins: barrels in a nutshell', *Molecular Microbiology*, 37(2), pp. 239–253. Available at: https://doi.org/10.1046/j.1365-2958.2000.01983.x.

Konovalova, A., Kahne, D.E. and Silhavy, T.J. (2017) 'Outer Membrane Biogenesis', *Annual Review of Microbiology*, 71, pp. 539–556. Available at: https://doi.org/10.1146/annurev-micro-090816-093754.

Kosinski, M.J., Rinas, U. and Bailey, J.E. (1992) 'Isopropyl-β-d-thiogalactopyranoside influences the metabolism of *Escherichia coli*', *Applied Microbiology and Biotechnology*, 36(6), pp. 782–784. Available at: https://doi.org/10.1007/BF00172194.

Kuhstoss, S., Richardson, M.A. and Rao, R.N. (1991) 'Plasmid cloning vectors that integrate site-specifically in *Streptomyces* spp', *Gene*, 97(1), pp. 143–146. Available at: https://doi.org/10.1016/0378-1119(91)90022-4.

Kwon, O., Georgellis, D. and Lin, E.C. (2000) 'Phosphorelay as the sole physiological route of signal transmission by the arc two-component system of *Escherichia coli*', *Journal of Bacteriology*, 182(13), pp. 3858–3862. Available at: https://doi.org/10.1128/JB.182.13.3858-3862.2000.

Laarmann, S. and Schmidt, M.A. (2003) 'The *Escherichia coli* AIDA autotransporter adhesin recognizes an integral membrane glycoprotein as receptor', *Microbiology (Reading, England)*, 149(Pt 7), pp. 1871–1882. Available at: https://doi.org/10.1099/mic.0.26264-0.

Lambin, P. *et al.* (1998) 'Colonisation of *Clostridium* in the body is restricted to hypoxic and necrotic areas of tumours', *Anaerobe*, 4(4), pp. 183–188. Available at: https://doi.org/10.1006/anae.1998.0161.

Landete, J.M. (2017) 'A review of food-grade vectors in lactic acid bacteria: from the laboratory to their application', *Critical Reviews in Biotechnology*, 37(3), pp. 296–308. Available at: https://doi.org/10.3109/07388551.2016.1144044.

Lara, A.R. *et al.* (2017) 'Characterization of Endogenous and Reduced Promoters for Oxygen-Limited Processes Using *Escherichia coli*', *ACS Synthetic Biology*, 6(2), pp. 344–356. Available at: https://doi.org/10.1021/acssynbio.6b00233.

Le Calvez, H., Green, J.M. and Baty, D. (1996) 'Increased efficiency of alkaline phosphatase production levels in *Escherichia coli* using a degenerate PelB signal sequence', *Gene*, 170(1), pp. 51–55. Available at: https://doi.org/10.1016/0378-1119(95)00850-0.

Lee, J.W. *et al.* (2018) 'Next-generation biocontainment systems for engineered organisms', *Nature Chemical Biology*, 14(6), pp. 530–537. Available at: https://doi.org/10.1038/s41589-018-0056-x.

Lee, Y.H. *et al.* (2008) 'The Membrane-Bound Transcriptional Regulator CadC Is Activated by Proteolytic Cleavage in Response to Acid Stress', *Journal of Bacteriology*, 190(14), pp. 5120–5126. Available at: https://doi.org/10.1128/JB.00012-08.

Lehning, C.E. *et al.* (2017) 'A Modular High-Throughput In Vivo Screening Platform Based on Chimeric Bacterial Receptors', *ACS Synthetic Biology*, 6(7), pp. 1315–1326. Available at: https://doi.org/10.1021/acssynbio.6b00288.

Lehouritis, P., Springer, C. and Tangney, M. (2013) 'Bacterial-directed enzyme prodrug therapy', *Journal of Controlled Release: Official Journal of the Controlled Release Society*, 170(1), pp. 120–131. Available at: https://doi.org/10.1016/j.jconrel.2013.05.005.

Lehti, T.A. *et al.* (2010) 'Mat fimbriae promote biofilm formation by meningitis-associated *Escherichia coli*', *Microbiology (Reading, England)*, 156(Pt 8), pp. 2408–2417. Available at: https://doi.org/10.1099/mic.0.039610-0.

Leo, J.C., Oberhettinger, P., Chaubey, M., *et al.* (2015) 'The Intimin periplasmic domain mediates dimerisation and binding to peptidoglycan', *Mol Microbiol*, 95(1), pp. 80–100. Available at: https://doi.org/10.1111/mmi.12840.

Leo, J.C., Oberhettinger, P., Schutz, M., *et al.* (2015) 'The inverse autotransporter family: intimin, invasin and related proteins', *Int J Med Microbiol*, 305(2), pp. 276–82. Available at: https://doi.org/10.1016/j.ijmm.2014.12.011.

Leo, J.C. *et al.* (2016) 'Secretion of the Intimin Passenger Domain Is Driven by Protein Folding', *J Biol Chem*, 291(38), pp. 20096–112. Available at: https://doi.org/10.1074/jbc.M116.731497.

Leo, J.C., Grin, I. and Linke, D. (2012) 'Type V secretion: mechanism(s) of autotransport through the bacterial outer membrane', *Philosophical Transactions of the Royal Society B: Biological Sciences*, 367(1592), pp. 1088–1101. Available at: https://doi.org/10.1098/rstb.2011.0208.

Leo, J.C. and Skurnik, M. (2011) 'Adhesins of human pathogens from the genus *Yersinia*', *Advances in Experimental Medicine and Biology*, 715, pp. 1–15. Available at: https://doi.org/10.1007/978-94-007-0940-9_1.

Leshem, Y. and Pastan, I. (2019) '*Pseudomonas* Exotoxin Immunotoxins and Anti-Tumor Immunity: From Observations at the Patient's Bedside to Evaluation in Preclinical Models', *Toxins*, 11(1), p. E20. Available at: https://doi.org/10.3390/toxins11010020.

Leventhal, D.S. *et al.* (2020) 'Immunotherapy with engineered bacteria by targeting the STING pathway for anti-tumor immunity', *Nature Communications*, 11(1), p. 2739. Available at: https://doi.org/10.1038/s41467-020-16602-0.

Leyton, D.L., Rossiter, A.E. and Henderson, I.R. (2012) 'From self sufficiency to dependence: mechanisms and factors important for autotransporter biogenesis', *Nature Reviews Microbiology*, 10(3), pp. 213–225. Available at: https://doi.org/10.1038/nrmicro2733.

Lillington, J., Geibel, S. and Waksman, G. (2014) 'Biogenesis and adhesion of type 1 and P pili', *Biochimica Et Biophysica Acta*, 1840(9), pp. 2783–2793. Available at: https://doi.org/10.1016/j.bbagen.2014.04.021.

Lim, D. *et al.* (2020) 'Targeted Delivery of the Mitochondrial Target Domain of Noxa to Tumor Tissue via Synthetic Secretion System in *E. coli*', *Frontiers in Bioengineering and Biotechnology*, 8, p. 840. Available at: https://doi.org/10.3389/fbioe.2020.00840.

Liou, G.-Y. and Storz, P. (2010) 'Reactive oxygen species in cancer', *Free Radical Research*, 44(5), pp. 479–496. Available at: https://doi.org/10.3109/10715761003667554.

Liu, X., Hoft, D.F. and Peng, G. (2022) 'Tumor microenvironment metabolites directing T cell differentiation and function', *Trends in Immunology*, 43(2), pp. 132–147. Available at: https://doi.org/10.1016/j.it.2021.12.004.

Loeffler, M. *et al.* (2008) 'IL-18-producing *Salmonella* inhibit tumor growth', *Cancer Gene Therapy*, 15(12), pp. 787–794. Available at: https://doi.org/10.1038/cgt.2008.48.

Loeffler, Markus *et al.* (2008) 'Inhibition of tumor growth using salmonella expressing Fas ligand', *Journal of the National Cancer Institute*, 100(15), pp. 1113–1116. Available at: https://doi.org/10.1093/jnci/djn205.

Loessner, H. *et al.* (2007) 'Remote control of tumour-targeted *Salmonella enterica* serovar Typhimurium by the use of L-arabinose as inducer of bacterial gene expression in vivo', *Cellular Microbiology*, 9(6), pp. 1529–1537. Available at: https://doi.org/10.1111/j.1462-5822.2007.00890.x.

Loessner, H. *et al.* (2009) 'Drug-inducible remote control of gene expression by probiotic *Escherichia coli* Nissle 1917 in intestine, tumor and gall bladder of mice', *Microbes and Infection*, 11(14–15), pp. 1097–1105. Available at: https://doi.org/10.1016/j.micinf.2009.08.002.

Luo, Y. *et al.* (2000) 'Crystal structure of enteropathogenic *Escherichia coli* intimin-receptor complex', *Nature*, 405(6790), pp. 1073–1077. Available at: https://doi.org/10.1038/35016618.

Lyssiotis, C.A. and Kimmelman, A.C. (2017) 'Metabolic Interactions in the Tumor Microenvironment', *Trends in Cell Biology*, 27(11), pp. 863–875. Available at: https://doi.org/10.1016/j.tcb.2017.06.003.

Maeda, H. (2013) 'The link between infection and cancer: tumor vasculature, free radicals, and drug delivery to tumors via the EPR effect', *Cancer Science*, 104(7), pp. 779–789. Available at: https://doi.org/10.1111/cas.12152.

Malmgren, R.A. and Flanigan, C.C. (1955) 'Localization of the vegetative form of *Clostridium tetani* in mouse tumors following intravenous spore administration', *Cancer Research*, 15(7), pp. 473–478.

Mamou, G. *et al.* (2022) 'Peptidoglycan maturation controls outer membrane protein assembly', *Nature*, 606(7916), pp. 953–959. Available at: https://doi.org/10.1038/s41586-022-04834-7.

Manzoni, R. *et al.* (2016) 'Synthetic biology: insights into biological computation', *Integrative Biology*, 8(4), pp. 518–532. Available at: https://doi.org/10.1039/C5IB00274E.

Marchès, O. *et al.* (2000) 'Role of Tir and Intimin in the Virulence of Rabbit Enteropathogenic *Escherichia coli* Serotype O103:H2', *Infection and Immunity*, 68(4), pp. 2171–2182.

Marin, E., Bodelon, G. and Fernandez, L.A. (2010) 'Comparative analysis of the biochemical and functional properties of C-terminal domains of autotransporters', *J Bacteriol*, 192(21), pp. 5588–602. Available at: https://doi.org/10.1128/JB.00432-10.

Massoud, T.F., Paulmurugan, R. and Gambhir, S.S. (2010) 'A molecularly engineered split reporter for imaging protein-protein interactions with positron emission tomography', *Nature Medicine*, 16(8), pp. 921–926. Available at: https://doi.org/10.1038/nm.2185.

McCarthy, E.F. (2006) 'The Toxins of William B. Coley and the Treatment of Bone and Soft-Tissue Sarcomas', *The Iowa Orthopaedic Journal*, 26, pp. 154–158.

McKay, R. *et al.* (2018) 'Development of Cell-Based Sentinels for Nitric Oxide: Ensuring Marker Expression and Unimodality', *ACS Synthetic Biology*, 7(7), pp. 1694–1701. Available at: https://doi.org/10.1021/acssynbio.8b00146.

McKee, M.L. *et al.* (1995) 'Enterohemorrhagic *Escherichia coli* O157:H7 requires intimin to colonize the gnotobiotic pig intestine and to adhere to HEp-2 cells', *Infection and Immunity*, 63(9), pp. 3739–3744. Available at: https://doi.org/10.1128/iai.63.9.3739-3744.1995.

Mellman, I., Coukos, G. and Dranoff, G. (2011) 'Cancer immunotherapy comes of age', *Nature*, 480(7378), pp. 480–489. Available at: https://doi.org/10.1038/nature10673.

Mellor, A.L. and Munn, D.H. (2008) 'Creating immune privilege: active local suppression that benefits friends, but protects foes', *Nature Reviews Immunology*, 8(1), pp. 74–80. Available at: https://doi.org/10.1038/nri2233.

Membrillo-Hernández, J. *et al.* (1998) 'A novel mechanism for upregulation of the *Escherichia coli* K-12 *hmp* (flavohaemoglobin) gene by the "NO releaser", S-nitrosoglutathione: nitrosation of homocysteine and modulation of MetR binding to the *glyA-hmp* intergenic region', *Molecular Microbiology*, 29(4), pp. 1101–1112. Available at: https://doi.org/10.1046/j.1365-2958.1998.01000.x.

Mengesha, A. *et al.* (2006) 'Development of a flexible and potent hypoxia-inducible promoter for tumor-targeted gene expression in attenuated *Salmonella'*, *Cancer Biology & Therapy*, 5(9), pp. 1120–1128. Available at: https://doi.org/10.4161/cbt.5.9.2951.

Merrick, C.A., Zhao, J. and Rosser, S.J. (2018) 'Serine Integrases: Advancing Synthetic Biology', *ACS Synthetic Biology*, 7(2), pp. 299–310. Available at: https://doi.org/10.1021/acssynbio.7b00308.

Meuskens, I. *et al.* (2019) 'Type V Secretion Systems: An Overview of Passenger Domain Functions', *Front Microbiol*, 10, p. 1163. Available at: https://doi.org/10.3389/fmicb.2019.01163.

Middlebrook, J.L. and Dorland, R.B. (1984) 'Bacterial toxins: cellular mechanisms of action', *Microbiological Reviews*, 48(3), pp. 199–221. Available at: https://doi.org/10.1128/mr.48.3.199-221.1984.

Morsut, L. *et al.* (2016) 'Engineering Customized Cell Sensing and Response Behaviors Using Synthetic Notch Receptors', *Cell*, 164(4), pp. 780–791. Available at: https://doi.org/10.1016/j.cell.2016.01.012.

Muñoz-Gutiérrez, I. *et al.* (2014) 'Ag43-mediated display of a thermostable β-glucosidase in *Escherichia coli* and its use for simultaneous saccharification and fermentation at high temperatures', *Microbial Cell Factories*, 13(1), p. 106. Available at: https://doi.org/10.1186/s12934-014-0106-3.

Mutalik, V.K. *et al.* (2013) 'Precise and reliable gene expression via standard transcription and translation initiation elements', *Nature Methods*, 10(4), pp. 354–360. Available at: https://doi.org/10.1038/nmeth.2404.

Muyldermans, S. (2013) 'Nanobodies: natural single-domain antibodies', *Annual Review of Biochemistry*, 82, pp. 775–797. Available at: https://doi.org/10.1146/annurev-biochem-063011-092449.

Nejman, D. *et al.* (2020) 'The human tumor microbiome is composed of tumor type-specific intracellular bacteria', *Science (New York, N.Y.)*, 368(6494), pp. 973–980. Available at: https://doi.org/10.1126/science.aay9189.

Noinaj, N. *et al.* (2013) 'Structural insight into the biogenesis of β-barrel membrane proteins', *Nature*, 501(7467), pp. 385–390. Available at: https://doi.org/10.1038/nature12521.

Noinaj, N., Gumbart, J.C. and Buchanan, S.K. (2017) 'The β-barrel assembly machinery in motion', *Nature Reviews Microbiology*, 15(4), pp. 197–204. Available at: https://doi.org/10.1038/nrmicro.2016.191.

Nuyts, S. *et al.* (2001) 'The use of radiation-induced bacterial promoters in anaerobic conditions: a means to control gene expression in clostridium-mediated therapy for cancer', *Radiation Research*, 155(5), pp. 716–723. Available at: https://doi.org/10.1667/0033-7587(2001)155[0716:tuorib]2.0.co;2.

Oberhettinger, P. *et al.* (2012) 'Intimin and invasin export their C-terminus to the bacterial cell surface using an inverse mechanism compared to classical autotransport', *PLoS One*, 7(10), p. e47069. Available at: https://doi.org/10.1371/journal.pone.0047069.

Oberhettinger, P. *et al.* (2015) 'The inverse autotransporter intimin exports its passenger domain via a hairpin intermediate', *The Journal of Biological Chemistry*, 290(3), pp. 1837–1849. Available at: https://doi.org/10.1074/jbc.M114.604769.

Oddershede, L. *et al.* (2002) 'The Motion of a Single Molecule, the λ-Receptor, in the Bacterial Outer Membrane', *Biophysical Journal*, 83(6), pp. 3152–3161. Available at: https://doi.org/10.1016/S0006-3495(02)75318-6.

Oomen, C.J. *et al.* (2004) 'Structure of the translocator domain of a bacterial autotransporter', *The EMBO journal*, 23(6), pp. 1257–1266. Available at: https://doi.org/10.1038/sj.emboj.7600148.

Ortiz-Suarez, M.L. *et al.* (2016) 'Full-Length OmpA: Structure, Function, and Membrane Interactions Predicted by Molecular Dynamics Simulations', *Biophysical Journal*, 111(8), pp. 1692–1702. Available at: https://doi.org/10.1016/j.bpj.2016.09.009.

Palumbo, R.N. and Wang, C. (2006) 'Bacterial invasin: structure, function, and implication for targeted oral gene delivery', *Current Drug Delivery*, 3(1), pp. 47–53. Available at: https://doi.org/10.2174/156720106775197475.

Panteli, J.T. and Forbes, N.S. (2016) 'Engineered bacteria detect spatial profiles in glucose concentration within solid tumor cell masses', *Biotechnology and Bioengineering*, 113(11), pp. 2474–2484. Available at: https://doi.org/10.1002/bit.26006.

Park, D.M. *et al.* (2013) 'The bacterial response regulator ArcA uses a diverse binding site architecture to regulate carbon oxidation globally', *PLoS genetics*, 9(10), p. e1003839. Available at: https://doi.org/10.1371/journal.pgen.1003839.

Pavlova, O. *et al.* (2013) 'Mechanistic link between β barrel assembly and the initiation of autotransporter secretion', *Proceedings of the National Academy of Sciences*, 110(10), pp. E938–E947. Available at: https://doi.org/10.1073/pnas.1219076110.

Pawelek, J.M., Low, K.B. and Bermudes, D. (1997) 'Tumor-targeted *Salmonella* as a novel anticancer vector', *Cancer Research*, 57(20), pp. 4537–4544.

Peterson, J.H. *et al.* (2010) 'Secretion of a bacterial virulence factor is driven by the folding of a C-terminal segment', *Proceedings of the National Academy of Sciences of the United States of America*, 107(41), pp. 17739–17744. Available at: https://doi.org/10.1073/pnas.1009491107.

Pettenati, C. and Ingersoll, M.A. (2018) 'Mechanisms of BCG immunotherapy and its outlook for bladder cancer', *Nature Reviews. Urology*, 15(10), pp. 615–625. Available at: https://doi.org/10.1038/s41585-018-0055-4.

Piñero-Lambea, C. *et al.* (2015) 'Programming Controlled Adhesion of *E. coli* to Target Surfaces, Cells, and Tumors with Synthetic Adhesins', *ACS Synthetic Biology*, 4(4), pp. 463–473. Available at: https://doi.org/10.1021/sb500252a.

Plavec, T.V. and Berlec, A. (2020) 'Safety Aspects of Genetically Modified Lactic Acid Bacteria', *Microorganisms*, 8(2), p. 297. Available at: https://doi.org/10.3390/microorganisms8020297.

Porter, J.R. *et al.* (2007) 'Split beta-lactamase sensor for the sequence-specific detection of DNA methylation', *Analytical Chemistry*, 79(17), pp. 6702–6708. Available at: https://doi.org/10.1021/ac071163+.

Pósfai, G. *et al.* (1999) 'Markerless gene replacement in *Escherichia coli* stimulated by a double-strand break in the chromosome', *Nucleic acids research*, 27(22), pp. 4409–4415. Available at: https://doi.org/10.1093/nar/27.22.4409.

Pósfai, G. *et al.* (2006) 'Emergent properties of reduced-genome *Escherichia coli'*, *Science (New York, N.Y.)*, 312(5776), pp. 1044–1046. Available at: https://doi.org/10.1126/science.1126439.

Prindle, A. *et al.* (2012) 'Genetic Circuits in *Salmonella typhimurium*', *ACS synthetic biology*, 1(10), pp. 458–464. Available at: https://doi.org/10.1021/sb300060e.

Pucadyil, T.J. and Chattopadhyay, A. (2006) 'Confocal fluorescence recovery after photobleaching of green fluorescent protein in solution', *Journal of Fluorescence*, 16(1), pp. 87–94. Available at: https://doi.org/10.1007/s10895-005-0019-y.

al-Ramadi, B.K. *et al.* (2009) 'Potent anti-tumor activity of systemically-administered IL2-expressing Salmonella correlates with decreased angiogenesis and enhanced tumor apoptosis', *Clinical Immunology (Orlando, Fla.)*, 130(1), pp. 89–97. Available at: https://doi.org/10.1016/j.clim.2008.08.021.

Rassam, P. *et al.* (2015) 'Supramolecular assemblies underpin turnover of outer membrane proteins in bacteria', *Nature*, 523(7560), pp. 333–336. Available at: https://doi.org/10.1038/nature14461.

Riglar, D.T. *et al.* (2017) 'Engineered bacteria can function in the mammalian gut long-term as live diagnostics of inflammation', *Nature Biotechnology*, 35(7), pp. 653–658. Available at: https://doi.org/10.1038/nbt.3879.

Ritchie, K. *et al.* (2013) 'Single-molecule imaging in live bacteria cells', *Philosophical Transactions of the Royal Society B: Biological Sciences*, 368(1611), p. 20120355. Available at: https://doi.org/10.1098/rstb.2012.0355.

Robert, V. *et al.* (2006) 'Assembly factor Omp85 recognizes its outer membrane protein substrates by a species-specific C-terminal motif', *PLoS biology*, 4(11), p. e377. Available at: https://doi.org/10.1371/journal.pbio.0040377.

Robinson, J.L. and Brynildsen, M.P. (2013) 'A Kinetic Platform to Determine the Fate of Nitric Oxide in *Escherichia coli*', *PLoS Computational Biology*. Edited by C.V. Rao, 9(5), p. e1003049. Available at: https://doi.org/10.1371/journal.pcbi.1003049.

Roman-Hernandez, G., Peterson, J.H. and Bernstein, H.D. (2014) 'Reconstitution of bacterial autotransporter assembly using purified components', *eLife*, 3, p. e04234. Available at: https://doi.org/10.7554/eLife.04234.

Roth, M. *et al.* (2022) 'Transcriptomic Analysis of *E. coli* after Exposure to a Sublethal Concentration of Hydrogen Peroxide Revealed a Coordinated Up-Regulation of the Cysteine Biosynthesis Pathway', *Antioxidants (Basel, Switzerland)*, 11(4), p. 655. Available at: https://doi.org/10.3390/antiox11040655.

Rothenberg, E. *et al.* (2011) 'Single-virus tracking reveals a spatial receptor-dependent search mechanism', *Biophysical Journal*, 100(12), pp. 2875–2882. Available at: https://doi.org/10.1016/j.bpj.2011.05.014.

Royo, J.L. *et al.* (2007) 'In vivo gene regulation in *Salmonella* spp. by a salicylate-dependent control circuit', *Nature Methods*, 4(11), pp. 937–942. Available at: https://doi.org/10.1038/nmeth1107.

Ruano-Gallego, D., Yara, D.A., *et al.* (2019) 'A nanobody targeting the translocated intimin receptor inhibits the attachment of enterohemorrhagic *E. coli* to human colonic mucosa', *PLoS pathogens*, 15(8), p. e1008031. Available at: https://doi.org/10.1371/journal.ppat.1008031.

Ruano-Gallego, D., Fraile, S., *et al.* (2019) 'Screening and purification of nanobodies from *E. coli* culture supernatants using the hemolysin secretion system', *Microbial Cell Factories*, 18(1), p. 47. Available at: https://doi.org/10.1186/s12934-019-1094-0.

Ruano-Gallego, D., Álvarez, B. and Fernández, L.Á. (2015) 'Engineering the Controlled Assembly of Filamentous Injectisomes in *E. coli* K-12 for Protein Translocation into Mammalian Cells', *ACS synthetic biology*, 4(9), pp. 1030–1041. Available at: https://doi.org/10.1021/acssynbio.5b00080.

Rubens, J.R., Selvaggio, G. and Lu, T.K. (2016) 'Synthetic mixed-signal computation in living cells', *Nature Communications*, 7(1), p. 11658. Available at: https://doi.org/10.1038/ncomms11658.

Ryan, R.M. *et al.* (2009) 'Bacterial delivery of a novel cytolysin to hypoxic areas of solid tumors', *Gene Therapy*, 16(3), pp. 329–339. Available at: https://doi.org/10.1038/gt.2008.188.

Sadelain, M., Brentjens, R. and Riviere, I. (2013) 'The basic principles of chimeric antigen receptor (CAR) design', *Cancer discovery*, 3(4), pp. 388–398. Available at: https://doi.org/10.1158/2159-8290.CD-12-0548.

Salema, V. *et al.* (2013) 'Selection of Single Domain Antibodies from Immune Libraries Displayed on the Surface of *E. coli* Cells with Two β-Domains of Opposite Topologies', *PLoS ONE*. Edited by J. Sturtevant, 8(9), p. e75126. Available at: https://doi.org/10.1371/journal.pone.0075126.

Salema, V., López-Guajardo, A., *et al.* (2016) 'Characterization of nanobodies binding human fibrinogen selected by *E. coli* display', *Journal of Biotechnology*, 234, pp. 58–65. Available at: https://doi.org/10.1016/j.jbiotec.2016.07.025.

Salema, V., Mañas, C., *et al.* (2016) 'High affinity nanobodies against human epidermal growth factor receptor selected on cells by *E. coli* display', *mAbs*, 8(7), pp. 1286–1301. Available at: https://doi.org/10.1080/19420862.2016.1216742.

Salema, V. and Fernández, L.Á. (2017) '*Escherichia coli* surface display for the selection of nanobodies', *Microbial Biotechnology*, 10(6), pp. 1468–1484. Available at: https://doi.org/10.1111/1751-7915.12819.

Samsudin, F. *et al.* (2016) 'OmpA: A Flexible Clamp for Bacterial Cell Wall Attachment', *Structure*, 24(12), pp. 2227–2235. Available at: https://doi.org/10.1016/j.str.2016.10.009.

Schlundt, A. *et al.* (2017) 'Structure-function analysis of the DNA-binding domain of a transmembrane transcriptional activator', *Scientific Reports*, 7(1), p. 1051. Available at: https://doi.org/10.1038/s41598-017-01031-9.

Schnaitman, C.A. (1971) 'Solubilization of the cytoplasmic membrane of *Escherichia coli* by Triton X-100.', *Journal of bacteriology*, 108(1), pp. 545–552. Available at: https://doi.org/10.1128/jb.108.1.545-552.1971.

Schnaitman, C.A. (1973) 'Outer membrane proteins of *Escherichia coli*: I. Effect of preparative conditions on the migration of protein in polyacrylamide gels', *Archives of Biochemistry and Biophysics*, 157(2), pp. 541–552. Available at: https://doi.org/10.1016/0003-9861(73)90673-5.

Schwarz, K.A. *et al.* (2017) 'Rewiring human cellular input–output using modular extracellular sensors', *Nature Chemical Biology*, 13(2), pp. 202–209. Available at: https://doi.org/10.1038/nchembio.2253.

Seco, E.M. and Fernández, L.Á. (2021) 'Efficient markerless integration of genes in the chromosome of probiotic *E. coli* Nissle 1917 by bacterial conjugation', *Microbial Biotechnology*, pp. 1751-7915.13967. Available at: https://doi.org/10.1111/1751-7915.13967.

Sehnal, D. *et al.* (2021) 'Mol* Viewer: modern web app for 3D visualization and analysis of large biomolecular structures', *Nucleic Acids Research*, 49(W1), pp. W431–W437. Available at: https://doi.org/10.1093/nar/gkab314.

Senok, A.C., Ismaeel, A.Y. and Botta, G.A. (2005) 'Probiotics: facts and myths', *Clinical Microbiology and Infection: The Official Publication of the European Society of Clinical Microbiology and Infectious Diseases*, 11(12), pp. 958–966. Available at: https://doi.org/10.1111/j.1469-0691.2005.01228.x.

Sherlock, O. *et al.* (2006) 'Glycosylation of the self-recognizing *Escherichia coli* Ag43 autotransporter protein', *Journal of Bacteriology*, 188(5), pp. 1798–1807. Available at: https://doi.org/10.1128/JB.188.5.1798-1807.2006.

Shreiner, A.B., Kao, J.Y. and Young, V.B. (2015) 'The gut microbiome in health and in disease', *Current Opinion in Gastroenterology*, 31(1), pp. 69–75. Available at: https://doi.org/10.1097/mog.0000000000000139

Silva-Rocha, R. *et al.* (2013) 'The Standard European Vector Architecture (SEVA): a coherent platform for the analysis and deployment of complex prokaryotic phenotypes', *Nucleic Acids Research*, 41(Database issue), pp. D666-675. Available at: https://doi.org/10.1093/nar/gks1119.

Siuti, P., Yazbek, J. and Lu, T.K. (2013) 'Synthetic circuits integrating logic and memory in living cells', *Nature Biotechnology*, 31(5), pp. 448–452. Available at: https://doi.org/10.1038/nbt.2510.

Skillman, K.M. *et al.* (2005) 'Efficient secretion of a folded protein domain by a monomeric bacterial autotransporter', *Molecular Microbiology*, 58(4), pp. 945–958. Available at: https://doi.org/10.1111/j.1365-2958.2005.04885.x.

Sklar, J.G. *et al.* (2007) 'Lipoprotein SmpA is a component of the YaeT complex that assembles outer membrane proteins in *Escherichia coli*', *Proceedings of the National Academy of Sciences*, 104(15), pp. 6400–6405. Available at: https://doi.org/10.1073/pnas.0701579104.

Somasundaram, V. *et al.* (2019) 'Molecular Mechanisms of Nitric Oxide in Cancer Progression, Signal Transduction, and Metabolism', *Antioxidants & Redox Signaling*, 30(8), pp. 1124–1143. Available at: https://doi.org/10.1089/ars.2018.7527.

Somerville, G.A. and Proctor, R.A. (2013) 'Cultivation conditions and the diffusion of oxygen into culture media: The rationale for the flask-to-medium ratio in microbiology', *BMC Microbiology*, 13(1), p. 9. Available at: https://doi.org/10.1186/1471-2180-13-9.

Song, S., Vuai, M.S. and Zhong, M. (2018) 'The role of bacteria in cancer therapy - enemies in the past, but allies at present', *Infectious Agents and Cancer*, 13, p. 9. Available at: https://doi.org/10.1186/s13027-018-0180-y.

Sonnenborn, U. (2016) '*Escherichia coli* strain Nissle 1917-from bench to bedside and back: history of a special *Escherichia coli* strain with probiotic properties', *FEMS microbiology letters*, 363(19), p. fnw212. Available at: https://doi.org/10.1093/femsle/fnw212.

Sonveaux, P. *et al.* (2008) 'Targeting lactate-fueled respiration selectively kills hypoxic tumor cells in mice', *The Journal of Clinical Investigation*, 118(12), pp. 3930–3942. Available at: https://doi.org/10.1172/JCI36843.

Spector, J. *et al.* (2010) 'Mobility of BtuB and OmpF in the *Escherichia coli* Outer Membrane: Implications for Dynamic Formation of a Translocon Complex', *Biophysical Journal*, 99(12), pp. 3880–3886. Available at: https://doi.org/10.1016/j.bpj.2010.10.029.

St. Jean, A.T., Zhang, M. and Forbes, N.S. (2008) 'Bacterial Therapies: Completing the Cancer Treatment Toolbox', *Current opinion in biotechnology*, 19(5), pp. 511–517. Available at: https://doi.org/10.1016/j.copbio.2008.08.004.

Stalker, D.M., Kolter, R. and Helinski, D.R. (1982) 'Plasmid R6K DNA replication. I. Complete nucleotide sequence of an autonomously replicating segment', *Journal of Molecular Biology*, 161(1), pp. 33–43. Available at: https://doi.org/10.1016/0022-2836(82)90276-5.

Stritzker, J. *et al.* (2007) 'Tumor-specific colonization, tissue distribution, and gene induction by probiotic *Escherichia coli* Nissle 1917 in live mice', *International journal of medical microbiology: IJMM*, 297(3), pp. 151–162. Available at: https://doi.org/10.1016/j.ijmm.2007.01.008.

Suhr, M., Benz, I. and Schmidt, M.A. (1996) 'Processing of the AIDA-I precursor: removal of AIDA ^{C} and evidence for the outer membrane anchoring as a β-barrel structure', *Molecular Microbiology*, 22(1), pp. 31–42. Available at: https://doi.org/10.1111/j.1365-2958.1996.tb02653.x.

Sullivan, L.B. and Chandel, N.S. (2014) 'Mitochondrial reactive oxygen species and cancer', *Cancer & Metabolism*, 2(1), p. 17. Available at: https://doi.org/10.1186/2049-3002-2-17.

Szatrowski, T.P. and Nathan, C.F. (1991) 'Production of large amounts of hydrogen peroxide by human tumor cells.', *Cancer research*, 51(3), pp. 794–798.

Thanabalu, T. (1998) 'Substrate-induced assembly of a contiguous channel for protein export from *E. coli*: reversible bridging of an inner-membrane translocase to an outer membrane exit pore', *The EMBO Journal*, 17(22), pp. 6487–6496. Available at: https://doi.org/10.1093/emboj/17.22.6487.

Theys, J. *et al.* (1999) 'Stable *Escherichia coli-Clostridium acetobutylicum* shuttle vector for secretion of murine tumor necrosis factor alpha', *Applied and Environmental Microbiology*, 65(10), pp. 4295–4300. Available at: https://doi.org/10.1128/AEM.65.10.4295-4300.1999.

Theys, J. *et al.* (2001) 'Specific targeting of cytosine deaminase to solid tumors by engineered *Clostridium acetobutylicum'*, *Cancer Gene Therapy*, 8(4), pp. 294–297. Available at: https://doi.org/10.1038/sj.cgt.7700303.

Thie, H. *et al.* (2008) 'SRP and Sec pathway leader peptides for antibody phage display and antibody fragment production in *E. coli*', *New Biotechnology*, 25(1), pp. 49–54. Available at: https://doi.org/10.1016/j.nbt.2008.01.001.

Thomas, D.D. *et al.* (2006) 'Superoxide Fluxes Limit Nitric Oxide-induced Signaling', *Journal of Biological Chemistry*, 281(36), pp. 25984–25993. Available at: https://doi.org/10.1074/jbc.M602242200.

Thomas, D.D. *et al.* (2008) 'The chemical biology of nitric oxide: Implications in cellular signaling', *Free Radical Biology and Medicine*, 45(1), pp. 18–31. Available at: https://doi.org/10.1016/j.freeradbiomed.2008.03.020.

Tomasek, D. *et al.* (2020) 'Structure of a nascent membrane protein as it folds on the BAM complex', *Nature*, 583(7816), pp. 473–478. Available at: https://doi.org/10.1038/s41586-020-2370-1.

Touzé, T. *et al.* (2003) 'Self-association of EPEC intimin mediated by the β-barrel-containing anchor domain: a role in clustering of the Tir receptor: Intimin-induced receptor clustering', *Molecular Microbiology*, 51(1), pp. 73–87. Available at: https://doi.org/10.1046/j.1365-2958.2003.03830.x.

Tsai, J.C. *et al.* (2010) 'The Bacterial Intimins and Invasins: A Large and Novel Family of Secreted Proteins', *PLoS ONE*. Edited by H.W. van Veen, 5(12), p. e14403. Available at: https://doi.org/10.1371/journal.pone.0014403.

Tsirigotaki, A. *et al.* (2017) 'Protein export through the bacterial Sec pathway', *Nature Reviews. Microbiology*, 15(1), pp. 21–36. Available at: https://doi.org/10.1038/nrmicro.2016.161.

Tsung, K. and Norton, J.A. (2006) 'Lessons from Coley's Toxin', *Surgical Oncology*, 15(1), pp. 25–28. Available at: https://doi.org/10.1016/j.suronc.2006.05.002.

Tucker, N.P. *et al.* (2004) 'DNA binding activity of the *Escherichia coli* nitric oxide sensor NorR suggests a conserved target sequence in diverse proteobacteria', *Journal of Bacteriology*, 186(19), pp. 6656–6660. Available at: https://doi.org/10.1128/JB.186.19.6656-6660.2004.

Tucker, N.P. *et al.* (2006) 'Mechanism of transcriptional regulation by the *Escherichia coli* nitric oxide sensor NorR', *Biochemical Society Transactions*, 34(Pt 1), pp. 191–194. Available at: https://doi.org/10.1042/BST0340191.

van Ulsen, P. *et al.* (2014) 'Type V secretion: from biogenesis to biotechnology', *Biochimica Et Biophysica Acta*, 1843(8), pp. 1592–1611. Available at: https://doi.org/10.1016/j.bbamcr.2013.11.006.

Ursell, T.S. *et al.* (2012) 'Analysis of surface protein expression reveals the growth pattern of the gram-negative outer membrane', *PLoS computational biology*, 8(9), p. e1002680. Available at: https://doi.org/10.1371/journal.pcbi.1002680.

Van Audenhove, I. and Gettemans, J. (2016) 'Nanobodies as Versatile Tools to Understand, Diagnose, Visualize and Treat Cancer', *EBioMedicine*, 8, pp. 40–48. Available at: https://doi.org/10.1016/j.ebiom.2016.04.028.

Varghese, S. *et al.* (2007) 'Submicromolar hydrogen peroxide disrupts the ability of Fur protein to control free-iron levels in *Escherichia coli*', *Molecular Microbiology*, 64(3), pp. 822–830. Available at: https://doi.org/10.1111/j.1365-2958.2007.05701.x.

Vecerek, B., Moll, I. and Bläsi, U. (2007) 'Control of Fur synthesis by the non-coding RNA RyhB and iron-responsive decoding', *The EMBO journal*, 26(4), pp. 965–975. Available at: https://doi.org/10.1038/sj.emboj.7601553.

Veiga, E. *et al.* (2002) 'Export of autotransported proteins proceeds through an oligomeric ring shaped by C-terminal domains', *The EMBO journal*, 21(9), pp. 2122–2131. Available at: https://doi.org/10.1093/emboj/21.9.2122.

Veiga, E., De Lorenzo, V. and Fernández, L.A. (1999) 'Probing secretion and translocation of a β-autotransporter using a reporter single-chain Fv as a cognate passenger domain: Protein translocation with β-autotransporters', *Molecular Microbiology*, 33(6), pp. 1232–1243. Available at: https://doi.org/10.1046/j.1365-2958.1999.01571.x.

Veiga, E., de Lorenzo, V. and Fernández, L.A. (2004) 'Structural tolerance of bacterial autotransporters for folded passenger protein domains', *Molecular Microbiology*, 52(4), pp. 1069–1080. Available at: https://doi.org/10.1111/j.1365-2958.2004.04014.x.

Verhoeven, G.S., Dogterom, M. and den Blaauwen, T. (2013) 'Absence of long-range diffusion of OmpA in *E. coli* is not caused by its peptidoglycan binding domain', *BMC Microbiology*, 13(1), p. 66. Available at: https://doi.org/10.1186/1471-2180-13-66.

Walenta, S. *et al.* (2000) 'High Lactate Levels Predict Likelihood of Metastases, Tumor Recurrence, and Restricted Patient Survival in Human Cervical Cancers', *Cancer Research*, 60, pp. 916–921.

Wallecha, A. *et al.* (2009) 'Construction and characterization of an attenuated *Listeria monocytogenes* strain for clinical use in cancer immunotherapy', *Clinical and vaccine immunology: CVI*, 16(1), pp. 96–103. Available at: https://doi.org/10.1128/CVI.00274-08.

Weikum, J. *et al.* (2020) 'The extracellular juncture domains in the intimin passenger adopt a constitutively extended conformation inducing restraints to its sphere of action', *Scientific Reports*, 10(1), p. 21249. Available at: https://doi.org/10.1038/s41598-020-77706-7.

Weinberg, F., Ramnath, N. and Nagrath, D. (2019) 'Reactive Oxygen Species in the Tumor Microenvironment: An Overview', *Cancers*, 11(8), p. 1191. Available at: https://doi.org/10.3390/cancers11081191.

Weirich, J. *et al.* (2017) 'Identifying components required for OMP biogenesis as novel targets for antiinfective drugs', *Virulence*, 8(7), pp. 1170–1188. Available at: https://doi.org/10.1080/21505594.2016.1278333.

Wells, T.J. *et al.* (2008) 'EhaA is a novel autotransporter protein of enterohemorrhagic *Escherichia coli* O157:H7 that contributes to adhesion and biofilm formation', *Environmental Microbiology*, p. 17.

Westphal, K. *et al.* (2008) 'Containment of tumor-colonizing bacteria by host neutrophils', *Cancer Research*, 68(8), pp. 2952–2960. Available at: https://doi.org/10.1158/0008-5472.CAN-07-2984.

Williams, N.T. (2010) 'Probiotics', *American Journal of Health-System Pharmacy*, 67(6), pp. 449–458. Available at: https://doi.org/10.2146/ajhp090168.

Wintgens, J.P., Rossner, M.J. and Wehr, M.C. (2017) 'Characterizing Dynamic Protein-Protein Interactions Using the Genetically Encoded Split Biosensor Assay Technique Split TEV', *Methods in Molecular Biology (Clifton, N.J.)*, 1596, pp. 219–238. Available at: https://doi.org/10.1007/978-1-4939-6940-1_14.

van der Woude, M.W. and Henderson, I.R. (2008) 'Regulation and Function of Ag43 (Flu)', *Annual Review of Microbiology*, 62(1), pp. 153–169. Available at: https://doi.org/10.1146/annurev.micro.62.081307.162938.

Wu, R. *et al.* (2020) 'The big BAM theory: An open and closed case?', *Biochimica Et Biophysica Acta. Biomembranes*, 1862(1), p. 183062. Available at: https://doi.org/10.1016/j.bbamem.2019.183062.

Wu, T. *et al.* (2005) 'Identification of a multicomponent complex required for outer membrane biogenesis in *Escherichia coli*', *Cell*, 121(2), pp. 235–245. Available at: https://doi.org/10.1016/j.cell.2005.02.015.

Wyborski, D.L. and Short, J.M. (1991) 'Analysis of inducers of the *E. coli lac* repressor system mammalian cells and whole animals', *Nucleic Acids Research*, 19(17), pp. 4647–4653. Available at: https://doi.org/10.1093/nar/19.17.4647.

Xiao, L. *et al.* (2021) 'Structures of the β-barrel assembly machine recognizing outer membrane protein substrates', *The FASEB Journal*, 35(1), p. e21207. Available at: https://doi.org/10.1096/fj.202001443RR.

Yang, L. *et al.* (2014) 'Permanent genetic memory with >1-byte capacity', *Nature Methods*, 11(12), pp. 1261–1266. Available at: https://doi.org/10.1038/nmeth.3147.

Yu, B. *et al.* (2012) 'Explicit hypoxia targeting with tumor suppression by creating an "obligate" anaerobic *Salmonella Typhimurium* strain', *Scientific Reports*, 2(1), p. 436. Available at: https://doi.org/10.1038/srep00436.

Yu, Y.A. *et al.* (2004) 'Visualization of tumors and metastases in live animals with bacteria and vaccinia virus encoding light-emitting proteins', *Nature Biotechnology*, 22(3), pp. 313–320. Available at: https://doi.org/10.1038/nbt937.

Zahaf, N.-I. *et al.* (2017) 'Targeted delivery of an ADP-ribosylating bacterial toxin into cancer cells', *Scientific Reports*, 7, p. 41252. Available at: https://doi.org/10.1038/srep41252.

Zhang, L., Zhao, G. and Ding, X. (2011) 'Tandem assembly of the epothilone biosynthetic gene cluster by in vitro site-specific recombination', *Scientific Reports*, 1(1), p. 141. Available at: https://doi.org/10.1038/srep00141.

Zheng, M. *et al.* (1999) 'OxyR and SoxRS regulation of *fur*', *Journal of Bacteriology*, 181(15), pp. 4639–4643.

Zhou, S. *et al.* (2018) 'Tumour-targeting bacteria engineered to fight cancer', *Nature Reviews. Cancer*, 18(12), pp. 727–743. Available at: https://doi.org/10.1038/s41568-018-0070-z.

Zschiedrich, C.P., Keidel, V. and Szurmant, H. (2016) 'Molecular mechanisms of two-component signal transduction', *Journal of molecular biology*, 428(19), pp. 3752–3775. Available at: https://doi.org/10.1016/j.jmb.2016.08.003.

Zúñiga, A. *et al.* (2020) 'Rational programming of history-dependent logic in cellular populations', *Nature Communications*, 11(1), p. 4758. Available at: https://doi.org/10.1038/s41467-020-18455-z.

Zúñiga, A. *et al.* (2021) 'Engineered l-Lactate Responding Promoter System Operating in Glucose-Rich and Anoxic Environments', *ACS synthetic biology*, 10(12), pp. 3527–3536. Available at: https://doi.org/10.1021/acssynbio.1c00456.

Zúñiga, A. *et al.* (2022) 'A rapid and standardized workflow for functional assessment of bacterial biosensors in fecal samples', *Frontiers in Bioengineering and Biotechnology*, 10, p. 859600. Available at: https://doi.org/10.3389/fbioe.2022.859600.